SUPERCONDUCTIVITY, HIGH-TEMPERATURE SUPERCONDUCTIVITY

Transport critical current in granular high-temperature superconductors

N. A. Bogolyubov

*Institute of Inorganic Chemistry, Siberian Branch of the Russian Academy of Sciences, 630090 Novosibirsk, Russia**)

(Submitted April 9, 1999)
Fiz. Nizk. Temp. **25**, 1243–1250 (December 1999)

The temperature and size dependences of critical current in three Bi-based ceramic HTSC samples with a circular cross section and in a sample with a right triangular cross section in zero magnetic field are studied by a contactless technique. It is shown that the critical current of ceramic HTSC can be presented as the product of the temperature- and size-dependent factors. The temperature-dependent factor describes individual properties of the Josephson net of each sample, while the size-dependent factor is a homogeneous function whose exponent does not depend on the shape of the sample cross section. An analysis of experimental data is used to find the radial distribution of critical current density in round samples and to determine its dependence on the magnetic induction in granular HTSC. © *1999 American Institute of Physics.* [S1063-777X(99)00112-7]

INTRODUCTION

The magnitude of critical current in high-temperature ceramic superconductors is determined by the properties of the random three-dimensional Josephson net formed by the set of weak links between superconducting grains of the material.[1,2] Considerable difficulties appear when the measurements of transport current are made in the range of magnetic fields smaller than the lower critical field of grains, since the role of the field induced by the transport current itself becomes significant. The only way to control such a field under these conditions is to vary the cross-sectional area of the sample. This leads to the so-called size effect, viz., the dependence of the critical current I_c and its average density $\langle j_c \rangle$ of the size of the sample cross section.[2–12] It was found in our earlier experiments with samples having a rectangular cross section[11,12] that the critical current as the function of temperature T and the size of the cross section (width X and height Y) in zero magnetic field has the form

$$I_c(X,Y,T)=G(X,Y)f(T). \tag{1}$$

Here the function $f(T)$ is determined only by the properties of the material of a given sample. It was found[12,13] that the critical current (namely, the function $G(X,Y)$) is a homogeneous function of the size of the cross section, i.e., is a function of the form[14,15]

$$I_c(kX,kY)=k^p I_c(X,Y). \tag{2}$$

For samples with a rectangular cross section, $p=1.39 \pm 0.02$.[12] It is reasonable to assume that the dependence of type (1) is preserved for other shapes of cross section, but the value of the exponent p in this case has to be determined in each case. This is due to the fact that individual intergrain links in the Josephson net of the sample are in the field of a varying magnetic induction since these fields are the resultant field of the currents flowing through other regions of the sample. The current in this case is distributed over the sample cross section as is dictated by the dependence of the local critical current density j_c on the magnitude of the magnetic field H. Under these conditions, the shape of the cross section can play a certain role.

The dependence of j_c on the field H (or the magnetic induction $B=\mu_0\mu H$, where μ_0 is the magnetic constant and μ the permeability of the material) is one of the central questions in the theory of critical state. In his pioneering works, Bean[16,17] proposed that $j_c=\text{const}$ in weak fields. Many models were recommended in order to take into account the effect of magnetic induction. Some of these models are generalized in the Xu–Shi–Fox three-parametric model:[18]

$$j_c(B)=A/(B_0+B)^{\beta}. \tag{3}$$

For $\beta=1$, we obtain the Kim–Anderson model.[19] However, alternative expressions for j_c were also proposed[3,7,20]:

$$j_c(B)=A/(B_0^2+B^2). \tag{4}$$

In expressions (3) and (4), A, B_0, and β are the model parameters (usually, $\beta=1/2$ or 1). These and some other relations are widely used in an analysis of the properties of HTSC systems.[2,3,7,21–24] The number of publications in which the $j_c(B)$ dependence was determined experimentally is small. For example, Johansen *et al.*[25] found on the basis of the magneto-optical method that the current distribution profile in thin strips and films corresponds to Bean's model. It should be noted that the Josephson net in such systems is rather two-dimensional, and the obtained results can hardly be used for describing the properties of $3D$ ceramic HTSC. Ginzburg *et al.*[20] proved (by measuring magnetic susceptibility) that model (4) is applicable in the limiting case of a ''thin sample.''

In order to verify the validity of expressions (1) and (2) for samples with cross sections other than rectangular and to determine the exponents p corresponding to such cross sections, we analyze here the critical current as a function of temperature and size of the cross sections of four ceramic HTSC samples in zero magnetic field. Three samples had circular cross section, while the fourth sample had a cross section of the shape of a right triangle. The current density and magnetic induction for samples with a round cross section depend only on the radius, which allows us to derive the relation $j_c = j_c(B)$ from experimental data.

OBJECTS AND METHODS OF INVESTIGATION

The samples under investigation differed in the preparation technology as well as in the ratio of initial components. The methods of sample synthesis and testing are described in Refs. 26 and 27. Sample 1 contained two superconducting phases (Bi-2212 and Bi-2223) and was characterized by the superconducting transition temperature $T_c = 105.75$ K and density 3.79 g/cm^3. Bismuth-based samples 2, 3, and 4 had only one phase (Bi-2223) and were characterized by the superconducting transition temperatures 104.8, 107.8, and 106.2 K and densities 4.91, 4.92, and 5.18 g/cm^3 respectively.

The critical current in ring-shaped samples with a circular or right-triangular cross section was measured with the help of the contactless transformer technique.[5,11,12,28] The sample with the primary and measuring windings was placed in a ferrite core of the armor type. If an alternating current flows in the primary, a current of the opposite direction is induced in the ring-shape sample. Its magnitude must be such that the magnetic flux accumulated in the central kernel of the core and passing through the gap between the ring and the winding remained unchanged and equal to zero. As a result, the magnetic induction in the central kernel, lateral and end faces of the core is equal to zero. In other words, the sample was placed in a ''jacket'' the field in whose walls is equal to zero. At the instant when the amplitude of current in the ring attained or exceeded the critical current, the signal induced in the measuring coil had the shape of a sharp peak. The amplitude I_1 of the primary current was recorded at the instant of the emergence of the signal, while the critical current was calculated by the formula $I_c = n_1 I_1$, where n_1 is the number of turns in the primary winding. The electric field induced in the sample at the instant of recording did not exceed 10 nV/cm. Measurements were made at a frequency of 14.3 Hz. The critical current of the initial sample was measured at a number of fixed temperatures. Then the sample was polished, and the critical current for the new cross sectional area was measured at the same temperatures. Such a procedure was repeated many times. As a result, two-dimensional arrays of values of I_c were obtained for various values of the cross-section diameter and the temperature. The values of I_c were measured 10–20 times at each temperature. The obtained values were averaged. The spread in the values obtained in individual measurements was usually of a few tenths of percent and exceeded 1% only in rare cases. The diameter D of the cross section was measured with the help of a clock-type indicator immediately after sample preparation as well as after completion of I_c measurements and sample heating. The temperature T_c was determined during sample cooling after each meachanical treatment. The critical current was measured at liquid nitrogen temperature for each value of the diameter of the cross section immediately after cooling, during the measurement of the $I_c(T)$ dependence, and after the completion of measurements before heating. Control measurements were made for some values of the diameter: the sample with an invariable size was cooled again after heating, and all the measuring procedures described above were repeated. The invariability of the obtained parameters was regarded as a proof of the fact that the superconducting properties of the sample had not changed as a result of mechanical processing and cooling–heating cycles. The critical current in sample 1 was measured for 10 values of the diameter of the cross section varying from 2.2 to 0.5 mm and for 14 values of temperature varying from 101 to 62.5 K. Sample 2 was investigated at eleven temperature points from the same interval and for 8 values of the diameter from 2.7 to 0.865 mm. In experiments with sample 3, the diameter varied from 1.23 to 0.7 mm (4 values), while the temperature varied from 90 to 66.25 K (6 values). Sample 4 whose critical current was studied at 77.33 K had a cross section in the form of a right triangle. The sizes of the sides of the triangle were varied in the course of the experiment in the same proportion from 1.43 to 1.08 mm and from 0.54 to 0.44 mm, and hence all the nine cross sections under investigation were similar.

DISCUSSION OF RESULTS

The results of measurements of critical current in samples 1 and 2 are shown in Figs. 1a and 1b respectively. It order to make experimental points distinguishable, temperature dependences are presented for 9 from 10 cross sections studied for sample 1 and for 7 from 8 for sample 2. The $I_c(T)$ curves for sample 1 in the temperature range 70–80 K have a typical bent associated with a superconducting transition of the Bi-2212 phase upon a decrease in temperature and with the emergence of a new Josephson net now formed by two phases Bi-2223 and Bi-2212. The critical current through the third sample had higher values than I_c in samples 1 and 2, but its temperature dependence was the same as for sample 2. At 66.25 K, the critical current in this sample attained values 14.3 and 6.75 A for the maximum and minimum diameters of the sample respectively. However, the magnetic field created in this case by the transport current even at the sample surface ($H = I_c/\pi D$) did not exceed the values of the first critical current for grains of the Bi-2223 phase.[29,30] Figure 2 shows the dependences of critical current for samples 1 and 2 as a function of their diameters. In spite of the fact that the curves correspond to different samples (Figs. 2a and 2b) and to different Josephson nets in the case of sample 1, they are of the same type.

If the expression for critical current in the samples under investigation has the same form as for samples with a rectangular cross section (i.e., (1)), the dependence on the sample diameter can be eliminated. Dividing the values of

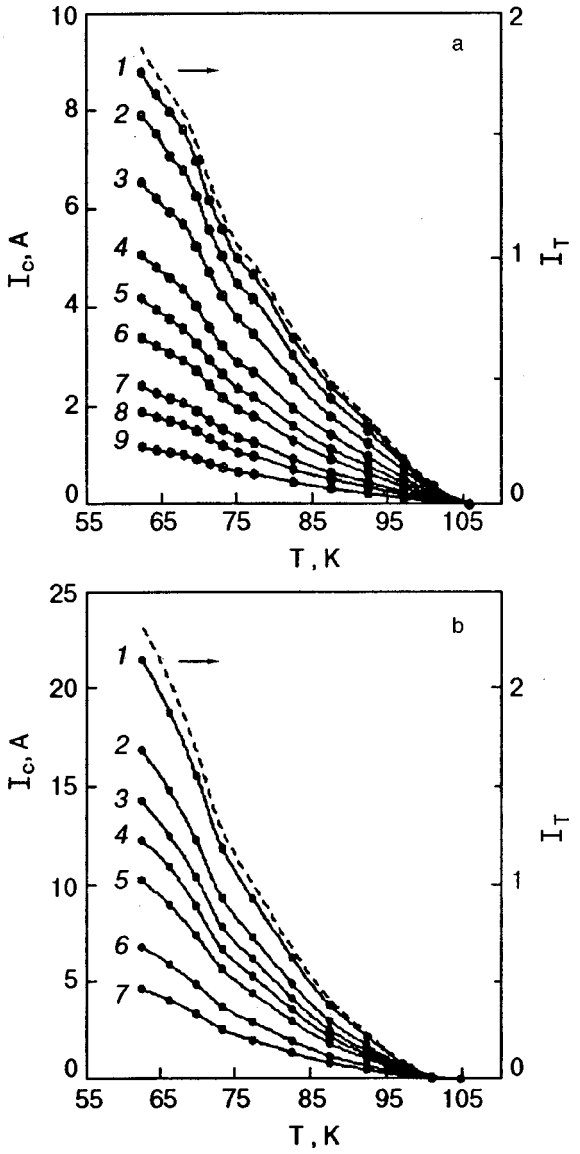

FIG. 1. Temperature dependences of critical current of the first (a) and second (b) samples. Cross section diameters, mm: 2.2 (curve *1*), 2.02 (curve *2*), 1.8 (curve *3*), 1.44 (curve *4*), 1.26 (curve *5*), 1.1 (curve *6*), 0.85 (curve *7*), 0.7 (curve *8*), and 0.5 (curve *9*) (a) and 2.7 (curve *1*), 2.32 (curve *2*), 2 (curve *3*), 1.78 (curve *4*), 1.54 (curve *5*), 1.14 (curve *6*), and 0.865 (curve *7*) (b) Dashed curves correspond to $I_T = I_c(D,T)/I_c(D,77.33K)$.

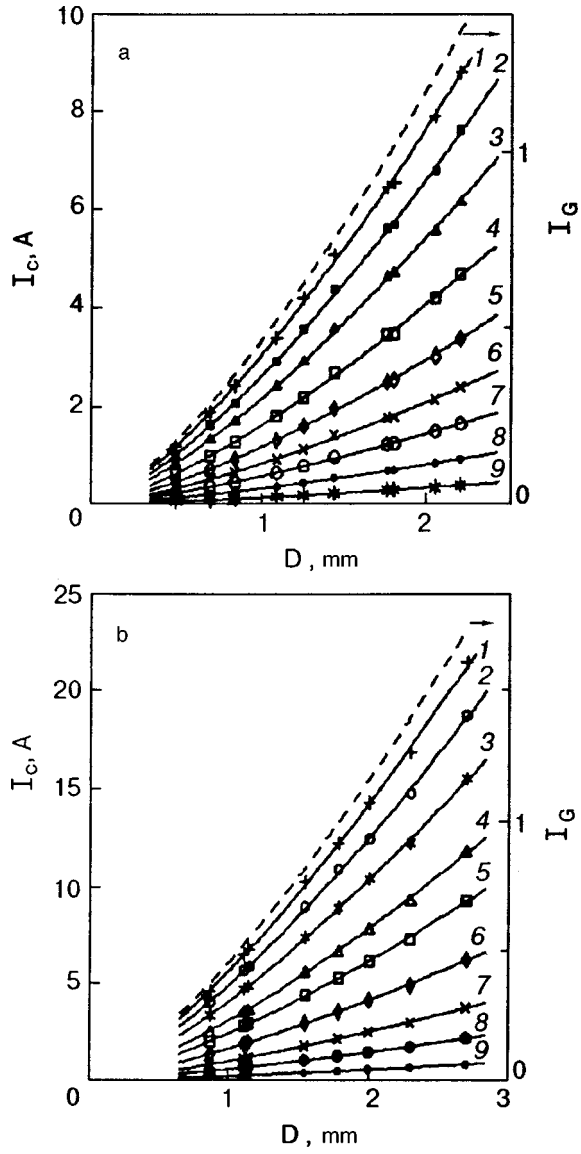

FIG. 2. Critical currents in samples 1 (a) and 2 (b) as functions of diameters of cross sections at various temperatures, K: 62 (curve *1*), 68.05 (curve *2*), 71.55 (curve *3*), 77.33 (curve *4*), 82.55 (curve *5*), 87.55 (curve *6*), 92.45 (curve *7*), 97.11 (curve *8*), and 101 (curve *9*) (a) and 62.5 (curve *1*), 66.25 (curve *2*), 69.85 (curve *3*), 73.3 (curve *4*), 77.33 (curve *5*), 82.55 (curve *6*), 87.55 (curve *7*), 92.45 (curve *8*), and 97.1 (curve *9*) (b) Dashed curves correspond to $I_G = I_c(D,T)/I_c(D_4,T)$.

critical current $I_c(D,T)$ for one of experimental curves in Fig. 1 by $I_c(D,T_0)$ for the same curve (T_0 is one of experimentally studied values of T), we must obtain the relative critical current I_T which is a function of temperature only:

$$I_T(T) = f(T)/f(T_0). \tag{5}$$

All the remaining experimental curves transformed in this way must be described by the same dependence. Indeed, the values of I_T calculated for cross sections with different diameters are close and differ from mean values by not more than 1%. For this reason, dashed curves in Fig. 1 for which $T_0 = 77.33$ K are the smoothed curves drawn through mean values. It should be noted that these dashed curves have the same shape as the temperature dependences of critical currents for individual samples, i.e., each curve reflects the individual behavior of $I_c(T)$ of a given sample. In order to eliminate the dependence on temperature, we introduce the relative current I_G by dividing the critical currents for each isotherm by the values of current determined at the same temperature for an intermediate value of the diameter D_0 of the sample cross section:

$$I_G(D) = I_c(D,T)/I_c(D_0,T). \tag{6}$$

The ratios calculated for different isotherms are quite close. Their deviation from mean values for each D are random. The scale of the figure does not allow us to demonstrate this, and Fig. 2 presents only the dashed curve drawn through mean values. Thus, the value of I_G is independent of temperature and the type of the Josephson net and is determined only by the diameter (or radius R) of the sample cross section. The critical current through sample 3 exhibits the same

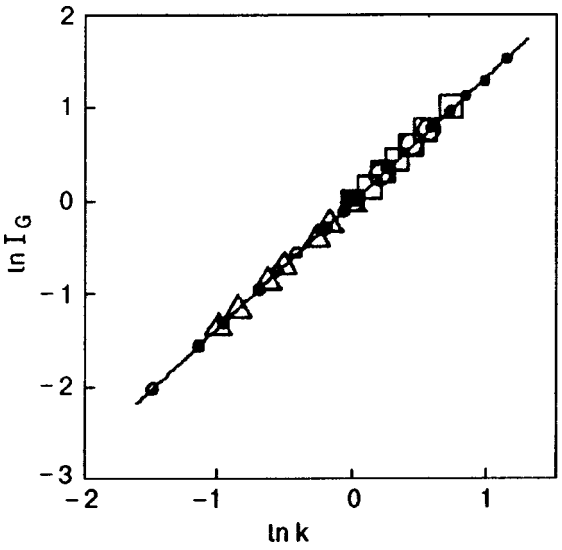

FIG. 3. Similitude law for critical current in ceramic samples with different shapes of cross section. Round samples: ○, ●, and ○ correspond to samples 1 (77.33 K), 2 (62.5 K), and 3 (90 K); △ correspond to sample 4 with a triangular cross section (77.33 K), □ correspond to sample 1 from Ref. 12 (rectangular cross section, 77.33 K).

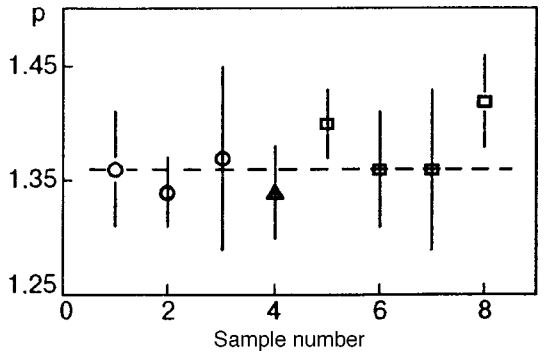

FIG. 4. Values of exponent of the homogeneous function and their confidence intervals obtained for samples with different shapes of cross sections: ○, △, and □ correspond to samples with circular, triangular, and rectangular cross sections (see text). The dashed line corresponds to the average value.

dependence on T and D. Since the critical current in round samples can be presented as (5) or (6), it has the form

$$I_c(R,T)=G(R)/(T), \tag{7}$$

i.e., the expression for critical current, as in the case of samples with a rectangular cross section, is the product of two functions one of which depends only on the size of the cross section, and the other only on temperature and material properties of an individual sample. Moreover, the analogy is much deeper. Let us consider the dependence of $I_G = I_c(kR)/I_c(R)$ on the relative size k ($k=R_j/R_i$, i and j being the numbers of sample cross sections). Statistical processing of the results of measurements shows that

$$I_c(kR,T)=k^p I_c(R,T),$$

for any sample, any isotherm, and any choice of R_i. Consequently, the critical current (to be more precise, the factor $G(R)$ depending on the sample radius) is a homogeneous function of R.[14,15] The dependence of $\ln I_G=\ln[I_c(kR)/I_c(R)]$ on $\ln k$ for samples 1–3 is shown by circles in Fig. 3. In order to minimize the overlapping of points corresponding to different samples, the normalizing quantities are chosen so that they correspond to the largest cross sections for sample 1 and to the smallest cross sections for samples 2 and 3. It can easily be seen that the dependence under investigation for each sample can be approximated by a straight line. Since the preceding equality is valid for any k, we find (putting $k=1/R$) that $G(R)$ is a power function and

$$I_c(R,T)=Cr^p f(T). \tag{8}$$

The averaged value of the exponent p determined for sample 1 is 1.36 ± 0.05. Here and below, the fractiles inverted Student distribution[31] with the confidence probability 0.95 is used for determining confidence intervals. The deviations of the value of exponent p determined for different isotherms of this sample from the average value are of random nature, i.e., the exponent is independent of temperature as well as the type of random Josephson medium existing in the sample at a certain temperature. The latter statement means that it must be independent of the properties of a specific sample also. Indeed, the $\ln I_G$ vs. $\ln k$ dependences plotted for samples 1–3 on the same graph coincide (see Fig 3). The exponent $p=1.34\pm0.03$ for the second sample and $p=1.37\pm0.08$ for sample 3. These values coincide within confidence intervals. Taking into account the facts mentioned above, we find the average value of $p=1.36\pm0.02$. Thus, the function $G(R)=CR^p$ for round ceramic HTSC samples is a homogeneous function of its argument, which is characterized by a universal exponent. In other words, we observe the same pattern as for samples with a rectangular cross section.

Experiments with sample 4 with a cross section in the form of a right triangle proved that its critical current is a homogeneous function of the dimensions of cross section (cathets X and Y), i.e., is described by expression (2). Since the condition $k=X_j/X_i=Y_j/Y_i$ cannot be fulfilled rigorously when the dimensions of this sample are varied, the quantity k was defined as in Ref. 12: $k=0.5(X_j/X_i+Y_j/Y_i)$. In the case of a triangular sample, the exponent $p=1.34\pm0.04$ (triangles in Fig. 3). On the other hand, in Ref. 12 we investigated four samples with rectangular cross sections and obtained the following values for the exponent p: 1.40 ± 0.04, 1.36 ± 0.05, 1.36 ± 0.07, and 1.42 ± 0.04, which coincide with the values of p determined in this research to within confidence intervals. Figure 4 shows the exponents and their confidence intervals determined by us here and in previous investigations.[12] Sample numbers are laid along the abscissa axis; samples 1–4 from Ref. 12 are labeled now by 5–8 respectively. The diagram displays no dependence of exponent p on the shape of the sample cross section. Consequently, we can introduce the universal average value of p. This has a physical meaning if the law of similitude in the dependence of the critical current of ceramic HTSC samples

on the relative size of cross section[12] is observed irrespective of the shape of cross section. In other words, the value of I_G must be a universal function of k for samples with any shape of the cross section (at least, for the shapes studied by us). Figure 3 shows the dependences of $\ln I_G$ on $\ln k$ obtained for round samples (1–3), as well as samples with triangular (4) and rectangular (sample 1 from Ref. 12) cross sections at various temperatures. It can easily be seen that all the points can be approximated by a single straight line, i.e., the similitude law is observed indeed. As an additional argument, we note that the statistical processing confirms the validity of zero-point hypothesis concerning the equality of general mean values (for a confidence probability 0.95).[31] Thus, for the weight-average value of the exponent of the homogeneous function, we obtain $p=1.36\pm 0.01$. It was proposed by us earlier[12,13] that the exponent p might depend on the shape of the sample cross section. However, subsequent experiments did not confirm this proposition. It should be noted that the cross sections of the samples under investigations are convex simply connected regions. Generalizing the results obtained by us, we can state that if samples cross sections are such regions, the critical current of ceramic samples in zero external field is a homogeneous function of the sample size with a universal exponent irrespective the shape of a cross section.

Let us return to an analysis of a round sample carrying current of the critical value. Obviously, the critical current density in this case has the critical value everywhere over the entire cross section. Consequently, we can write

$$I_c(R,T)=CR^p f(T)=\int j_c r\,d\,r\,d\varphi. \tag{9}$$

The integration is carried out here over the entire cross-sectional area of the sample, and r and φ are polar coordinates. Since the integration concerns only spatial variables, the factor $f(T)$ appearing in the expression for $I_c(R,T)$ is also contained in j_c. In the case of a round sample, the current density does not depend on the azimuthal angle, and hence

$$j_c(r,T)=cf(T)r^{p-2}, \tag{10}$$

where c is a constant. Using relations (9) and (10), we obtain $C=2\pi c/p$. Since $p=1.36$, we have $j_c\propto r^{-0.64}$. It follows from formula (10) that the value of j_c in the central part of the sample increases unlimitedly. It should be noted in this connection that this expression was derived by interpreting the results of macroscopic measurements in which a $3D$ Josephson net in the sample behaves as a continuous medium. If the radius of the region in the central part of the sample (or in any other its part) becomes smaller than r_0 which is equal to tens and even hundreds of diameters of individual superconducting granules, we go over to a discrete Josephson medium, and expression (10) is not applicable any longer. The critical current density itself remains finite everywhere. The average critical current density

$$\langle j_c\rangle = I_c/\pi R^2 = C/(T)/\pi R^{2-p} \tag{11}$$

is a homogeneous function of R with the exponent $p-2$ and increases upon a decrease in the sample cross section. Samokhvalov[32] who studied the emergence of vortices in a cylindrical sample came to the same conclusion. When the decreasing value of R approaches r_0, the form of the dependence $\langle j_c\rangle$ changes for the above reasons. If we write $\langle j_c\rangle$ as a function of the cross-sectional area S, we have $\langle j_c\rangle\sim S^{p/2-1}\sim S^{-0.32\pm 0.01}$. The authors of Refs. 7, 2, 33, and 3 presented the results of their analysis of $\langle j_c\rangle$ in the form of a power function of S and obtained exponents -1, $-1/2$, and $-1/3$ respectively. It can be seen that our result is in very god agreement with that obtained by Zakharchenko *et al.*[3]

The magnetic field created in the sample by transport current, and hence the magnetic induction have only azimuthal components depending on r. Using the integral Maxwell equation for the circulation of magnetic field, we obtain

$$B(r)=\mu_0\mu H(r)=\frac{c}{p}\mu_0 u r^{p-1}f(T). \tag{12}$$

The values of B and H are equal to zero at the center of the sample and increase towards the periphery in proportion to $r^{0.36}$. Besides, the values of B and H as well as $\langle j_c\rangle$ depend on $f(T)$, i.e., on individual properties of the sample. At the sample surface, we have

$$H(R)=CR^{p-1}f(T).$$

Thus, $H(R)$ is also a homogeneous function of the sample radius with the exponent $p-1$. Eliminating r from (10) and (12), we obtain the following equation connecting the critical current density and magnetic induction:

$$j_c(B)=\left(\frac{pc^{1/(p-2)}}{\mu_0\mu}\right)^{(p-2)/(p-1)} B^{(p-2)/(p-1)}f(T)^{1/(p-1)}. \tag{13}$$

Thus, $j_c\propto B^{-1.78\pm 0.08}$. The behavior of the critical current density in the vicinity of the sample center, where the magnetic field and induction tend to zero, has been considered earlier.

Expression (13) obtained for the $j_c(B)$ dependence differs from (3) or (4) primarily in the value of exponent. If we assume that $B_0=0$, we arrive at (3) for $\beta=(p-2)/(p-1)$. If we round off the exponent of B to -2, expression (13) is transformed to formula (4) (for $B_0=0$). The presence of terms with B_0 in (3) and (4) allows us to eliminate divergence of j_c at the center of the sample. Using the results obtained by us as well as quite natural assumptions, we can derive expressions for $j_c(r)$ and $j_c(B)$ which give a finite value of j_c at the sample center. In this work, however, we confine our analysis only to corollaries following directly from experiments. Equation (13) connecting the critical current density with the magnetic induction was obtained by us for a round sample. However, it is a characteristic of a random Josephson medium realized in granular HTSC materials. Consequently, it is valid for any sample and does not depend on whether the magnetic field is applied or is induced

by transport current, and the properties of a specific material medium are taken into account in (13) due to the presence of the function $f(T)$.

We shall use Eq. (13) for analyzing the state emerging in the sample having the shape of a tube carrying the critical transport current I_{c1}. The radii of inner and outer surface of the tube are R_1 and R respectively. In this case, j_c and B depend only on r. Maxwell's equation for the case under investigation has the form

$$\frac{d(rB)}{dr} = \mu_0 \mu r j_c .$$

Taking into account the fact that magnetic induction on the inner surface of the tube is equal to zero, we obtain

$$B(r) = (\mu_0 \mu c/p) r^{p-1} \gamma(r) f(T), \tag{14}$$

$$j_c(r) = c r^{p-2} [\gamma(r)\Gamma]^{-1} f(T).$$

$$\gamma(r) = [1 - (R_1/r)^{p/(p-1)}]^{p-1}. \tag{15}$$

When $r - R_1 \sim r_0$, we can make the same remark on the applicability of expression (15) as while discussing formula (10). The expressions for critical current, its average density, and magnetic field on the surface of such a sample have the form

$$I_{c1} = C R^p \gamma(R) f(T), \tag{16}$$

$$\langle j_c \rangle = \frac{I_{c1}}{\pi R^2}(1 - R_1^2/R^2), \tag{17}$$

$$H(R) = \frac{C}{2\pi} R^{p-1} [\gamma(R)]^{p-1} f(T). \tag{18}$$

This means that as in the case of a continuous round sample, these three quantities are homogeneous function of degree p, $p-2$, and $p-1$ respectively, but now of two arguments R_1 and R. In the example under consideration, the sample has the cross section in the form of a doubly-connected region possessing a central symmetry. Consequently, the generalization made by us earlier remains unchanged (see the end of discussion Fig. 3).

Let a round continuous sample carry a transport current I_1 smaller than critical. Following the hypothesis of critical state,[16,17] we assume that this current is distributed over the sample cross section starting from the surface region so that the current density is equal to its critical value everywhere. Consequently, the current flows over the part of the sample having the shape of a tube with inner radius R_1 and outer radius R. The current in the central part is equal to zero. On the inner surface of this tube, $H = 0$, while $H = I_1/2\pi R$ on the outer surface. In this case, formulas (14) and (15) describe the radial distribution of magnetic induction and critical current density. The current I_1 is critical for the tube under investigation. Comparing it with the critical current (8) for the entire sample, we obtain

$$R_1 = R[1 - (I_1/I_c)^{1/(p-1)}]^{(p-1)/p}.$$

Thus, the internal boundary of the region carrying current is displaced towards the center with increasing current I_1 according to the power law.

CONCLUSION

An analysis of experimental results shows that the expression for critical current in ceramic HTSC in zero magnetic field can be written as the product of two functions. One of the functions reflects individual properties of the sample material and is a function of temperature only. The other is a homogeneous function of the sigl of sample cross section with a universal value of exponent p for all samples irrespective of the shape of cross section ($p = 1.36 \pm 0.01$). Using experimental results, we have established the form of field dependence of critical current density: $j_c \sim B^{(p-2)/(p-1)}$.

*)E-mail: mart@casper.che.nsk.su

[1] J. R. Clem, Physica C **153–155**, 50 (1988).
[2] H. Dearch and G. Blatter, Phys. Rev. B **38**, 11391 (1988).
[3] S. I. Zakharchenko, V. B. Mityushin, N. A. Podlevskikh, and L. M. Fisher, Sverkhprovodimost: Fiz., Khim., Tekh. **2**, 136 (1989).
[4] A. A. Zhukov, D. F. Komarkov, V. V. Moshchalkov *et al.*, Sverkhprovodimost: Fiz., Khim., Tekh. **3**, 1234 (1990).
[5] G. P. Meisner and C. A. Taylor, Physica C **169**, 303 (1990).
[6] C.-W. Cheng, A. C. Rose-Innes, N. McAlford, and T. W. Button, Supercond. Sci. Technol. **3**, 90 (1990).
[7] A. A. Zhukov, V. V. Moshchalkov, D. F. Komarkov *et al.*, Jpn. J. Appl. Phys., Part 1 **29**, L760 (1990).
[8] B. H. Kliem, A. Wegers, and J. Lutzner, J. Appl. Phys. **69**, 1534 (1991).
[9] C. A. D'Ovido, J. E. Fiscina, and D. A. Esparza, J. Appl. Phys. **69**, 8265 (1991).
[10] E. Babic, M. Prester, D. Drobac *et al.*, Phys. Rev. B **45**, 913 (1992).
[11] N. A. Bogoliubov, Sverkhprovodimost: Fiz., Khim., Tekh. **7**, 294 (1994).
[12] N. A. Bogoliubov, Fiz. Nizk. Temp. **23**, 808 (1997) [Low Temp. Phys. **23**, 606 (1997)].
[13] N. A. Bogoliubov, Czech. J. Phys. **46**, Suppl., 1261 (1996).
[14] J. Aczel, *Lectures on Functional Equations and Their Applications*, Academic Press, New York, London (1966).
[15] R. Courant, *Differential and Integral Calculus*, vol. 2 [Russian transl.], Nauka, Moscow (1970).
[16] C. P. Bean, Phys. Rev. Lett. **8**, 250 (1962).
[17] C. P. Bean, Rev. Mod. Phys. **36**, 31 (1964).
[18] M. Xu, D. Shi, and R. F. Fox, Phys. Rev. B **42**, 10773 (1990).
[19] P. W. Anderson and Y. B. Kim, Rev. Mod. Phys. **36**, 39 (1964).
[20] S. L. Ginzburg, G. Yu. Logvinova, I. D. Luzyanin *et al.*, Zh. Éksp. Teor. Fiz. **100**, 532 (1991) [Sov. Phys. JETP **73**, 292 (1991)].
[21] K. V. Bhagwat and P. Chaddah, Phys. Rev. B **44**, 6950 (1991).
[22] E. H. Brandt, Phys. Rev. B **52**, 15442 (1995).
[23] X. N. Xu, A. M. Sun, S. A. Aruna *et al.*, J. Supercond. **10**, 151 (1997).
[24] A. B. Riise, T. H. Johansen, and H. Bratsberg, J. Supercond. **11**, 353 (1998).
[25] T. H. Johansen, M. Bazilievich, H. Bratsberg, and Y. Galperin, Phys. Rev. B **54**, 16264 (1996).
[26] V. S. Kravtchenko, M. A. Zhuravleva, Y. M. Uskov *et al.*, Superlattices Microstruct. **21**, Suppl. A, 87 (1997).
[27] V. S. Kravchenko, M. A. Zhuravleva, Y. M. Uskov *et al.*, Neorg. Mater. **34**, 1274 (1998).
[28] E. A. Harris, J. E. L. Bishop, R. L. Havill, and P. J. Ward, J. Phys. C **221**, L673 (1988).
[29] E. V. Matizen, P. P. Bezverkhii, V. G. Martynets, and N. V. Kuskova, Sverkhprovodimost: Fiz., Khim., Tekh. **7**, 294 (1994).

[30] P. Mune, J. Lopez, and E. Altshuler, Physica C **292**, 48 (1997).
[31] E. I. Pustyl'nik, *Statistical Methods of Analysis and Processing of Observations* [in Russian], Nauka, Moscow (1968).
[32] A. V. Samokhvalov, Physica C **308**, 74 (1998).
[33] V. F. Khirnyi, V. P. Seminizhenko, and A. A. Kozlovskii, Fiz. Tverd. Tela (St. Petersburg) **38**, 2951 (1996) [Phys. Solid State **38**, 1614 (1996)].

Translated by R. S. Wadhwa

A crossover in the temperature behavior of the perpendicular upper critical magnetic field of layered superconductors and thin films

V. M. Gvozdikov

Department of Physics, Kharkov State University, 310077, Svobody sq. 4, Kharkov, Ukraine
(Submitted May 12, 1999)
Fiz. Nizk. Temp. **25**, 1251–1258 (December 1999)

A mechanism which relates the upturn of the perpendicular upper critical magnetic field $H_{c2}^{\perp}(T)$ in layered superconductors and thin films with the structural inhomogeneity in the bulk of the sample, provided that the local critical temperature T_c^* inside the inhomogeneity is higher than in the rest of the sample (T_c) is proposed. Within the Ginzburg–Landau approach an equation which describes two types of experimentally observed nonlinearities in $H_{c2}^{\perp}(T)$ near T_c for ISN (insulator-superconductor-normal metal) and NSN layer configurations, is found. In the NSN case a crossover from the linear branch $H_{c2}^{\perp}(T) \propto (T_c - T)$, for fields $H \leqslant H_m$, to the nonlinear branch with the upturn, if $H > H_m$, takes place. The crossover field H_m is inversely proportional to the local enhancement of the critical temperature $(T_c^* - T_c)$ and the distance R to the surface (the nearest surface, in case of a thin film). In the ISN case the upturn holds for $H < H_m$, whereas for higher fields $H_{c2}^{\perp}(T)$ crosses over to the linear branch. In the ISI case the $H_{c2}^{\perp}(T)$ is a linear function. © *1999 American Institute of Physics.* [S1063-777X(99)00212-1]

1. INTRODUCTION

The nonlinear behavior of the upper critical field H_{c2} has been observed first in the layered dichalcogenides of transient metals in the beginning of the 1970s[1] and was given then much attention as a possible signal of non-BCS pairing in these materials. In the 1980s, artificially prepared superconducting superlattices (SL) have been an object of intensive studies which revealed a number of nonlinearity types in the temperature behavior of the $H_{c2}(T)$: the positive curvature [an upturn of the $H_{c2}(T)$ near the critical temperature T_c], square-root and linear crossovers, the Takahashi–Tachiki crossover (in S/S' superlattices), and the power law $H_{c2}^{\parallel} \sim [1-(T/T_c)]^{\gamma}$ with $1/2 < \gamma < 1$ in quasiperiodic[2] and fractal[3,4] superlattices. The control over the width of layers, their number and content, as well as the deposition sequence order made it possible to clear up in detail the relationship between the structure of the artificial superlattices and the form of the $H_{c2}(T)$. A review of the temperature behavior of the upper critical field $H_{c2}(T)$ in superlattices is given in Ref. 5. The nonlinearities of the $H_{c2}(T)$ have been observed in different types of high-T_c layered cuprates and superlattices made from novel materials such as YBaCuO/PrBaCuO superlattices.[6]

Theoretically, the problem of calculation of $H_c(T)$ reduces to the eigenvalue problem for a fictitious particle in an external magnetic field. In the case of parallel fields this problem has been solved both numerically[7] and analytically[8–10] for different types of periodic SI and SN superlattices. A theory of the temperature dependence of the $H_{c2}^{\parallel}(T)$ for quasi-periodic SL was developed in Refs. 10 and 11. In contrast with the parallel field $H_{c2}^{\parallel}(T)$, where the nonlinearities are due to the lifting of degeneracy of the lowest Landau level on the orbit center position, the perpendicular field $H_{c2}^{\perp}(T)$ in all existing theories is a linear function of T, because the lowest Landau level in this geometry equals its standard value $\hbar\Omega/2$ ($\Omega = eH/mc$ is the cyclotron frequency). Setting this value equal to the coefficient $\alpha(T)$ of the Ginzburg–Landau expansion, we obtain the linear dependence $H_{c2}^{\perp} \sim 1-(T/T_c)$. The exceptions are twinned crystals of the YBaCuO type and the artificial superlattices PbTe/PbS (Ref. 12) where the mismatch dislocations make a quasi-square two-dimensional lattice at the boundaries between the neighboring layers. A theory for the positive curvature of the $H_{c2}^{\parallel}$ in PbTe/PbS superlattices was given in Ref. 10. On the other hand, the positive curvature of the $H_{c2}^{\perp}(T)$ has been observed in a periodic SL,[13–16] fractal SL, superconducting SL with magnetic interlayers,[17] and intercalated layered crystals,[18,19] including high-T_c cuprates.[20] (In the latter a positive curvature close to zero temperature also has been observed.[21] We do not consider it here.) In contrast with the specific case of PbTe/PbS superlattice, in other artificially fabricated SL this nonlinearity cannot be related to some superstructure in the plane perpendicular to the external field, so that the above-mentioned mechanisms of the Landau level broadening cannot explain an upturn in the $H_{c2}^{\perp}(T)$. The positive curvature of the $H_{c2}^{\perp}(T)$ is a property inherent to all types of SL, regardless of the layer stacking sequence order. On the other hand, it seems rather sensitive to the quality of layers in SL, because an upturn in the $H_{c2}^{\perp}(T)$ was observed only in a small portion of the samples studied so far. The physical reason behind this phenomenon is not understood yet. The relationship between the quality of a layered crystal and the positive curvature of the $H_{c2}^{\perp}(T)$ has been clearly demonstrated in Refs. 18 and 19, where a positive curvature was observed after the intercalation of layered single crystals of $2H$-$NbSe_2$ by molecules of TCNQ and Sn atoms.

Very instructive observations were made in some experimental studies.[4,17] An upturn in the $H_{c2}^{\perp}(T)$ of a single Nb layer deposited on a dielectric substrate was not found in those studies,[4,17] whereas it has appeared in triple layers and SLs Nb/Gd and Nb/Cu fabricated in the same series of experiments. These results show that boundary conditions at interfaces between superconducting and metal (or insulator) layers play a crucial role in physics driving the nonlinearities in the $H_{c2}^{\perp}(T)$.

In this paper we propose a mechanism of the positive curvature of the $H_{c2}^{\perp}(T)$ near T_c due to the structural inhomogeneities in the bulk of a layer. This mechanism gives a qualitative description of all types of nonlinearities in the $H_{c2}^{\perp}(T)$ observed near T_c in artificially fabricated SLs.

Our paper is organized as follows. In Sec. 2 the problem of calculations of the perpendicular critical field is reduced, in the adiabatic approximation, to the eigenvalue problem for a ''particle'' in a one-dimensional potential well which experiences an additional action from the surface. In Sec. 3 the equations for $H_{c2}^{\perp}(T)$ are derived. They describe nonlinearities in the $H_{c2}^{\perp}(T)$ of a thin film and SLs near T_c with a decrease in temperature. The discussion and comparison of the results with experiments on layered superconductors are given in Sec. 4.

2. FORMULATION OF THE PROBLEM AND THE MODEL

The problem of calculations of the upper critical field $H_{c2}^{\perp}(T)$, as is well known, reduces to the eigenvalue problem for the lowest Landau level. In the case of the Ginzburg–Landau approach an appropriate Schrödinger equation for a ''particle'' is

$$\hat{H}\Psi = -\alpha(T)\Psi, \tag{1}$$

where Ψ is the order parameter, and $\alpha(T)$ stands for the coefficient in front of the term $|\Psi|^2$ in the Ginzburg–Landau expansion. The physics of nonlinearities of the function $H_{c2}^{\perp}(T)$ in different types of regular and quasi-periodic superlattices is based on the fact that in these structures, due to the lift of the Landau level degeneracy on the orbit center position, the lowest edge of the energy spectrum $\epsilon_{\min}(H)$ is below $\hbar\Omega/2$. Nonlinearity of the function $\epsilon_{\min}(H)$ results then in the nonlinearity of the function $H_{c2}^{\perp}(T)$, which is a solution of the equation $\epsilon_{\min}(H_{c2}) = -\alpha(T)$. This approach proved to be very useful for studies of the $H_{c2}^{\parallel}(T)$, as was discussed in the previous section. In the case of a perpendicular orientation of the magnetic field, the problem of the positive curvature of the $H_{c2}^{\perp}(T)$ in thin layers and superlattices remains unsolved. The explanation of the positive curvature of the perpendicular critical fields in superlattices of the type PbTe/PbS, given in Ref. 10, is essentially based on the same idea that holds for calculations of the $H_{c2}^{\parallel}(T)$ in superlattices, because the upturn in the $H_{c2}^{\perp}(T)$ in these materials is attributable to the two-dimensional net of mismatch dislocations.

The situation with the $H_{c2}^{\perp}(T)$ is absolutely different because artificial SLs are assumed to be uniform along the layers and, hence, cannot broaden the Landau levels into bands. On the other hand, among the numerous superlattices fabricated so far[5] only a few[4,13–19] have displayed a positive curvature in the $H_{c2}^{\perp}(T)$, while the great majority of them yield a linear temperature behavior near T_c. This linearity in T is in agreement with theory, since the lowest energy level, $\epsilon_{\min}$, in this case is $\hbar\Omega/2$ and, hence, $H_{c2}^{\perp} \sim T_c - T$. Of course, perfectly uniform SL is no more than a mere theoretical model and real SLs are far from being ideal periodic structures because of uncontrollable inhomogeneities introduced during the process of their fabrication. We will show in what follows that a structural inhomogeneity of content, which locally enhances the superconductivity of a layer or thin film, gives rise to the positive curvature of $H_{c2}^{\perp}(T)$.

Let us assume that an inhomogeneity exists in a thin superconducting film at a distance a from its surface, where local conditions for superconductivity are better than those in the rest of the sample, so that the local critical temperature T_c^* is higher than the temperature T_c. In high-T_c cuprates, for example, such an inhomogeneity may be due to the oxygen concentration fluctuations since the local oxygen content is a factor which mainly determines the local T_c. Nonuniform distribution of intercalating molecules can also cause a local enhancement of the superconductivity in intercalated layered superconductors. For simplicity we assume a cylindrical-shape inhomogeneity, so that the Schrödinger equation can be written in the symmetric gauge, $\mathrm{A} = 1/2[\mathbf{Hr}]$, in the form

$$\hat{H}\Psi_E(\rho,z) = E\Psi_E(\rho,z), \tag{2}$$

where

$$\hat{H} = \hat{H}_1(\rho) + \hat{H}_2(z) + U(\rho,z). \tag{3}$$

Here $\hat{H}_2(z)$ is a Hamiltonian which is related to the particle motion along the field, $\rho = (\rho,\varphi)$ are the polar coordinates in the plane perpendicular to the external field $\mathbf{H}$; z is the coordinate along the field $\mathbf{H}$, and $U(\rho,z) < 0$ is a ''potential well'' associated with the inhomogeneity. The Hamiltonian, relevant to the motion of a ''particle'' in an external magnetic field in the plane, is

$$\hat{H}_1(\rho,\varphi) = -\frac{\hbar^2}{2\mu}\left[\frac{1}{\rho}\frac{\partial}{\partial\rho}\rho\frac{\partial}{\partial\rho} + \frac{1}{\rho^2}\frac{\partial^2}{\partial\varphi^2} + \frac{eH}{\hbar c}\hat{l}_z\right] + \frac{e^2H^2}{8mc^2}\rho^2. \tag{4}$$

The eigenfunctions of the Hamiltonian (4) can be written in the form

$$\Psi_{Em}(\rho,\varphi) = \frac{\mathrm{e}^{im\varphi}}{\sqrt{2\pi}}\sqrt{\rho}f(\rho), \tag{5}$$

where $f(\rho)$ satisfies the equation

$$f'' + \frac{2}{\rho}f' + \left[\frac{2\mu E}{\hbar^2} + \frac{eHm}{c\hbar} - \frac{m^2 - 1/4}{\rho^2} - \frac{\rho^2}{4L^2}\right]f = 0. \tag{6}$$

The solution of Eq. (6) is given by

$$\sqrt{\rho}f(\rho) = C\exp\left(\frac{-\rho^2}{4L^2}\right)\left(\frac{\rho}{L}\right)^{|m|}F\left(-n_\rho, |m|+1, \frac{\rho^2}{2L^2}\right). \tag{7}$$

The energy spectrum is determined by the condition that the hypergeometric function $F(a,b,c)$ reduces to a polynomial, which yields

$$E_m=\hbar\Omega\left(n+\frac{1}{2}\right), \tag{8}$$

$n=n_\rho+(|m|+m)/2$ and $m=-\infty\ldots,-1,0,\ldots n$. Here n and n_ρ are integers; $\Omega=eH/\mu c$ is the cyclotron frequency, and $L=(\hbar/\mu\Omega)^{1/2}$ stands for the magnetic length.

The normalization constant C in Eq. (7) is

$$C=\left[\frac{(|m|+n_\rho)!}{n_\rho!}\right]^{1/2}(|m|!L)^{-1}. \tag{9}$$

Since T_c^* is only slightly greater than T_c, we can assume that influence of the potential $U(\rho,z)$ is weak compared to the action that the external field exerts on a particle. This means that an adiabatic approximation can be applied to the eigenvalue equation (2). Since we are interested in the lowest energy level $n=0$, the adiabatic approximation in this case means that the energy and the wave function should be taken in the following approximate form:[22]

$$\Psi_{Em\epsilon}(\mathbf{r})\approx\Psi_{0m}(\rho,\varphi)\Psi_{\epsilon m}(z), \tag{10}$$

$$E=\frac{\hbar\Omega}{2}+\epsilon \tag{11}$$

where

$$\Psi_{0m}(\rho,\varphi)=\left(\frac{\rho}{\sqrt{2}L}\right)^{|m|}\exp\left(im\varphi-\frac{\rho^2}{4L^2}\right)/\sqrt{2\pi|m|!}L. \tag{12}$$

Substituting (10) into Eq. (2) and eliminating $\Psi_{0m}(\rho,\varphi)$, we obtain the Schrödinger equation for the wave function $\Psi_{\epsilon m}(z)$

$$\hat{H}_2(z)\Psi_{\epsilon m}(z)+[U_{\rm eff}^m(z)-\epsilon]\Psi_{\epsilon m}=0, \tag{13}$$

where $\hat{H}_2=-(\hbar^2/2\mu)(d^2/dz^2)$, and the effective potential energy is introduced

$$U_{\rm eff}^m(z)=\int U(\rho,z)|\Psi_{0m}(\rho)|^2d^2\rho. \tag{14}$$

Since (13) is a one-dimensional Schrödinger equation, and $U_{\rm eff}^m(z)$ is negative, there should be at least one bound state in the potential well made by $U_{\rm eff}^m(z)$. In the case of boundless sample the eignevalue ϵ in Eq. (13) is negative and strongly depends on the magnitude of the external field H, so that the minimal energy in the eigenvalue problem (2) in adiabatic approximation is given by

$$E_{\rm min}=\frac{\hbar\Omega}{2}-\epsilon_0(H). \tag{15}$$

Thus, $E_{\rm min}(H)$ is lower than $\hbar\Omega/2$ and, in general, is a nonlinear function of H, because $\epsilon_0(H)$ is a nonlinear function of H, as one can see from Eqs. (12) and (14), which yield the following expression for the potential well in this case:

$$U_{\rm eff}^m(z)=\frac{2}{|m|!}\int_0^\infty U(\rho,z)\tilde{\rho}^{2|m|+1}\exp(-\tilde{\rho}^2)d\tilde{\rho}, \tag{16}$$

where $\tilde{\rho}=\rho/\sqrt{2L}$.

For small (compared to $\hbar\Omega$) potential $U(\rho,z)$ the one-dimensional potential well, given by Eq. (16), is shallow and $\epsilon_0(H)$ can be evaluated as[22]

$$\epsilon_0(H)\simeq\frac{mU_0^2}{2\hbar^2}, \tag{17}$$

$$U_0=\int_{-\infty}^{\infty}U_{\rm eff}^0(z)dz. \tag{18}$$

The presence of a boundary, as is well known, can dramatically change the situation with the bound state because the value which Ψ takes at the boundaries of a film strongly affects the possibility of a potential well to create a bound state. Two different types of the boundary conditions take place at the interfaces: $\Psi=0$ for insulator-superconductor (IS) boundary and $d\Psi/dx=0$ for the NS boundary of the normal metal with the superconductor.[23] Thus, we have three different cases for the superconductor layer (S) sandwiched between the insulating (I) or the normal metal (N), which we denote as ISI, ISN, and NSN. The analysis given in the next section shows that conditions for the creation of a bound state of the particle in the potential well are different for these three cases.

Since the depth of a well, $U_{\rm eff}^0(z)$, grows with the enhancement of an external field H, we can expect a crossover from the regime $E_{\rm min}(H)=\hbar\Omega/2$ to the regime where $E_{\rm min}(H)=\hbar\Omega/2-\epsilon_0(H)$, when H crosses over some value H^*. The crossover field H^* corresponds to such a depth of the potential well which permits to create a bound state in the well for a given value of distance between the boundary and the well. In the context of our analysis, this crossover corresponds to the transition from the linear branch, $H_{c2}^\perp\propto T_c-T$, to the nonlinear branch which goes above the linear branch as the field H increases to a value larger than H^*. The temperature dependence of the upper critical field, $H_{c2}^\perp(T)$, can then be determined from the equation $E_{\rm min}(H_{c2}^\perp)=-\alpha(T)$. To simplify further calculations, we will make some additional assumptions which do not change the physics beyond the above crossover. We first assume that the radius of the inhomogeneity, R, is less than the magnetic length, $L=(\hbar c/eH_{c2})^{1/2}$, which near T_c is of the order of the coherence length $\xi(T)=\xi_0/(1-T/T_c)^{1/2}$ because $H_{c2}=\Phi_0/2\pi\xi^2(T)$. Therefore, the condition $R\ll L$ reduces to the inequality $R\ll\xi(T)$, which is easy to satisfy near T_c even for sufficiently large (in the lattice constant scale) R. The quantity Φ_0 stands for the flux quantum. Under this condition assuming $U(\rho,z)=-|U(z)|$ if $\rho\leqslant R$ and $U(\rho,z)=0$ otherwise, we have from Eq. (16)

$$U_{\rm eff}^0=-|U(z)|I(H), \tag{19}$$

where

$$I(H)\approx\frac{2\pi R^2H}{\Phi_0}. \tag{20}$$

Thus, the effective potential well depth is proportional to the flux, $\Phi = 2\pi R^2 H$,

$$U_{\text{eff}}^0 = -|U(z)|\frac{\Phi}{\Phi_0}. \tag{21}$$

Since the precise form of the potential well is unknown, we will simulate it, as is generally accepted, with the δ-well:

$$U_{\text{eff}}^0 = -V\frac{\Phi}{\Phi_0}\delta(z), \tag{22}$$

where

$$V = \int_{-\infty}^{\infty} dz|U(z)|.$$

In the particular case of a layered superconductor such as $NbSe_2$ or the one from the family of high-T_c cuprates, the approximation given by Eq. (22) is quite acceptable because the inhomogeneity that belongs to a certain layer has a form of a ''pancake.'' Such ''pancakes'' may be due to the nonuniform distribution of intercalating molecules in dichalcogenides of transient metals or oxygen (in the case of cuprates) since local concentration of these elements determines the local value of the critical temperature T_c.

3. ANALYTIC CONSIDERATION OF THE POSITIVE CURVATURE AND CROSSOVER OF THE UPPER CRITICAL FIELD $H_{c2}^{\perp}(T)$

Consider a thin superconducting film of thickness d, which amounts to a few ξ or less and which contains an inhomogeneity with the effective potential (22) located at a distance a from the surface. The problem of calculation of the $H_{c2}^{\perp}(T)$ then reduces to finding the lowest eigenvalue of the Schrödinger equation (13) with

$$U_{\text{eff}}^0 = -V\frac{\Phi}{\Phi_0}\delta(z-a) \tag{23}$$

and appropriate boundary conditions. We first consider the case of NSN sandwich, for which the boundary conditions are $\Psi(0) = \Psi(d) = 0$. To satisfy these conditions, we write the solution in the form

$$\Psi_1(x) = A\sinh\kappa x, \quad \text{for } 0 \leqslant x \leqslant a,$$
$$\Psi_2(x) = B\sinh\kappa(x-d), \quad \text{for } a \leqslant x \leqslant d. \tag{24}$$

Here $\kappa^2 = 2m|\epsilon|/\hbar^2$. The constants A and B can be found from the corresponding boundary conditions at the δ-well

$$\Psi_2'(a) - \Psi_1'(a) = -\frac{2mV\Phi}{\hbar\Phi_0}\Psi_1(a),$$
$$\Psi_1(a) = \Psi_2(a). \tag{25}$$

It follows immediately from Eqs. (24) and (25) that the energy of the bound state ϵ_0 is determined by the only root of the equation

$$\frac{H}{H_m} = YF(Y), \tag{26}$$

where

$$F(Y) = \coth Y + \coth(Yb/a). \tag{27}$$

The energy of the bound state is then given by

$$\epsilon_0 = -\frac{\hbar^2 Y^2}{2ma^2}. \tag{28}$$

We have assumed here for certainty that $b = d - a > a$. In the opposite case a should be replaced by b. It is easy to see that the eigenvalue equation (26) has a solution only if $H > H^*$, where

$$H^* = H_m\left(1 + \frac{a}{b}\right), \tag{29}$$

and H_m is a threshold field given by

$$H_m = \frac{\Phi_0\hbar^2}{\pi R^2 maV}. \tag{30}$$

A sample which occupies a half-space corresponds to the limit $b \to \infty$ in Eqs. (27)–(29). We thus obtain the following picture. If $H \leqslant H_m$, the lowest eigenvalue of the problem under study is $E_{\min} = \hbar\Omega/2$. For fields $H > H_m$ the minimal energy is $E_{\min} = \hbar\Omega/2 - \epsilon_0(H)$. Equating then $E_{\min}$ to the Ginzburg–Landau coefficient α, we have

$$H_{c2}^{\perp} = H(0)\left(1 - \frac{T}{T_c}\right), \quad \text{if } H \leqslant H^*, \tag{31}$$

$$H_{c2}^{\perp} = H(0)\left(1 - \frac{T}{T_c}\right) + Y^2 H(0)\left(\frac{\xi}{a}\right)^2, \quad \text{if } H > H^*, \tag{32}$$

where $H(0) = \Phi_0/(2\pi a^2)$, and $Y(H/H_m)$ is determined by Eq. (26). We see that for $H \leqslant H_m$ the perpendicular critical field, given by Eq. (31), is a linear function of temperature T and at $H = H_m$ it crosses over to the nonlinear branch of Eq. (32), which goes higher than (31) and has an upturn or a so-called ''positive curvature.'' The dependence of the reduced critical field, $B_{c2} = H_{c2}^{\perp}/H_m$, on the reduced temperature T/T_c for different values of the parameters $G = H(0)/H_m$ and $W = (\xi/a)^2$ is shown in Fig. 1.

Since Eq. (13) is valid for

$$|\epsilon_0| \ll \frac{\hbar\Omega}{2}, \tag{33}$$

the second term on the right-hand side of Eq. (32) should be small compared to the first term. This condition determines the formal validity of Eq. (32). It follows then from Eq. (32) that the smallness of the parameter $W \propto a^{-2}$ is favorable for the applicability condition (33). On the other hand, $H_m \propto a^{-1}$, so values of W and H_m decrease with increasing of the separation between the surface and the inhomogeneity.

In the case of a film sandwiched between an insulating and a normal-metal (or ferromagnet) layer, i.e., in the ISN case, the boundary conditions are $d\Psi(0)/dx = 0$ and $\Psi(L) = 0$. The appropriate function $F(Y)$ in Eq. (26) is

$$F(Y) = \coth Y - \tanh\left(Y\frac{b}{a}\right). \tag{34}$$

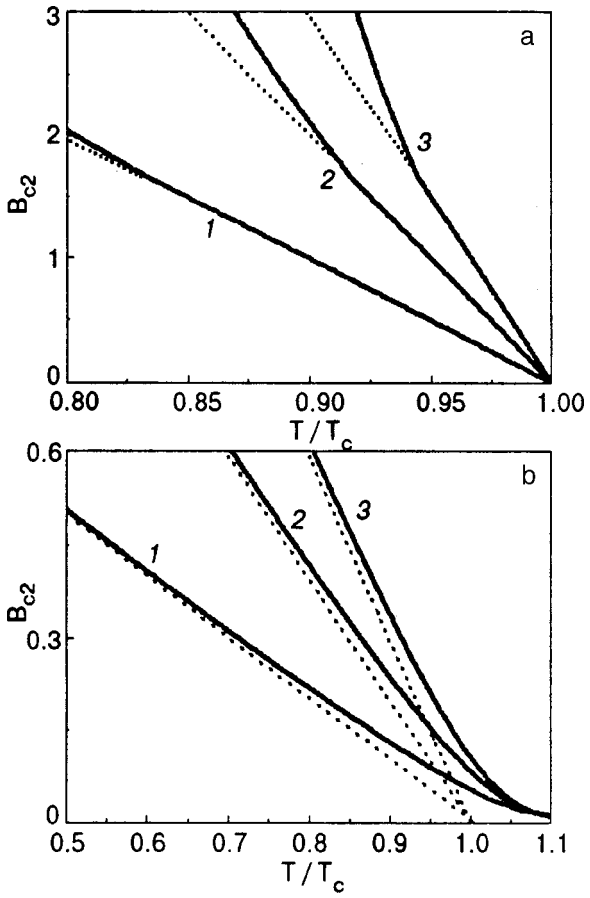

FIG. 1. The dependence of the reduced perpendicular critical magnetic field B_{c2} on the temperature T/T_c for the NSN (a) and ISN (b) cases calculated from Eq. (26) with: (a) $F(Y)$ given by Eq. (27), $W=(\xi/a)^2=0.1$ and $G=10;20;30$ (curves *1, 2, 3*); (b) $F(Y)$ given by Eq. (34), $W=0.1$ and $G=1;2;3$ (curves *1, 2, 3*). The parameter $G=H(0)/H_m$ and the ratio $b/a=1.5$ for both cases.

The solution of Eq. (26), with the $F(Y)$ given by Eq. (34), yields a nonzero root only for $H<H_m$. This means that a crossover in $H_{c2}^{\perp}(T)$ for the ISN case is somewhat different from that we have described above for the NSN sandwich: an upward-like branch (32) for $H<H^*$ crosses over to the linear branch (31) when the field exceeds the value H_*. The results of a numerical analysis for the $H_{c2}^{\perp}(T)$ in the ISN case are shown in Fig. 1(b).

In the ISI case the function $F(Y)$ is determined by the Schrödinger equation (13) and by the boundary conditions $d\Psi(0)/dx=d\Psi(L)/dx=0$, which yield

$$F(Y)=\tanh Y-\tanh\left(Y\frac{b}{a}\right). \tag{35}$$

Substitution of Eq. (35) into Eq. (26) gives an equation which has no solution for positive Y. This means that $\epsilon_0=0$ and $H_{c2}^{\perp}(T)$ for the ISI sandwich is given by the linear function (31) in accordance with the experiments.[4,17] In the next section we will discuss the physical meaning of the results obtained in the context of a current experimental situation in the field.

4. DISCUSSION AND CONCLUSIONS

Let us summarize the results obtained in the previous sections from the viewpoint of their relevance to experiments done so far. We see that at least two major preconditions are necessary for deviation of the $H_{c2}^{\perp}(T)$ from the linear behavior (31): a) structural inhomogeneities with local enhancement of the critical temperature and b) an appropriate boundary condition of the NSN or ISN type. Therefore, structurally perfect films and multilayers should not display nonlinearities of the $H_{c2}^{\perp}(T)$ near T_c. This assertion is in agreement with the fact that an upturn in $H_{c2}^{\perp}(T)$ has been observed only in a limited number of experiments on different superconducting SLs, whereas the rest of them show linear behavior of the perpendicular critical field.[5] But even the prerequisite a) is satisfied in a single film; it does not display a nonlinearity in $H_{c2}^{\perp}(T)$ when sandwiched between the insulators, i.e., in the ISI case. This conclusion of our theory is confirmed by experiments reported elsewhere.[4,17] Those experiments showed that the $H_{c2}^{\perp}(T)$ of a single Nb film deposited on a dielectric substrate in vacuum is a linear function of T near the phase transition, but it becomes upturned in triple layers and multilayers Nb/Gd (Ref. 17) and Nb/Cu (Ref. 4) fabricated from the Nb films. The latter, as was found in Nb/Gd and Nb/Cu superlattices, have a grained structure necessary for our approach. Thus, we can explain the above experimental observations as follows. A single layer deposited on an insulating sapphire substrate in vacuum belongs to the ISI case in our classification and, hence, has no nonlinearities in the $H_{c2}^{\perp}(T)$ behavior. The situation changes in the case of triple layers Nb/Cu/Nb and Nb/Gd/Nb, because they are of the ISN type (since each of the two Nb layers in the triple layer makes contact with one insulator and one normal metal layer) and should display a crossover of the kind shown in Fig. 1(b). The multilayers Nb/Cu and Nb/Gd are of the NSN type in the bulk of the sample and of the ISN type for the marginal layers at the top and the bottom of a SL (where the superconductor layer contacts either with the vacuum or with an insulating substrate). Therefore, the nonlinearity (see Fig. 1) which displays a specific SL depends on which of its layers (marginal or the one in the bulk of a SL) yields the largest $H_{c2}^{\perp}(T)$.

The intercalation of a layered crystal $NbSe_2$, as was shown in Refs. 18 and 19, also gives rise to the upturn in the $H_{c2}^{\perp}(T)$. Let us consider in more detail the case reported in Ref. 18, where the temperature behavior of the $H_{c2}^{\perp}(T)$ of layered single crystals $2H$-$NbSe_2$, intercalated by molecules of TCNQ, has been studied. Before the intercalation, the $H_{c2}^{\perp}(T)$ was found to be a linear function of the temperature. After the intercalation, the $H_{c2}^{\perp}(T)$ became a nonlinear function, whose shape near T_c reported in Ref. 18 is as follows: a linear branch up to $H_m\approx 0.8\,\mathrm{T}$ and then a smooth upturn with further decrease in temperature. The critical temperature of intercalated $2H$-$NbSe_2$, $T_c^*=6.5\,\mathrm{K}$, is lower than that of a nonintercalated crystal, where $T_c=7.2\,\mathrm{K}$. The physical reason behind the lowering of T_c after the intercalation is that molecules of the TCNQ, when placed between the superconducting sheets, diminish the concentration of electrons in them since the TCNQ is a very active acceptor. On the other

hand, the intercalation procedure cannot provide a perfectly uniform distribution of the TCNQ molecules across the sample. The latter means that after the intercalation some inhomogeneities must inevitably appear with the lower local concentrations of the TCNQ molecules. The corresponding local critical temperatures in them are higher than in the rest of the sample. The above data allow us to estimate the local enhancement as $\Delta T_c = T_c - T_c^* \approx 0.7\,\mathrm{K} \ll T_c$. Therefore, the value of V in Eq. (30) can be taken as $V = \Delta T_c\, d$, where d is of the order of the distance between the superconducting sheets in the intercalated $2H$-$NbSe_2$. Assuming $d \approx 10$ Å, $a \approx 10-100$ Å, and $H_m \approx 1$ T, we can estimate R from Eq. (28) as $R \approx 10^3 - 10^4$ Å, which seems plausible for the reported[18] concentrations of the TCNQ molecules in the intercalated $2H$-$NbSe_2$. One can check the above theoretical model by measurements of the $H_{c2}^{\perp}(T)$ and by concurrent control of the spatial distribution of the TCNQ molecules at different stages of the intercalation.

It is rather tempting to apply our model to another yet unresolved problem—nonlinearity of the $H_{c2}^{\perp}(T)$ near T_c in layered high-T_c cuprates. In these materials the oxygen is the agent which controls the local values of the critical temperature. Thus, spatial fluctuations of the oxygen in the plane would result in ''pancakes'' where the local T_c is higher than in the rest of a sample. According to the previous consideration, such a type of inhomogeneity is a prerequisite for the positive curvature of the $H_{c2}^{\perp}(T)$. Although an upturn in the $H_{c2}^{\perp}(T)$ near T_c in layered high-T_c cuprates has been reported in many publications, it is well known that to measure this quantity in detail is very difficult in these materials because of the resistive transition broadening in an external magnetic field.[20] In contrast, the melting line $B_m(t)$ is a much better measurable quantity in high-T_c cuprates. Its shape via the elastic moduli, $c_{i,j} = c_{i,j}(b)$, depends on the $H_{c2}(T)$, where $b = H/H_{c2}(T)$. Therefore, a crossover in the line $H_{c2}(T)$ inevitably should manifest itself in the form of the function $B_m(T)$. This rather evident fact, as was shown in Ref. 24, must be taken into account in calculating the shape of the melting line $B_m(T)$.

Consider now briefly a defect which extends through the bulk of a layered crystal. In this case the potential $U_{\mathrm{eff}}^0(z)$ in the eigenvalue problem of Eq. (13) is given by the infinite set of periodic potential wells of the form

$$U_{\mathrm{eff}}^0(z) = -\frac{\Phi}{\Phi_0} V \sum_n \delta(z - an), \tag{36}$$

where a is the interlayer spacing. The eigenvalue problem of Eq. (13) is now exactly the well-known Kronig–Penny model, whose lowest energy level $E_{\min} = -(\hbar^2 Y^2)/(2ma^2)$ is given by the solution of the equation

$$\cosh Y - \frac{H}{H_m Y} \sinh Y = 1. \tag{37}$$

The critical field is determined by Eq. (32) which describes the curve that gradually upturns with a decrease in temperature from the point of T_c. The analytic solutions can be easily found for two cases. Near the critical temperature, i.e., for $H \ll H_m$ the $H_{c2}^{\perp}(T)$ is a linear function of the temperature:

$$H_{c2}^{\perp}(T) \approx H(0)\left[1 + 2\frac{H(0)}{H_m}\left(\frac{\xi}{a}\right)^2\right]\left(1 - \frac{T}{T_c}\right).$$

When $H \gg H_m$, which corresponds to lower temperatures, and if the additional condition $\xi \ll a$ is satisfied, which implies that $[H\xi/(H_m a)]^2 \ll 1$ (the latter is the case, for example, in some highly anisotropic high-T_c cuprates), the upper critical field is given by

$$H_{c2}^{\perp}(T) \approx \left(\frac{H(T)\xi}{H_m a}\right)^2 H(0)(1 - 2\mathrm{e}^{-H(T)/H_m}) + H(T).$$

Here $H(T)$ equals the right-hand side of Eq. (31), which is a linear function of the temperature and, hence, the $H_{c2}^{\perp}(T)$ experiences an upturn known also in the literature as the positive curvature.

In summary, we conclude that the presence of a particular type of inhomogeneity in thin films and layered superconductors, which enhances the local value of the critical temperature, is one of the physical reasons beyond the positive curvature in the temperature behavior of the $H_{c2}^{\perp}(T)$ observed in some multilayers near T_c.

The discussions with M. A. Obolenskii, H. B. Chashka, A. I. Sidorenko, N. Ya. Fogel, L. I. Glazman, and O. Fisher are gratefully acknowledged. This work was supported in part by International Soros Education Program through Grant No. APU 072017.

[1] L. N. Bulaevskii, Usp. Fiz. Nauk **116**, 449 (1975) [Sov. Phys. Usp. **18**, 514 (1975)].
[2] M. G. Karkut, J. M. Triscone, D. Ariosa, and O. Fisher, Phys. Rev. B **34**, 4390 (1986).
[3] V. Matijasevic and M. R. Beasley, Phys. Rev. B **35**, 3175 (1987).
[4] A. Sidorenko, C. Surgers, T. Trappmann, and H. V. Lohneysen, Phys. Rev. B **53**, 11751 (1996).
[5] B. Y. Jin and J. B. Ketterson, Adv. Phys. **38**, 189 (1989).
[6] E. Fullerton, J. Guimpel, O. Nakamura, and I. Schuller, Phys. Rev. Lett. **69**, 2859 (1992).
[7] S. Takahashi and M. Tachiki, Phys. Rev. B **33**, 4620 (1986); **34**, 3162 (1987).
[8] L. I. Glazman, I. M. Dmitrenko, V. L. Tovazhnyanskii, V. G. Cherkasova, and N. Ya. Fogel, Zh. Éksp. Teor. Fiz. **93**, 1384 (1987) [Sov. Phys. JETP **66**, 787 (1967)].
[9] V. M. Gvozdikov, Fiz. Nizk. Temp. **16**, 5 (1990) [Sov. J. Low Temp. Phys. **16**, 1 (1990)].
[10] V. M. Gvozdikov and M. Teisheira, Fiz. Nizk. Temp. **19**, 1302 (1993) [Low Temp. Phys. **19**, 922 (1993)].
[11] A. Yu. Kitaev and L. S. Levitov, Zh. Éksp. Teor. Fiz. **95**, 311 (1989) [Sov. Phys. JETP **68**, 176 (1989)].
[12] O. A. Mironov, B. A. Savitskii, A. Yu. Sipatov, A. I. Fedorenko, A. N. Chirkin, S. V. Chistyakov, and L. P. Shpakovskaya, Pis'ma Zh. Éksp. Teor. Fiz. **48**, 100 (1988) [JETP Lett. **48**, 106 (1988)].
[13] T. W. Haywood and D. G. Ast, Phys. Rev. B **18**, 225 (1978).
[14] C. S. Chun, G. Zheng, J. L. Vincent, and I. K. Schuller, Phys. Rev. B **29**, 4915 (1984).
[15] K. Kanoda, H. Mazaki, T. Yamada, N. Hosito, and T. Hinjo, Phys. Rev. B **33**, 2052 (1987).
[16] P. R. Broussard and T. Geballe, Phys. Rev. B **35**, 1664 (1987).
[17] C. Strunk, C. Surgers, U. Pashen, and H. V. Lohneysen, Phys. Rev. B **49**, 4053 (1994).
[18] M. A. Obolenskii, H. B. Chashka, and V. I. Beletskii, Fiz. Nizk. Temp. **8**, 174 (1982) [Sov. J. Low Temp. Phys. **8**, N2 (1982)].

[19] H. B. Chashka, V. I. Beletskii, M. A. Obolenskii, and Yu. B. Poltoratskii, Fiz. Nizk. Temp. **17**, 833 (1991) [Sov. J. Low Temp. Phys. **17**, 435 (1991)].
[20] *Physical Properties of High-temperature Superconductors*, D. M. Ginsberg (Ed.) (World Scientific, 1989).
[21] K. Moloni, M. Friessen, S. Li, V. Souw, P. Metcalf, L. How, and M. Mc. Elfresh, Phys. Rev. Lett. **78**, 3173 (1997).
[22] V. M. Galitskii, B. M. Karnakov, and V. I. Kogan, *Problems in Quantum Mechanics*, Nauka, Moscow (1992) [in Russian].
[23] A. A. Abrikosov, *Fundamentals of the Theory of Metals*, North-Holland, Amsterdam (1988).
[24] V. M. Gvozdikov and L. Z. Kaganovsky, Czech. J. Phys. **46**, 1811 (1996).

This article was published in English in the original journal. It was edited by S. J. Amoretty.

Relaxation of the electric resistance of YBaCuO single crystals due to hydrostatic pressure and jumpwise temperature variation

M. A. Obolenskiĭ, D. D. Balla, A. V. Bondarenko, R. V. Vovk, A. A. Prodan, and T. F. Ivanova

*Kharkov State University, 310077 Kharkov, Ukraine**

(Submitted July 9, 1999)
Fiz. Nizk. Temp. **25**, 1259–1264 (December 1999)

The effect of hydrostatic pressure on pressure, temperature, and time dependences of the conductivity in the *ab-plane* of $YBa_2Cu_3O_{7-x}$ single crystals with different oxygen concentrations ($0.1<x<0.5$) is studied. It is shown that in oxygen-deficient samples with $x>0.2$, temperature and pressure variations may induce a nonequilibrium state in which effects associated with the variation of unit cell volume and redistribution of oxygen in Cu–O planes must be distinguished. Characteristic conductivity relaxation times under the effect of pressure and during annealing at room temperature are determined. It is concluded that these processes have the same origin. © *1999 American Institute of Physics.* [S1063-777X(99)00312-6]

High-temperature superconductors (HTSC) are characterized by the presence of a labile element, viz., oxygen. Under the effect of external agencies like temperature and pressure, the lattice parameters may change and the labile component may be redistributed. In turn, these changes affect the critical parameters of the superconductor. In order to determine the origin of superconductivity in HTSC compounds, it is important to separate processes associated with the variation of lattice parameters and redistribution of labile oxygen. However, very few authors[1–4] have studied the effect of pressure on T_c in nonequilibrium state, and only ceramic samples were investigated. In the present work, we consider the results of investigations of pressure, temperature and time dependences of the resistivity of $YBa_2Cu_3O_{7-x}$ single crystals with different levels of oxygen deficiency ($0.1<x<0.5$) in a wide range of temperatures (30–350 K) and pressures (0–11 kbar).

The hydrostatic pressure was created in an independent piston–cylinder type chamber by using the technique described in Ref. 4. The pressure was determined by a manganine pressure gauge, and the temperature by a copper–constantan thermocouple mounted on the outer surface of the chamber. The resistance in the ab-plane was measured by the standard four-probe technique in a constant current 1–10 mA.

Single crystals were grown by the solution–melting technique in a gold crucible by the method described in detail in Ref. 5. The single crystals had a characteristic size $3\times4\times0.03$ mm. Oxygen-deficient samples were obtained by annealing in air at 600–650° for a period ranging from ten hours to two days. Table I shows the parameters of seven single crystals with different superconducting transition temperatures.

According to the data available in the literature, three types of processes (depending on oxygen concentration) may lead to the superconducting transition in the YBaCuO compounds: (1) a narrow transition occurring at $T_c=90$ K for $x<0.1$ expands in the interval from 90 to 60 K upon an increase in x, and then narrows down at $T=60$ K; (Refs. 6 and 7) (2) for $x>0$, the transition is of two-step type with $T_{c1}=90$ K and $T_{c2}=60$ K (Ref. 8) and (3) a transition can occur for any $T_c<90$ K, the transition width depending insignificantly on the value of T_c (Refs. 9 and 10). The experimental results presented in Table I speak rather in favor of the first two versions, which is also confirmed indirectly by the step form of the resistive transitions to the superconducting state observed in a majority of the investigated objects. The absence of steps on the resistive transitions of the crystals K4 and K7 does not rule out the possibility of coexistence of two or more phases with difference values of T_c since the presence of percolation paths of current flow in a phase with high T_c means that a transition to the superconducting state of this very phase will be observed at the resistive transition.

The conductivity increases with pressure, and the pressure derivatives of samples with different oxygen concentrations may differ by a factor of several units. By way of an example, Fig. 1 shows the $R(T)$ dependences for different values of P in the K4 single crystal. The insets *a* and *b* show the dependences $R_{300}(P)$ and $[dT_c/dP](x)$ for samples K2, K4 and K7. It can be seen that an increase in the oxygen deficiency leads to an increase in dT_c/dP and dR/dP, which is in accord with the available data (see, for example, Ref. 11). The figure also shows that nonstoichiometric samples ($x\sim0.5$) show a considerable increase in the baric derivatives dT_c/dP and dR/dP, the quantity dT_c/dP attaining values (0.63–0.85) $\mathrm{K\cdot kbar^{-1}}$, which are much higher than the values for perfect samples. The nonmonotonic nature of the dependence $T_c(x)$ creates additional difficulties in the interpretation of the obtained results. One possible explanation for the singularities observed in the $T_c(P)$ dependence for the system 123 was proposed by Saiko and Gusakov[12] in their theoretical model which connects the variation of the superconducting transition temperature with the peculiarities of the dynamics of apical O(4) atoms forming a bistable sublattice which can be controlled by applying

TABLE I. Parameters of single crystals with different superconducting transition temperature.

Single crystal	T_c, K	ΔT_c, K	ρ_{300}, $\mu\Omega\cdot$cm	x
K1	42	14	8200	0.52
K2	45	10	7500	0.50
K3	48	8	5200	0.48
K4	50	2.4	750	0.46
K5	68	10	620	0.15
K6	82	5	450	0.10
K7	90	0.3	200	<0.1

an external pressure and by varying the oxygen nonstoichiometry. Indeed, it can be seen from Fig. 2 that an explicit correlation exists between the T_c variation and the separation $d_{\mathrm{Cu(2)\text{-}O(4)}}$ (Ref 13). According to Saiko and Gusakov,[12] the formation of the 90°-phase under the action of a pressure applied on a 60°-phase sample, or an alternation of these phases upon a variation of oxygen nonstoichiometry is associated with the ''switching'' of the mode frequency Ω which dominates in BCS pairing due to a transformation of the bistable potential of apical oxygen atoms. The value of the pressure required for transforming the system into the 90°-phase also decreases with x. Thus, a considerable increase in T_c under pressure is interpreted as an extension of the transition from the 60°-phase to the 90°-phase. Indeed, it can be seen from Fig. 3 showing the $T_c - d\ln T_c/d\ln V$ diagram for K2, K4, and K7 crystals calculated taking into account bulk moduli (100 GPa for $x<0.1$ and 115 GPa for $x>0.1$)[14] that $[d\ln T_c/d\ln V](T_c)$ curves have a kink that might be an indication of a transition from the 60°-phase to the 90°-phase which is characterized by a different value of dT_c/dP. However, the anomalous increase in dT_c/dP from 1.5 to 2.5 K·kbar^{-1} observed by us for low pressures up to 1.2 kbar for an insignificant difference in oxygen concentration in the samples with $T_c=45$ and 50 K as well as the sign reversal of dT_c/dP under an axial pressure applied along different crystallographic directions[15] apparently do not allow us to explain unambiguously the peculiarities in the behavior of $T_c(P,x)$ dependences on the basis of the above theoretical model only.

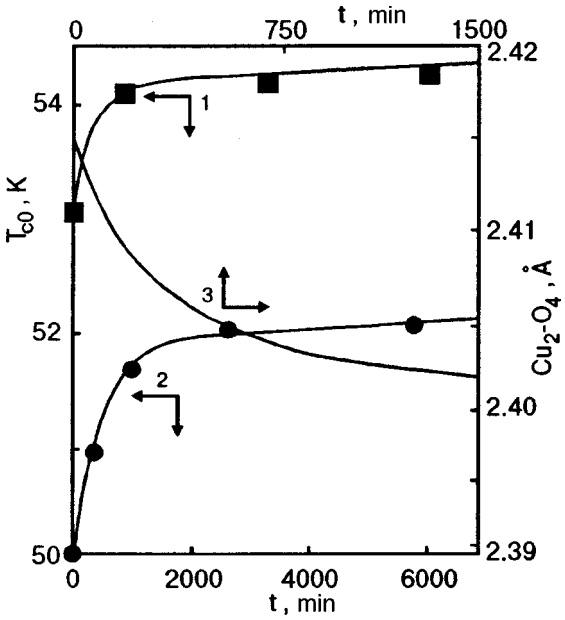

FIG. 2. Dependence $T_{co}(t)$ (of the temperature corresponding to the onset of the superconducting transition) for sample K2 (curve *1*) at $P=6.3$ kbar, for sample K3 (curve *2*) during annealing at room temperature, and time dependence of the separation $d_{\mathrm{Cu_2-O_4}}$ obtained in Ref. 13 (curve *3*). Solid curves are calculated by formula (3).

In all probability, peculiarities in the behavior of $T_c(P,x)$ dependences are due to several mechanisms one of which is associated with a change of the band structure under bulk compression. The observed linear relation between of $d\ln T_c/d\ln V$ and $d\ln T_c$ can be obtained using the Labbe–Bok theoretical model[16] taking into account the contribution of logarithmic singularity to the density of states of the half-filled band. In this model, T_c is defined as

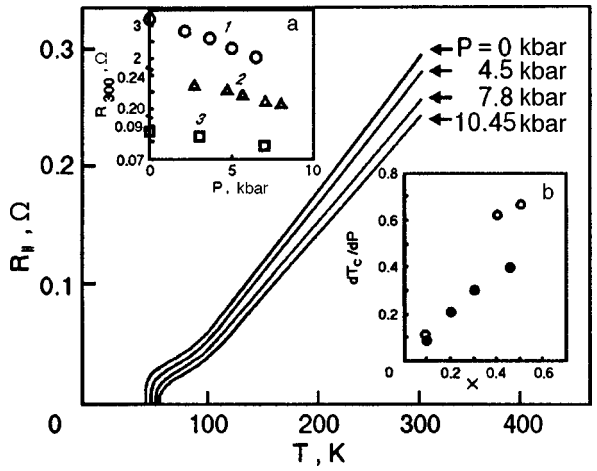

FIG. 1. Dependence $R(T)$ for sample K4 under pressures 0, 4.5, 7.8, and 10.45 kbar. The inset (a) shows the $R_{300}(T)$ dependence under different pressures for samples K2, K4, and K7 (curves *1*, *2* and *3*, respectively). The inset (b) shows the dependence $[dT_c/dP](x)$; dark circles correspond to the results obtained in Ref. 11 for ceramic samples.

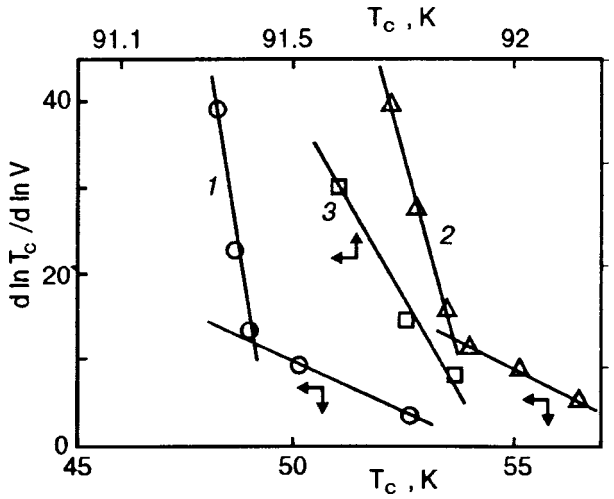

FIG. 3. Diagram $T_c - d\ln T_c/d\ln V$ for crystals K2, K4, and K7 (curves *1*, *2*, and *3*, respectively) calculated taking into account bulk moduli (100 GPa for $x<0.1$ and 115 GPa for $x>0.1$).[14]

$$T_c = D \exp(-1/\lambda^{0.5}), \tag{1}$$

where D is the singularity ''width.'' In this case, for the volume dependence of T_c we have

$$\frac{d \ln T_c}{d \ln V} = \frac{d \ln D}{d \ln V} + \frac{1}{2\lambda^{0.5}} \frac{d \ln \lambda}{d \ln V}.$$

This gives

$$d \ln T_c / d \ln V = a_1 \ln T_c + a_2,$$
$$a_1 = -\frac{1}{2} \frac{d \ln \lambda}{d \ln V}; \quad a_2 = \frac{d \ln D}{d \ln V} - a_2 \ln D. \tag{2}$$

The kinks on the $(d \ln T_c/d \ln V)(T_c)$ curves can be due to the cluster structure of the sample, which is confirmed by the presence of steps on resistive transitions to the superconducting state. It was proved by us earlier[17] hat the observed step form of resistive transitions indicates the nonstoichiometric ratio of oxygen and vacancies concentrations leading to the formation of a mixture of phases, viz., clusters characterized by different concentrations of oxygen and its ordering and naturally have different critical temperatures and the values of dT_c/dP. It is interesting to note that similar peculiarities in the behavior of pressure derivatives dT_c/dP as functions of composition were observed by us for $NbSe_2$ single crystals that also belong to systems of two-dimensional lattices and are characterized by close values of anisotropy parameter.[18,19] For example, intercalation with deuterium up to 2 at.% and the introduction of tin impurities into $NbSe_2$ lead to an increase in the value of dT_c/dP by a factor of 2–3 as compared to a pure sample. In this case, the value of dT_c/dP increases with the tin impurity concentration. It should also be noted that the pressure dependences $T_c(P)$ for $NbSe_2$ and YBaCuO single crystals display a qualitatively similar behavior. The above peculiarities of $T_c(P)$ dependences were interpreted as a consequence of a displacement of the Fermi level relative to the root singularities of the density of states.

Taking into account the above analogies as well as the results obtained in Refs. 16 and 20 where the model presuming the presence of a singularity in the electron spectrum of $2D$ lattices with a strong coupling was considered, we can suggest that a change in the composition of such compounds may lead to a displacement of the Fermi level relative to singularities of the density of states. Indeed, according to the results of x-ray diffraction studies,[21] the saturation with oxygen changes the crystal lattice parameters from $a = 3.872$ Å, $b = 3.879$ Å, $c = 11.809$ Å to $a = 3.833$ Å, $b = 3.898$ Å, $c = 11.700$ Å i.e., increases the orthorhombic distortion. This in turn leads to splitting of the Van Hove critical point. It is well known that the Fermi level for crystals with $T_c \approx 90$ K lies in the valley between two peaks of the density of states, and the density of states $N(E_F)$ at the Fermi level depends considerably on the ratio $(a-b)/a$.[20] An increase in this ratio leads to an increase in the separation between the peaks of the density of states and accordingly to a decrease in $N(E_F)$ and T_c. On the contrary, a decrease in the ratio $(a-b)/a$ reduces the separation between the peaks of the density of states, which leads to an increase in $N(E_F)$ and T_c. A similar regularity in the variation of T_c was observed during an analysis of the effect of axial compression along the axes **a** and **b** on the superconducting transition temperature of single crystals with $T_c \approx 90$ K.[15] The superconducting transition temperature increased when the pressure was applied along the axis **a** and decreased when the load was applied along the axis **b**. The application of hydrostatic pressure affects the ratio $(a-b)/a$ insignificantly since the value of the ratio is determined only by the difference in compression moduli along the axes **a** and **b**. For this reason, the change in critical temperature under hydrostatic pressure is relatively small.

TABLE II. Results of measurements of $T_c(P)$ and $\Delta T_c(P)$.

	T_c, K	ΔT_c, K	T_c, K	ΔT_c, K
P, kbar	before holding at 300 K		after holding at 300 K	
0	50.6	2.4	50.6	2.4
1.26	52.4	2.4	52.5	2.7
2.53	53.0	2.8	53.0	2.9
3.90	54.0	2.9	54.1	3.2
5.00	54.8	3.2	54.8	3.4
8.00	56.6	3.5	56.7	4.1
After pressure removal	50.6	3.5	50.6	2.8
Three days after pressure removal	50.6	3.5	50.5	2.4

For crystals with $T_c \approx 60$ K, the Fermi level is shifted from the middle of the band and lies at a distance form the Van Hove singularity. Consequently, if the superconducting transition temperature is determined primarily by the density of electron states, the Fermi level must be displaced under a hydrostatic pressure towards the peak of the density of states.

It should be noted in this connection that Fig. 1 shows the dependences associated with the ''true'' effect of pressure caused by a direct compression of the sample. Since it was proved in Refs. 2 and 3 that two effects connected with a decrease in the unit cell volume and with a redistribution of oxygen must be taken into consideration while determining dT_c/dP, we used an approach permitting the separation of these effects. In order to reduce the effect of redistribution of oxygen to the maximum possible extent, we rapidly (during 15–20 min) cooled the bomb with the sample immediately after the application of pressure to temperatures at which relaxation effects are absent. Then the values of $R(T)$ were measured during heating to room temperature. This was followed by the measurement of time dependences $R(t)$, which are described in detail in Ref. 4.

After this, the $R(T)$ dependence was measured repeatedly during a cooling–heating cycle. The results of measurements of $T_c(P)$ and $\Delta T_c(P)$ are presented in Table II. The value of T_c was determined from the middle of the resistive transition to the superconducting state at the level $R = R_N/2$, where R_N is the residual electrical resistance in the normal state. The superconducting transition width ΔT_c was determined as the difference between the temperatures T_{co} and T_{cf} (the onset and end of the superconducting transition), corresponding to the resistance $0.95R_N$ and $0.05R_N$.

The results described above show that the critical temperature determined from the middle of the superconducting transition is practically independent of the time of holding the sample at room temperature and is determined only by the applied pressure. On the contrary, the superconducting transition width increases under similar conditions and practically does not change during measurements made immediately after the application–removal of pressure, which is apparently due to the effect of oxygen redistribution. This assumption is also confirmed by the results of measurements (see Fig. 2) of time dependences $T_{co}(t)$ (the temperature of the onset of superconducting transition) for sample K2 (curve *1*) obtained for $P=6.3$ kbar as well as the dependences $T_{co}(t)$ for K3 crystal (curve *2*) obtained during annealing at room temperature following rapid cooling from temperatures $\sim 650\,^{\circ}$C.

Solid curves *1* and *2* show the results of calculations based on the method proposed by Jorgensen *et al.*[13] We assume that the process of oxygen redistribution can be divided conditionally into the main rapid process with the time constant τ_1, which is responsible for oxygen ordering within fragments of Cu–O chains, and a slower process with the characteristic time τ_2 determining the formation of a $2D$ ordered structure. In this case, the dependence $T_c(t)$ for $P=\text{const}$ can be described by a two-exponential law of the form

$$T_c(t,a,\tau_1,\tau_2)=T_c(\infty)-[T_c(\infty)-T_c(0)]\times[a\exp(-t/\tau_1)^{0.5}+(1-a)\times\exp(-t/\tau_2)^{0.5}], \quad (3)$$

where a is the weight factor for two relaxation processes and $T_c(0)$ and $T_c(\infty)$ are the temperatures of superconducting transitions before and after relaxation respectively.

The values $\tau_1\approx 50-90$ min and $\tau_2\approx(2-4)\cdot 10^3$ min obtained from calculations based on this formula are in satisfactory agreement with the dependences *1* and *2* as well as with the results obtained in Refs. 3 and 13. This is an indication of the fact that the evolution of superconducting transitions under pressure as well as during annealing at room temperature is determined by the redistribution of labile oxygen within Cu–O planes.

Let us consider briefly the difference in the results obtained by us here and by Baran and Gladchuk.[3] In Ref. 3, the superconducting transition temperature relaxes under pressure during holding at room temperature. In our experiments, the critical temperature determined from the middle of the superconducting transition depends only on the applied pressure and does not depend on the time of holding the sample at room temperature. It can be seen from Fig. 4, however, that hysteresis phenomena are observed on the pressure dependences $T_c(P)$ for crystals K2 and K4 at T_{co} and T_{cf}. The temperature T_{co} corresponding to the onset of the superconducting transition is shifted to higher temperatures in the case of holding at T_{300}, while the end of the superconducting transition is displaced towards lower temperatures, the middle of the transition remaining unchanged. On the other hand, such a variation can be due to the fact that Baran and Gladchuk[3] studied ceramic samples in which hydrostatic nature of pressure can be disturbed due to possible porosity and disorientation of crystallites. On the other hand, the compounds with admixtures of Sr and Gd used in Ref. 3 have a qualitatively different $T_c(x)$ dependence, although they belong to the 123 system. In contrast to the $T_c(x)$ dependence for YBaCuO with two plateaus at 60 and 90 K, partial substitution Sr for Ba leads to a nonmonotonic dependence $T_c(x)$, while the plateau at 90 K disappears and a new plateau is formed at 40 K for a system with Sr and Gd. The third important difference lies in the method of determining T_c by a linear extrapolation of magnetization to its zero value. It remains unclear whether T_c corresponds to the onset or end of the transition.

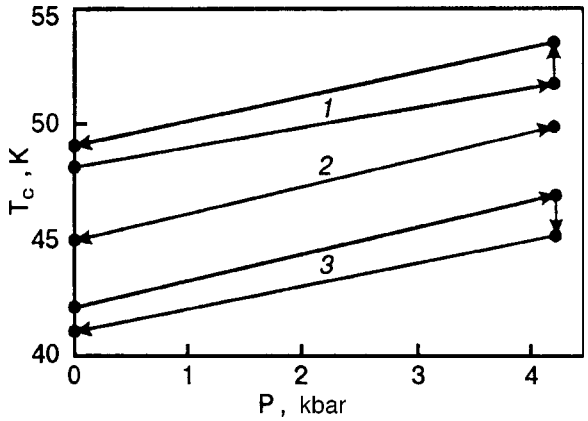

FIG. 4. Evolution of temperatures corresponding to the onset (T_{co}), middle (T_c), and end (T_{cf}) of the superconducting transition (curves *1*, *2*, and *3*, respectively) for sample K2 during the application–removal of pressure of 4.2 kbar.

*)E-mail: mikhail.a.obolenskii@univer.kharkov.ua

[1] J. S. Shilling and S. Klotz, in *Physical Properties of High Temperature Superconductors* (ed. by D. M. Ginzberg), World Scientific, Singapore (1992).
[2] J. Meltzler, T. Weber, and W. H. Fietz *et al.*, Physica C **C214**, 371 (1993).
[3] M. Baran, L. Gladchuk, and V. P. D'yakonov *et al.*, Fiz. Nizk. Temp. **22** 1360 (1996) [Low Temp. Phys. **22**, 1034 (1996)].
[4] D. D. Bala, A. V. Bondarenko, and R. V. Vovk *et al.*, Fiz. Nizk. Temp. **23**, 1035 (1997) [Low Temp. Phys. **23**, 777 (1997)].
[5] M. A. Obolenskii, A. V. Bondarenko, and M. O. Zubarev, Fiz. Nizk. Temp. **15**, 1152 (1989) [Sov. J. Low Temp. Phys. **15**, 635 (1989)].
[6] J. M. Tarascon, E. Wang, S. Kivelson *et al.*, in *Novel Superconductivity* (ed. by S. A. Wolf and V. Z. Kresin), Plenum Press, New York (1989).
[7] A. Mazaki, K. Hirata, and K. Yamamoto *et al.*, Jpn. J. Appl. Phys., Part 1 **28**, 368 (1989).
[8] L. H. Creene and B. G. Bangley, in *Physical Properties of High Temperature Superconductors II* (ed. by D. M. Ginzberg), World Scientific, Singapore (1990).
[9] Y. Kubo, I. Ichihashi, and T. Monako *et al.*, Phys. Rev. B **B37**, 7858 (1988).
[10] Y. Narazava and M. Ishikava, Physica C **C158**, 381 (1989).
[11] M. A. Il'ina, Sverkhprovodimost: Fiz., Khim., Tekh. **4**, 726 (1991).
[12] A. P. Saiko and V. E. Gusakov, Fiz. Nizk. Temp. **22**, 748 (1996) [Low Temp. Phys. **22**, 575 (1996)].
[13] D. Jorgensen, S. Pei, and P. Lightfoot *et al.*, Physica C **C167**, 571 (1990).
[14] I. V. Aleksandrov, A. F. Goncharov, and S. M. Stishov, Pis'ma Zh. Éksp. Teor. Fiz. **47**, 357 (1988) [JETP Lett. **47**, 428 (1988)].

[15] U. Welp, M. Grimsditch, and S. Flesher *et al.*, Phys. Rev. Lett. **69**, 2130 (1992).
[16] J. Labbe and J. Bok, Europhys. Lett. **3**, 1225 (1987).
[17] M. A. Obolenskii, A. V. Bondarenko, P. V. Vovk, and A. A. Prodan, Fiz. Nizk. Temp. **23**, 1178 (1997) [Low Temp. Phys. **23**, 882 (1997)]
[18] Kh. B. Chashka, M. A. Obolenskii, and D. D. Bala *et al.*, Fiz. Nizk. Temp. **19**, 450 (1993) [Low Temp. Phys. **19**, 317 (1993)].
[19] M. A. Obolenskii, Kh. B. Chashka, V. I. Beletskii, and V. M. Gvozdikov, Fiz. Nizk. Temp. **15**, 484(5?) (1989) [Sov. J. Low Temp. Phys. **15**, 272 (1989)].
[20] V. M. Gvozdikov, Fiz. Nizk. Temp. **19**, 1285 (1993) [Low Temp. Phys. **19**, 914 (1993)].
[21] A. V. Bondarenko, B. I. Verkin, M. O. Zubareva, and M. A. Obolenskii, Preprint PTILTE, Kharkov (1998).

Translated by R. S. Wadhwa

Upper critical fields in superconductor–normal metal type superlattices in the Ginzburg–Landau approximation

V. N. Kushnir, A. Yu. Petrov, and S. L. Prishchepa

*Byelorussian State University of Informatics and Radioelectronics, 220027 Minsk, Byelorussia**)
(Submitted June 15, 1999)
Fiz. Nizk. Temp. **25**, 1265–1270 (December 1999)

The application of the Ginzburg–Landau theory to the superconductor–normal metal–superconductor (SNS) superlattices is considered in the case when normal and superconducting layers have the same thickness. The temperature dependences of the transverse and longitudinal upper critical fields are considered. The theoretical curves are compared with the available experimental results on SNS superlattices [C. Coccorese *et al.*, Phys. Rev. **B57**, 7922 (1998)]. It is shown that the theoretical model can provide a correct interpretation of the experimental results with the minimum number of fitting parameters. The peculiarities of the order parameter behavior at the dimensional crossover in a parallel magnetic field as a function of the sample symmetry axis are discussed, and practical recommendations are given for an experimental verification of the role of symmetry of SNS-type structures. © *1999 American Institute of Physics.* [S1063-777X(99)00412-0]

INTRODUCTION

The properties of multilayer structures of the type superconductor–normal metal–superconductor (SNS) in the vicinity of the superconducting transition temperature T_c were described in the framework of the microscopic theory at the beginning of the seventies.[1,2] An exhaustive interpretation of the temperature dependence of the upper critical fields was also given by Takahashi and Tachiki[3] using the microscopic theory. However, it is technically quite difficult to use this theory for describing the properties of SNS away from the critical temperature region. Hence it seems quite natural to use the Ginzburg–Landau (GL) theory for studying the transport properties, vortex lattice dynamics, pinning forces, etc.. The conditions of applicability of the GL theory (see, for example, Ref. 4) make it possible to use it for studying SNS in which action of normal layer serves as a perturbation of the superconducting state. This requirement was taken into consideration for studying the properties of superconducting superlattices by various researchers.[5–8] But the most interesting effects (like the peak effect[9,10]) are observed in SNS in which the effect of normal layers cannot be treated as a perturbation (the normal layer thickness is of the order of the superconducting layer thickness and is of the order of the correlation length $\xi_\perp(0)$ in a direction normal to the surface of the layers). In this case, the inadequacy of the GL theory becomes obvious. It can be asked whether the GL theory can describe such phenomena qualitatively. This question was answered partially by using the GL theory to determine the temperature dependence of the peak-effect field in an SNS, which coincide with the experimental dependence for reasonable values of fitting parameters.[11] Hence it is expedient to construct a GL model which can be used not only in the vicinity of T_c. Dediu *et al.*[12] proposed a version of such amodel restoring the temperature dependences of the upper critical fields, which were obtained in the microscopic theory and are in accord with the experimental curves. In the present work, we present another version of the GL model and compare th results with the experimental temperature dependences of the upper critical fields obtained for Nb/Pd superlattices.[13]

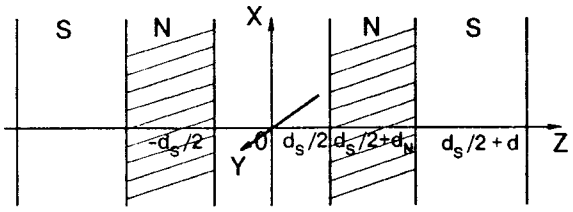

FIG. 1. Geometry of an infinite multilayer SNS structure with the center of symmetry in the *S*-layer

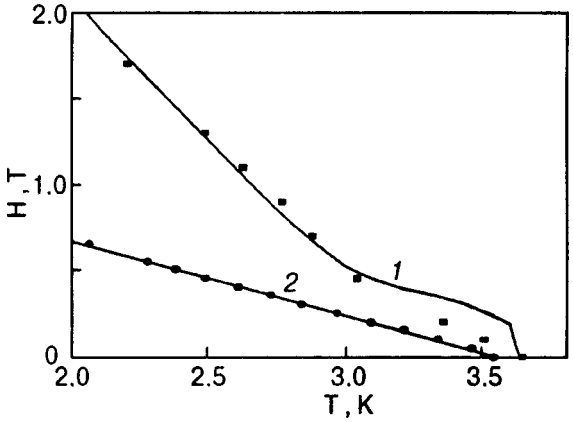

FIG. 2. Experimental temperature dependences of the upper critical field in a multilayer Nb/Pd structure ($d_{Nb}=170$ Å, $d_{Pd}=187$ Å) for parallel (curve *1*) and perpendicular (curve *2*) orientation of the the external magnetic field relative to the surface layers,[13] and the theoretical dependences $H_{c2\parallel}(T)$ and $H_{c2\perp}(T)$ (solid curves).

MODEL

We define the coordinate system as follows: the z-axis is directed at right angles to the surface of the layers, the xy plane coincides with the middle of the superconducting layer and is one of the symmetry planes of the infinite superlattice (see Fig. 1). According to Jin and Ketterson,[2] the GL equations for the wave function in the vicinity of critical fields can be written in the form

$$\left(\nabla - i\frac{2\pi}{\Phi_0}A(r)\right)^2 \Psi(r) + \eta(z)\Psi(z) = 0. \tag{1}$$

Here, the step function has the form

$$\eta(z) = \begin{cases} \dfrac{1}{\xi_S^2(T)}, -\dfrac{d_S}{2} + md < z \leqslant \dfrac{d_S}{2} + md, & m = 0, \pm 1 \pm 2, \ldots \\ -\dfrac{1}{\xi_N^2(T)}, \dfrac{d_S}{2} + md < z \leqslant \dfrac{d_S}{2} + d_N + md, & m = 0, \pm 1, \pm 2, \ldots, \end{cases} \tag{2}$$

where d_S and d_N are the thicknesses of the superconducting and normal layers, $d = d_S + d_N$ is the superlattice period,

$$\xi_S(T) = \xi_{S0}\left(1 - \frac{T}{T_{cS}}\right)^{-1/2}, \quad \xi_N(T) = \xi_{Nc}\left(\frac{T}{T_c}\right)^{-1/2} \tag{3}$$

are the correlation lengths in the superconducting and normal layers, ξ_{S0} is the coherence length in the superconducting layer at zero temperature, ξ_{Nc} the coherence length in the normal layer at the critical temperature T_c of the multilayer structure, T_{cS} the transition temperature for the superconducting material, and $\Phi_0 = 2.07 \times 10^{-15}$ Wb the magnetic flux quantum. The function $\eta(z)$ in the normal layers (second row in formula (2)) was defined on the basis of the simple consideration that the normal layer in conventional experiments is chosen from metals with $T_{cN} \to 0$. It should be noted, however, that the GL model used for describing superlattices uses ''renormalized'' correlation lengths $\xi_S(T)$ and $\xi_N(T)$ as well as the parameter function $\eta(z)$. Hence the sign of the function $\eta(z)$ in the normal layer is determined from the experiment. For example, the temperature dependences of the upper critical fields were calculated by Dediu *et al.*[12] using the model (1)–(2) with the function $\eta(z)$ that is positive in the N-layer. Obviously, our choice of the sign of this function in the N-layer indicates a weak proximity effect.

The GL equation (1) must be supplemented with the boundary conditions at the superconductor–normal metal interfaces:

$$\frac{1}{\Psi}\left(\frac{\partial\Psi}{\partial z} - i\frac{2\pi}{\Phi_0}A_z\right)\bigg|_b = P\frac{1}{\Psi}\left(\frac{\partial\Psi}{\partial z} - i\frac{2\pi}{\Phi_0}A_z\right)\bigg|_b, \tag{4}$$

where $P \in (0,1)$ is a parameter which is defined in the macroscopic theory[1–3] and is a phenomenological parameter here.

TRANSVERSE UPPER CRITICAL FIELD $H_{c2\perp}(T)$

Let us consider the behavior of the system in the vicinity of the upper critical field $H_{c2\perp}(T)$ (at right angles to the layer surface). Taking into account the expression for the vector potential $\mathbf{A} = (0, Hx, 0)$ in this case, we can write Eq. (1) in the form

$$\left\{\frac{\partial^2}{\partial x^2} + \frac{\partial^2}{\partial z^2} - \frac{x^2}{\zeta_H^4} + \eta(z)\right\}\Psi(x,z) = 0, \tag{5}$$

where $\xi_H^2(T) \equiv \Phi_0/2\pi H$.

Separation of variables $\Psi(x,z) = \varphi(x)\psi(z)$ in Eq. (5) gives a solution for $\varphi(x)$ corresponding to the minimum eigenvalue (maximum field H) in the form of a Gaussian function. In this case, we obtain for $\psi(z)$ the following equation:

$$\left\{\frac{\partial^2}{\partial z^2} - \frac{1}{\zeta_H^2} + \eta(z)\right\}\psi(z) = 0. \tag{6}$$

The boundary conditions (4) for the wave function $\Psi(x,z)$ is transformed into the de Gennes boundary conditions[1] for $\psi(z)$:

$$\frac{1}{\psi(z)}\frac{\partial\psi(z)}{\partial z}\bigg|_b = P\frac{1}{\psi(z)}\frac{\partial\psi(z)}{\partial z}\bigg|_b. \tag{7}$$

In the problem under consideration, the field $H_{c2\perp}(T)$ is defined as the boundary of the region of values of the external magnetic field H corresponding to steady-state solutions of an equation with periodic coefficients (in other words, $H_{c2\perp}$ is determined from the condition that the multipliers in Eq. (6) with the boundary condition (7) become equal to unity).[14] The corresponding solution is even and d-periodic. This leads to the following equation defining the transverse upper critical field as a function of temperature:

$$k_S \tan\left(\frac{d_S k_S}{2}\right) = p\kappa_N \tanh\left(\frac{d_N\kappa_N}{2}\right). \tag{8}$$

Here

$$k_S = \frac{1}{d_S}\left(\frac{H_S(T) - H}{H_{ds}}\right)^{1/2}; \tag{9}$$

$$\kappa_N = \frac{1}{d_N}\left(\frac{H + H_N(T)}{H_{dn}}\right)^{1/2}, \tag{10}$$

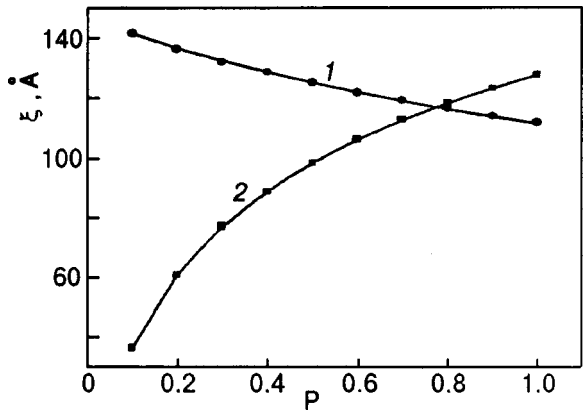

FIG. 3. Dependence of the coherence lengths in superconducting (curve *1*) and normal (curve *2*) layers on the parameter P of the wave function discontinuity at the metal–superconductor boundary.

and the following notation has been used for the sake of convenience:

$$H_{ds}=\frac{\Phi_0}{2\pi d_S^2};\quad H_S(T)=\frac{\Phi_0}{2\pi\xi_s^2(T)};\tag{11}$$

$$H_{dn}=\frac{\Phi_0}{2\pi d_N^2};\quad H_N(T)=\frac{\Phi_0}{2\pi\xi_N^2(T)}.$$

Note that Eqs. (6)–(11) essentially coincide with the Takahashi–Tachiki equations[3] for finding the transverse upper critical field, with the exception of one important factor: the parameters $H_S(0)$ and $H_N(0)$ in the microscopic theory[3] are presented in terms of material constants, and the temperature dependence of $H_{c2\perp}$ is obtained from the secular equation defining the kernel of the integral equation for the order parameter (see formulas (20), (30), (35), (38), and (46) in Ref 3). In the model constructed on the basis of the Ginzburg–Landau theory, the temperature dependence of $H_{c2\perp}$ is defined by the quantities $\xi_S(T)$ and $\xi_S(T)$ (or $H_S(T)$ and $H_N(T)$) as the phenomenological parameters-functions (although their functional form (3) is quite obvious).

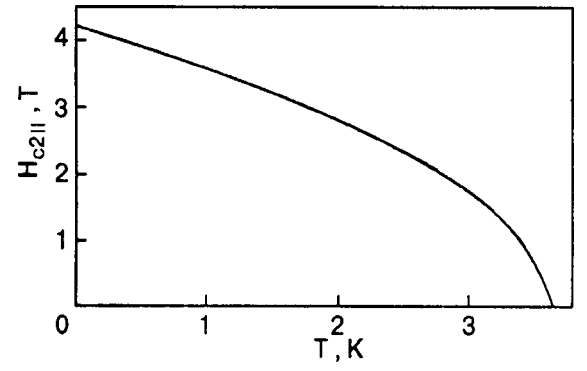

FIG. 4. The dependence $H_{c2\parallel}(T)$ ($d_S=170$ Å, $d_N=187$ Å) with coherence lengths $\xi_{S0}=135$ Å and $\xi_{Nc}=37$ Å, and the parameter $z_0=0$ corresponding to the solution symmetric relative to the middle of the superconducting layer.

PARALLEL UPPER CRITICAL FIELD $H_{c2\parallel}(T)$

We shall use the following standard procedure for determining the parallel upper critical field.[2,4] Let the external magnetic field $\mathbf{H}$ be directed along the plane of the layers, i.e., along the y-axis. We present the vector potential in the form $\mathbf{A}=(Hz,0,0)$ and separate the variables in Eq. (1):

$$\psi(\mathbf{r})=\exp(ikx)\,\psi(z).\tag{12}$$

In this case, we obtain instead of Eq. (1)

$$\left\{\frac{\partial^2}{\partial z^2}+\eta(z)-H_0^2(z-z_0)^2\right\}\psi(z)=0,\tag{13}$$

where $z_0\equiv k/H_0$, and the notation $H_0\equiv 2\pi H/\Phi_0$ is introduced for the sake of convenience.

Equation (13) is supplemented by the conditions (7) at the superconductor/normal metal boundary, as well as by the conditions at infinity

$$\psi(z\to\pm\infty)\to 0.\tag{14}$$

The maximum value of the external magnetic field parameter for which condition (14) is satisfied is the upper critical field.

It should be reiterated that the procedure of determining the upper critical field is formally the same as the procedure based on the microscopic theory[3] with the only exception mentioned in the preceding section.

DISCUSSION OF RESULTS

Computations of $H_{c2\perp}(T)$ and $H_{c2\parallel}(T)$ were made by us for the Nb/Pd superlattices investigated in Ref. 13.

It was found that the experimental dependence $H_{c2\perp}(T)$ can be described by formulas (3), (8)–(11) using the fitting parameters ξ_{S0} and ξ_{Nc} for any fixed value of the parameter P (see Fig. 2). Figure 3 shows by way of an example the dependence of the correlation lengths ξ_{S0} and ξ_{Nc} on parameter P calculated for an Nb/Pd sample with $d_S=187$ Å and $d_N=170$ Å.

The obtained values of the parameters ξ_{S0} and ξ_{Nc} were used to study numerically the solutions of the problem (7), (13), (14) for any fixed value of the parameter z_0. (It should be recalled that solutions of Eq. (13) are obtained by joining successively linear combinations of the functions of a parabolic cylinder with the help of boundary conditions (7).) As expected, the highest among the maximum values of the external magnetic field $H(z_0)$ corresponds to the values of the parameter $z_0=ld$ ($l=0,\pm1,\pm2,\ldots$) as well as the wave functions that are symmetric with respect to the middle of the lth S-layer. The temperature dependence $H_{c2\parallel}(T;z_0=ld)$ is of ''$2D$-type''[2] (see Fig. 4), and hence does not match with the experimental curve (see Fig. 2). Note that the values of the parameter z_0 are obtained form the variational principle for the GL-functional and, as can be seen easily, are determined from the equation

$$z_0=\frac{\int z\psi^2(z;z_0)dz}{\int\psi^2(z;z_0)dz}.\tag{15}$$

It follows from this equation that the values of the parameter z_0 corresponding to the ''$2D$-type'' temperature dependence of $H_{c2\parallel}$ are solutions of Eq. (15) (after substitution of wave

functions symmetric with respect to the middle of the lth S-layer) only for an infinite superlattice. The ''$2D$-type'' temperature dependence of $H_{c2\|}$ is also realized for a finite superlattice with an even number of S-layers and an odd number of N-layers since the presence of a symmetry plane in the middle of the central S-layer means that Eq. (15) has an exact zero as a solution corresponding to an even wave function $\psi(z)$.

In the experimental situation of Nb/Pd (11 layers of Pd and 10 layers of Nb) considered by Coccorese *et al.*,[13] the symmetry is exact relative to the middle N-layer. In this case, the integrals in Eq. (15) are taken over nonsymmetric limits, and hence substitution of the even wave function into (15) gives a nonzero value of the parameter z_0 which, in turn, contradicts the condition of parity of $\psi(z)$. However, the wave function is localized within a single S-layer for large values of the external magnetic fields (or for $T \ll T_c$). Consequently, the sample is practically equivalent to an infinite superlattice, and a ''$2D$-type'' behavior of the dependence $H_{c2\|}(T)$ is observed at low temperatures again. With increasing temperature, the ''blurring'' of the wave function over layers increases so that the parameter z_0 becomes perceptibly nonzero, and hence odd modes of the wave function also start competing. As a result, the curve $H_{c2\|}(T)$ will deviate noticeably downwards from the corresponding curve for an infinite superlattice. As the temperature attains a certain value T^*, the parameter z_0 becomes equal to $d/2$, which corresponds to a wave function symmetric relative to the middle of the N-layer. A comparison of the values of $H_{c2\|}(T^*)$ obtained from (13) and (14) with experimental results shows that the temperature T^* is the point of $2D-3D$ transition. At temperatures quite close to the transition temperature (or for small values of the external magnetic field), the solution of the system (13), (14) must be nearly identical (for not too large z) with the d-periodic solution of the GL equations for zero external magnetic field. The solution corresponding to zero applied magnetic field is independent of the variable x. This imposes certain constraints on the wave number k, viz., $k(H \to 0) \to 0$. Due to symmetry considerations, we choose $k \propto \sqrt{H_0}$ or $z_0 \propto 1/\sqrt{H_0}$. (Note that such a functional form of $z_0(H)$ also follows indirectly from (15) since the solution of Eq. (13) depends effectively on the dimensionless argument of $H_0 z^2$.) In this case, as $H \to 0$, we can present Eq. (13) for finite z (i.e., for $z \ll z_0$) in the following approximate form:

$$\left\{ \frac{\partial^2}{\partial z^2} + \eta(z) - H_0 Z_0^2 \right\} \psi(z) = 0,$$

where $Z_0 \equiv z_0 \sqrt{H_0}$. The condition for the existence of a d-periodic solution of this equation together with the boundary condition (7) leads to equations for $H_{c2\|}(T \to T_c)$ that are analogous to Eqs. (8)–(11) for $H_{c2\perp}(T)$ and give a linear dependence $H_{c2\|}(T - T_c)$.

It follows from what has been stated above that in order to determine the dependence $H_{c2\|}(T)$ for a superlattice with an even number of S layers and an odd number of N layers, we can use the following reasonable approximation for the parameter z_0:

$$z_0(H) = (Z_0/\sqrt{H_0}) - Z_1, \tag{16}$$

where Z_0 and Z_l are obtained from the conditions $z_0(H(T=0)) \approx 0$, $z_0(H(T=T^*)) = d/2$. Such an approximation makes it possible to avoid complex technical problems in the solution of the self-consistent problem (13)–(15). Using Eq. (16) and solving Eqs. (13) and (14) numerically, we calculated the dependence $H_{c2\|}(T)$ for the superlattice Nb/Pd. The parameter P was chosen from the condition of equality of the calculated value of $H_{c2\|}(0)$ and the experimental value of the upper critical field extrapolated to zero temperature. It can be seen from Fig. 2 that the theoretical dependence $H_{c2\|}(T)$ describes the experimental results quite satisfactorily.

CONCLUSION

The main results obtained in this work can be formulated as follows.

The Ginzburg–Landau theory is used to calculate the temperature dependences of the upper critical magnetic fields $H_{c2\perp}$ and $H_{c2\|}$ of a multilayered system of the superconductor– normal metal–superconductor type. It is shown that the theoretical curves $H_{c2\perp}(T)$ and $H_{c2\|}(T)$ can be used to reconstruct quite satisfactorily the experimental dependences of the upper critical fields for reasonable values of the Ginzburg–Landau model parameters.

It was proposed that the transition from $2D$ to $3D$ behavior in a multilayer superconducting structure with comparable thicknesses of the superconducting and normal layers can be attributed to a change in the symmetry of the Ginzburg–Landau order parameter from the infinite superlattice symmetry for large values of the applied parallel magnetic field to the symmetry of a real structure for small values of the field.

Note that the existence of such a ''symmetry effect'' can be easily verified experimentally in samples with an odd number of superconducting (Nb) and an even number of normal (Pd) layers. The rigorous mathematical problem on the form of the wave function corresponding to the parallel upper critical field can be solved, for example, with the help of the mathematical analysis used by Hastings and Troy[15] for investigating the symmetry properties of the solutions of one-dimensional Ginzburg–Landau equations for a superconducting film. However, the scope and style of the present communication do not allow us a detailed analysis of such a problem. It would be more expedient to study a more general form of the function $\eta(z)$ in the normal layer, viz., $\eta(z) \propto (T_{cN} - T)$. However, the introduction an ''extra'' fitting parameter T_{cN} does not appear to be justified from the methodical point of view.

*E-mail: aleks@gw.bsuir.unibel.by

[1] P. G. de Gennes, Rev. Mod. Phys. **36**, 225 (1964).
[2] B. Y. Jin and J. B. Ketterson, Adv. Phys. **38**, 189 (1989).
[3] S. Takahashi and M. Tachiki, Phys. Rev. B **33**, 4620 (1986).
[4] A. A. Abrikosov, *Fundamentals of the Theory of Metals* [in Russian], Nauka, Moscow (1987).

[5] S. K. Ami and K. Maki, Prog. Theor. Phys. **53**, 1 (1975).
[6] M. Kulic' and F. S. Rys, J. Low Temp. Phys. **76**, 167 (1989).
[7] V. Prokic', D. Davidovic', and L. Dobrosavljevic'-Grujic', Phys. Rev. B **51**, 6013 (1995).
[8] K. I. Kugel, T. Matsushita, E. Z. Melikhov, and A. L. Rakhmanov, Physica C **C**, 373 (1994).
[9] H. Raffy, J. C. Renard, and E. Guyon, Solid State Commun. **11**, 1679 (1972).
[10] H. Raffy, J. C. Renard, and E. Guyon, Solid State Commun. **14**, 427 (1974).
[11] S. L. Prischepa, V. N. Kushnir, A. Y. Petrov *et al.*, in *Proc. SPIE: Superconducting Superlattices II Naturel and Artificial* (Ed. by I. Bozovich and D. Pavuna) (1998).
[12] V. I. Dediu, V. V. Kabanov, and A. A. Sidorenko, Phys. Rev. B **49**, 4027 (1994).
[13] C. Coccorese, C. Attanasio, L. V. Mercaldo *et al.*, Phys. Rev. B **57**, 7922 (1998).
[14] V. A. Yakubovich and V. M. Starzhinskii, *Linear Differential Equations with Periodic Coefficients and Their Application*, Nauka, Moscow (1972).
[15] S. P. Hastings and W. C. Troy, Cond. Mat. **9903253**, 18 (1999).

Translated by R. S. Wadhwa

LOW-TEMPERATURE MAGNETISM

Description of critical behavior of Ising ferromagnet in the ρ^6 model approximation taking into account the confluent correction. II. Region below the phase transition point

I. V. Pylyuk

*Institute of Condensed Matter Physics, National Academy of Sciences of the Ukraine, 290011 Lviv, Ukraine**)

(Submitted December 15, 1998; revised June 9, 1999)
Fiz. Nizk. Temp. **25**, 1271–1281 (December 1999)

A scheme for calculating the thermodynamic characteristics of a $3D$ one-component spin system in the temperature range below the critical temperature is described on the basis of the sextic measure density (ρ^6 model) taking into account the first confluent correction. A microscopic analog of the Landau free energy is calculated. The coefficients of average spin moment, leading critical amplitudes, and the amplitudes of the confluent correction to specific heat and susceptibility of the system are calculated for different values of effective radius of the exponentially decreasing interaction potential. Plots of temperature dependence of entropy and other thermodynamic characteristics in the vicinity of T_c are given for various values of effective radius. The variation of the free energy of the system at the phase transition point, average spin moment, and specific heat with increasing ratio of the potential effective radius to the constant of a simple cubic lattice is traced. The results of calculations and their comparison with the data obtained by other authors show that the ρ^6 model provides a better quantitative description of the critical behavior of a $3D$ Ising ferromagnet than the ρ^4 model. © *1999 American Institute of Physics.* [S1063-777X(99)00512-5]

INTRODUCTION

This research is devoted to the theory of phase transitions and critical phenomena which remain the subject of intense studies (see, for example, Refs. 1–4). The approach to description of second-order phase transitions based on the method of collective variables (CV)[5] has been developed further. The object of investigation is the $3D$ Ising model on a simple cubic lattice with an exponentially decreasing interaction potential (see, for example, Ref. 6). The Ising model, which is simple and convenient for mathematical analysis, is widely used in the theory of phase transitions for an analysis of properties of various magnetic and nonmagnetic systems (ferromagnets, antiferromagnets, ferroelectrics, binary mixtures, lattice model of liquids, etc.).

The behavior of a $3D$ Ising ferromagnet will be studied here at temperatures $T<T_c$ (low-temperature region) in the approximation of the non-Gaussian sextic distribution of spin density oscillation modes (the ρ^6 model).[5] A method of taking into account the first confluent correction is developed in the course of calculation of thermodynamic characteristics. The dependences of these characteristics on temperature and microscopic parameters of the system are plotted. The case of $T>T_c$ was considered in Ref. 7. The present publication supplements the cycle of works[8–16] in which the CV method is used for calculating the thermodynamic functions of a $3D$ Ising system in the low-temperature region. The calculations on the basis of the ρ^4 model without taking into account confluent corrections were made in Ref. 8, taking into account the first and second confluent corrections in Refs. 9–14, and in the ρ^6 model approximation without confluent corrections, in Refs. 15 and 16.

The method of calculation of thermodynamic characteristics of a one-component spin system can be extended to the n-component model applied for spin dimensions $n=2$ as a lattice model of transition of a Bose liquid to the superfluid state. The main points of such a generalization to the n-component case are given in Ref. 5.

1. ALGORITHM OF CALCULATION OF FREE ENERGY OF THE SYSTEM AT $T<T_C$

As in the case of $T>T_c$,[7] we shall calculate the free energy of the system by separating the contributions from short- and long-wave modes of spin density oscillations. For $T<T_c$, we have

$$F=F_0+F_{CR}+F_{IGR}, \tag{1}$$

where $F_0=-kTN\ln 2$ corresponds to the free energy of N noninteracting spins, and F_{CR} to the contribution of short-wave modes of spin moment density oscillations to the free energy of the system (critical regime (CR) region), and F_{IGR} to the contribution of long-wave oscillation modes (the region of inverse Gaussian regime (IGR)).

While calculating the free energy of the system, we shall use extensively the solutions of recurrence relations (RR) between the coefficients of effective sextic distributions (see, for example, Ref. 17). In the CR region, the solutions of RR

of the renormalization group (RG) type are valid. In contrast to the limiting Gaussian regime (LGR) observed for $T>T_c$, the IGR is described by a non-Gaussian density of measure. It should be emphasized that at $T<T_c$, the system acquires a nonzero order parameter. It is not introduced as an independent quantity, but is determined as a result of direct calculation. This is possible since the set of CV contains the variable ρ_0 associated with the order parameter. The distribution acquires a Gaussian form as a result of separation of free energy of ordering.

Calculating the partition function of the Ising model, we divide the CV space into layers with the division parameter s and use the average value of the Fourier transform of the interaction potential (arithmetic mean in the given case) corresponding to the given layer.[5] Short- and long-wave modes of spin density oscillations at $T<T_c$ are separated by the layer number μ_τ. The CR takes place for layers of the CV phase space with $n\leqslant\mu_\tau$, while IGR is observed for $n>\mu_\tau$. The condition for determining μ_τ is the equality[6,18]

$$\frac{r_{\mu_\tau+1}-r^{(0)}}{r^{(0)}}=\delta. \tag{2}$$

Here δ is a constant quantity ($\delta\leqslant 1$), $r_{\mu_\tau+1}$ is determined from the solutions of RR, and $r^{(0)}$ corresponds to a coordinate of the fixed point.[17] In numerical calculations, we shall put $\delta=1$, which is in accord with the same condition for δ used by us for $T>T_c$.[7] In analogy with the case $T>T_c$,[7] we obtain the following expression for μ_τ:

$$\mu_\tau=\mu_\tau^{(0)}-m_{\Delta_1}|\tau|^{\Delta_1},$$
$$\mu_\tau^{(0)}=-\frac{\ln|\tau|}{\ln E_1}+\mu_0-1,\quad \mu_0=m_c. \tag{3}$$

The values of m_{Δ_1}, Δ_1, and m_c coincide with the corresponding values for $T>T_c$ (see Ref. 7), $\tau=(T-T_c)/T_c$, and E_1 is the largest eigenvalue of the matrix of RG linear transformation.

The expression for the layer μ_τ determining the point of exit of the system from the CR region at $T<T_c$ makes it possible to determine F_{CR} as well as F_{IGR}. We shall consider these calculations schematically. It should be noted that the thermodynamic characteristics are calculated taking into account the term proportional to $|\tau|^{\Delta_1}$ and determining the first confluent correction.

2. THERMODYNAMIC FUNCTIONS OF THE SYSTEM CORRESPONDING TO THE CRITICAL REGIME REGION

As in the case of $T>T_c$, the contribution F_{CR} to the free energy of the system from the CR region is calculated through the summation of partial free energies over the layers of the CV phase space. Using formulas (3) and singling out temperature explicitly in the calculations, we arrive at the following expression:

$$F_{CR}=-kTN'[\gamma_0^{(CR)}-\gamma_1|\tau|+\gamma_2|\tau|^2-\gamma_3^{(CR)(0)-}|\tau|^{3\nu}-\gamma_3^{(CR)(1)-}|\tau|^{3\nu+\Delta_1}], \tag{4}$$

where $\nu=\ln s/\ln E_1$ is the critical exponent of correlation length, N' and $\gamma_0^{(CR)}$, γ_1, and γ_2 (which are functions of microscopic parameters of the system) are the same as for $T>T_c$.[7,17] We present the coefficients $\gamma_3^{(CR)(l)-}$ in the form in which the universal factor $\overline{\gamma}_3^{(CR)(l)-}$ independent of microscopic parameters of the system is separated. The latter parameters in our case include the parameters of exponentially decreasing interaction potential (the effective radius b of the potential and its Fourier transform $\tilde{\Phi}(0)$ for zero value of wave vector) as well as the constant c of the simple cubic lattice. We have

$$\gamma_3^{(CR)(l)-}=c_\nu^3 c_{\Delta_1}^l\,\overline{\gamma}_3^{(CR)(l)-},\quad l=0,1,$$
$$\overline{\gamma}_3^{(CR)(0)-}=\gamma^-,\quad \overline{\gamma}_3^{(CR)(1)-}=\gamma_{\Delta_1}^- -\Phi_0(\gamma_{11}^-+3\nu\gamma^-). \tag{5}$$

Here

$$\gamma^-=\frac{f_{CR}^{(0)}}{1-s^{-3}}-\frac{f_{CR}^{(1)}\varphi_0^{-1/2}f_0\delta}{1-E_1s^{-3}}+\frac{f_{CR}^{(7)}\varphi_0^{-1}(f_0\delta)^2}{1-E_1^2s^{-3}},$$
$$\gamma_{\Delta_1}^-=\frac{f_{CR}^{(2)}\varphi_0^{-1}}{1-E_2s^{-3}}-\frac{f_{CR}^{(4)}\varphi_0^{-3/2}f_0\delta}{1-E_1E_2s^{-3}}+\frac{f_{CR}^{(8)}\varphi_0^{-2}(f_0\delta)^2}{1-E_1^2E_2s^{-3}}, \tag{6}$$
$$\gamma_{11}^-=\frac{f_{CR}^{(1)}\varphi^{-1/2}f_0\delta}{1-E_1s^{-3}}-\frac{2\,f_{CR}^{(7)}\varphi_0^{-1}(f_0\delta)^2}{1-E_1^2s^{-3}}.$$

The nonuniversal factors c_ν, c_{Δ_1}, the factor Φ_0, the eigenvalues E_l of the matrix of RG transformation, the expressions for three coordinates of the fixed point and the quantities characterizing them (including f_0 and φ_0) as well as for $f_{CR}^{(i)}$ depending on the values of variables at the fixed point are presented in Ref. 17.

Differentiating expression (4) for F_{CR} with respect to temperature, we obtain the following expressions for entropy S_{CR}, internal energy U_{CR}, and specific heat C_{CR} in the CR region:

$$S_{CR}=kN'[s^{(CR)(0)}-c_0|\tau|+u_3^{(CR)(0)-}|\tau|^{1-\alpha}+u_3^{(CR)(1)-}|\tau|^{1-\alpha+\Delta_1}],$$
$$U_{CR}=kTN'[\gamma_1-u_1|\tau|+u_3^{(CR)(0)-}|\tau|^{1-\alpha}+u_3^{(CR)(1)-}|\tau|^{1-\alpha+\Delta_1}], \tag{7}$$
$$C_{CR}=kN'[c_0-c_3^{(CR)(0)-}|\tau|^{-\alpha}-c_3^{(CR)(1)-}|\tau|^{\Delta_1-\alpha}],$$

where $\alpha=2-3\nu$ is the critical exponent of specific heat, and

$$u_3^{(CR)(l)-}=c_\nu^3 c_{\Delta_1}^l\,\overline{u}_3^{(CR)(l)-},\quad l=0,1;$$
$$\overline{u}_3^{(CR)(0)-}=3\nu\overline{\gamma}_3^{(CR)(0)-};$$
$$\overline{u}_3^{(CR)(1)-}=(3\nu+\Delta_1)\overline{\gamma}_3^{(CR)(1)-};$$
$$c_3^{(CR)(l)-}=c_\nu^3 c_{\Delta_1}^l\,\overline{c}_3^{(CR)(l)-}; \tag{8}$$
$$\overline{c}_3^{(CR)(0)-}=3\nu(3\nu-1)\overline{\gamma}_3^{(CR)(0)-};$$
$$\overline{c}_3^{(CR)(1)-}=(3\nu+\Delta_1)(3\nu+\Delta_1-1)\overline{\gamma}_3^{(CR)(1)-}.$$

The remaining coefficients are defined by corresponding expressions obtained from an analysis of temperatures above T_c.[7,17]

3. THERMODYNAMIC FUNCTIONS OF THE SYSTEM CORRESPONDING TO THE REGION OF INVERSE GAUSSIAN REGIME

We shall write the final result for the contribution of the IGR region

$$F_{IGR}=-kTN's^{-3(\mu_\tau+1)}\ln[\sqrt{2}Q(P_{\mu_\tau})]-kT\ln Z_{\mu_\tau+1} \tag{9}$$

to the free energy of the system. The calculations of the first and second terms in (9), associated with the calculations of

$$\sqrt{2}Q(P_{\mu_\tau})=\left(\frac{4s^3u_{\mu_\tau}s^{-4\mu_\tau}}{\pi^4C(h_{\mu_\tau},\alpha_{\mu_\tau})}\right)^{1/4}I_0(\eta_{\mu_\tau},\xi_{\mu_\tau}) \tag{10}$$

and

$$Z_{\mu_\tau+1}=\int\exp\left[-\frac{1}{2}\sum_{k\leqslant B_{\mu_\tau+1}}d_{\mu_\tau+1}(k)\rho_k\rho_{-k}-\sum_{l=2}^{3}\frac{a_{2l}^{(\mu_\tau+1)}}{(2l)!N_{\mu_\tau+1}^{l-1}}\sum_{k_1\ldots,k_2\leqslant B_{\mu_\tau+1}}\rho_{k_1}\ldots\rho_{k_{2l}}\delta_{k_1+\ldots+k_{2l}}\right](d\rho)^{N_{\mu_\tau+1}}, \tag{11}$$

are described in detail in Ref. 18 (see Ref. 13 for the ρ^4 model). We obtain

$$F_{IGR}=-kTN'[\gamma_{IGR}^{(0)}|\tau|^{3\nu}+\gamma_{IGR}^{(1)}|\tau|^{3\nu+\Delta_1}],$$
$$\gamma_{IGR}^{(l)}=\gamma_3^{(l)(\mu_\tau)}+\gamma_3^{(l)(\sigma)},\quad l=0,1. \tag{12}$$

The term $\gamma_3^{(l)(\mu_\tau)}$ defines free energy after the exit from the CR, and $\gamma_3^{(l)\langle\sigma\rangle}$ defines the free energy of ordering. These terms can be calculated by the formulas

$$\gamma_3^{(l)(\mu_\tau)}=\gamma_g^{(l)}+\gamma_\rho^{(l)},\quad \gamma_g^{(l)}=c_\nu^3c_{\Delta_l}^l\overline{\gamma}_g^{(l)},$$
$$\gamma_\rho^{(l)}=c_\nu^3c_{\Delta_l}^l\overline{\gamma}_\rho^{(l)},\quad \gamma_3^{(l)\langle\sigma\rangle}=c_\nu^3c_{\Delta_l}^l\overline{\gamma}_3^{(l)\langle\sigma\rangle}. \tag{13}$$

The expressions for the quantities $\overline{\gamma}_g^{(l)},\overline{\gamma}_\rho^{(l)},\overline{\gamma}_3^{(l)\langle\sigma\rangle}$ independent of microscopic parameters are given in Ref. 18.

The entropy S_{IGR}, internal energy U_{IGR}, and specific heat C_{IGR} corresponding to IGR can be written in the form

$$S_{IGR}=S_{\mu_\tau}+S_{\langle\sigma\rangle},\quad U_{IGR}=U_{\mu_\tau}+U_{\langle\sigma\rangle},$$
$$C_{IGR}=C_{\mu_\tau}+C_{\langle\sigma\rangle}. \tag{14}$$

The components of these thermodynamic characteristics satisfy the following relations:

$$S_\eta=-kN'[u_3^{(0)\langle\eta\rangle}|\tau|^{1-\alpha}+u_3^{(1)\langle\eta\rangle}|\tau|^{1-\alpha+\Delta_1}],$$
$$U_\eta=-kTN'[u_3^{(0)(\eta)}|\tau|^{1-\alpha}+u_3^{(1)(\eta)}|\tau|^{1-\alpha+\Delta_1}],$$
$$C_\eta=kN'[c_3^{(0)(\eta)}|\tau|^{-\alpha}+c_3^{(1)(\eta)}|\tau|^{\Delta_1-\alpha}],$$
$$u_3^{(l)(\eta)}=c_\nu^3c_{\Delta_1}^l\overline{u}_3^{(l)(\eta)},\quad l=0,1,$$
$$\overline{u}_3^{(0)(\eta)}=3\nu\overline{\gamma}_3^{(0)(\eta)},\quad \overline{u}_3^{(l)(\eta)}=(3\nu+\Delta_1)\overline{\gamma}_3^{(1)(\eta)},$$
$$c_3^{(l)(\eta)}=c_\nu^3c_{\Delta_1}^l\overline{c}_3^{(l)(\eta)},\quad \overline{c}_3^{(0)(\eta)}=3\nu(3\nu-1)\overline{\gamma}_3^{(0)(\eta)},$$
$$\overline{c}_3^{(1)(\eta)}=(3\nu+\Delta_1)(3\nu+\Delta_1-1)\overline{\gamma}_3^{(1)(\eta)}. \tag{15}$$

The exponent η can assume two values: μ_τ and $\langle\sigma\rangle$. Here $\overline{\gamma}_3^{(l)(\mu_c)}=\overline{\gamma}_g^{(l)}$ $(l=0,1)$, and $\overline{\gamma}_3^{(l)\langle\sigma\rangle}$ are universal factors appearing in $\gamma_3^{(l)\langle\sigma\rangle}$ (see (13)).

Thus, we have calculated free energy in the IGR region. Proceeding from the expression (12) for F_{IGR}, we have obtained other thermodynamic functions corresponding to IGR. Expression (12) contains the free energy of ordering determined by integration with respect to CV ρ_0, whose average value is proportional to the order parameter which is an important characteristic of the phase transition.

4. ORDER PARAMETER OF A 3*D* ISING SYSTEM

The role of the order parameter for the system under investigation is played by the average spin moment. It is associated with the existence of a nonzero value $\overline{\rho_0}$ below the phase transition temperature, for which the integrand of the expression

$$Z_{\mu_\tau+1}=\exp(-\beta F'_{\mu_\tau+1})\times\int\exp\left[\beta\sqrt{N}\rho_0h+\tilde{B}\rho_0^2-\frac{G}{N}\rho_0^4-\frac{D}{N^2}\rho_0^6\right]d\rho_0, \tag{16}$$

attains its extremum value. Here $\beta=1/(kT)$ is the inverse thermodynamic temperature and h is determined by the value of the constant external field $\mathcal{H}$ introduced in our analysis ($h=\mu_B\mathcal{H}$, μ_B being the Bohr magneton). The expression for $-\beta F'_{\mu_\tau+1}$ corresponding to the contribution to the free energy of the system from $\rho_{\mathbf{k}}$ with the values of wave vectors $k\to0$ (but not equal to zero) as well as the coefficients

$$\tilde{B}=\tilde{B}^{(0)}|\tau|^\nu\beta\tilde{\Phi}(0)(1+\overline{B}^{(1)}|\tau|^{\Delta_1}),$$
$$G=G^{(0)}|\tau|^\nu(\beta\tilde{\Phi}(0))^2(1+G^{(1)}|\tau|^{\Delta_1}), \tag{17}$$
$$D=D^{(0)}(\beta\tilde{\Phi}(0))^3(1+D^{(1)}|\tau|^{\Delta_1})$$

are given in Ref. 18. Carrying out in (16) the substitution of the variable

$$\rho_0=\sqrt{N}\rho, \tag{18}$$

we obtain

$$Z_{\mu_\tau+1}=\exp(-\beta F'_{\mu_\tau+1})\sqrt{N}\int\exp(-NE_0(\rho))d\rho, \tag{19}$$

TABLE I. Values of quantities determining the coefficients in expression for a microscopic analog of the Landau free energy.

b	$\tilde{B}(0)$	$\tilde{B}(1)$	$G(0)$	$G(1)$	$D(0)$	$D(1)$
			$s=2.0000$			
b_{I}	1.0106	−0.2733	0.0550	−0.8919	0.0009	−0.6952
b_{II}	0.9530	−0.3959	0.0857	−1.2918	0.0023	−0.9377
b_{III}	0.9305	−0.4420	0.1010	−1.4423	0.0033	−1.0470
c	0.7258	−0.8188	1.9382	−2.6720	1.5614	−1.9396
$2c$	0.7149	−0.8375	15.3880	−2.7330	99.9318	−1.9839
			$s=2.7349$			
b_{I}	0.9417	−0.4451	0.0690	−1.1718	0.0012	−0.8853
b_{II}	0.8888	−0.5124	0.1074	−1.3491	0.0031	−1.0193
b_{III}	0.8683	−0.5377	0.1267	−1.4157	0.0044	−1.0696
c	0.6865	−0.7445	2.4478	−1.9601	2.0825	−1.4809
$2c$	0.6768	−0.7550	19.4434	−1.9876	133.281	−1.5017
			$s=3000$			
b_{I}	0.9115	−0.4755	0.0732	−1.1967	0.0013	−0.9113
b_{II}	0.8610	−0.5321	0.1141	−1.3392	0.0033	−1.0199
b_{III}	0.8415	−0.5533	0.1346	−1.3926	0.0047	−1.0606
c	0.6697	−0.7261	2.6087	−1.8275	2.2185	−1.3918
$2c$	0.6605	−0.7348	20.7264	−1.8495	141.986	−1.4085

TABLE II. Coefficients of the average spin moment $\langle\sigma\rangle$ in (25) for some values of the effective radius b of potential and RG parameter s.

b	$\langle\sigma\rangle^{(0)}$	$\langle\sigma\rangle^{(1)}$
	$s=2.0000$	
b_{I}	2.7329	0.2499
b_{II}	2.0684	0.3619
b_{III}	1.8700	0.4040
c	0.3747	0.7485
$2c$	0.1321	0.7656
	$s=2.7349$	
b_{I}	2.3854	0.3034
b_{II}	1.8027	0.3493
b_{III}	1.6288	0.3666
c	0.3248	0.5076
$2c$	0.1145	0.5147
	$s=3.0000$	
b_{I}	2.2861	0.3046
b_{II}	1.7269	0.3409
b_{III}	1.5600	0.3545
c	0.3107	0.4651
$2c$	0.1095	0.4707

and the evaluation of the order parameter is reduced to determining the extremum point $\overline{\rho}$ of the expression

$$E_0(\rho)=D\rho^6+G\rho^4-\tilde{B}\rho^2-\beta h\rho. \tag{20}$$

The value of $\overline{\rho}$ coincides with the average value of ρ corresponding to the equilibrium value of the order parameter.[5,15,16] The expression for $E_0(\rho)$ defines the fraction of free energy associated with the order parameter. It corresponds to the microscopic analog of the Landau free energy. The quantity $Z_{\mu_\tau+1}$ will be expressed in terms of $E_0(\overline{\rho})$ (coinciding in form with the expansion of free energy into a power series in the order parameter) by using the steepest descent method for evaluating the integral (19) (see Ref. 18).

Expression (20) was derived by successive elimination of ''insignificant'' variables $\rho_{\mathbf{k}}$ with $k\neq 0$, which allowed us to calculate the coefficients of $E_0(\rho)$ (see Table I).

Numerical values in Table I are given for some values of effective radius b of the potential and the RG parameter s. As in the case of $T>T_c$,[7,17] the parabolic approximation of the Fourier transform of the exponentially decreasing potential of interaction in the region of small values of wave vectors for $b=b_I=c/(2\sqrt{3})$ corresponds to a similar approximation of the Fourier transform for the potential of interaction between nearest neighbors, nearest and next nearest neighbors for $b=b_{II}=0.3379c$, and first, second, and third neighbors for $b=b_{III}=0.3584c$. The value of $s=s^*=2.7349$ corresponds to the average value of the coefficient of the second power of the variable in the expression for density of measure of the nth layer, which is equal to zero at a fixed point (in the ρ^4 model, this corresponds to $s^*=3.5862$). Thus, there is no need to postulate a temperature dependence of the coefficients in formula (20) (as in the case of the Landau expansion) since the analytic form of their dependence on temperature and microscopic parameters of the system has been obtained as a result of direct calculations. In contrast to the Landau theory, the temperature dependence of these coefficients is nonanalytic (see (17)).

Let us go over to direct calculation of the average spin moment. The point $\overline{\rho}$ can be determined from the condition of extremum $\partial E_0(\rho)/\partial\rho=0$ or

$$6D\overline{\rho}^5+4G\overline{\rho}^3-2\tilde{B}\overline{\rho}-\frac{h}{kT}=0. \tag{21}$$

For $h=0$, we obtain the biquadratic equation

$$6D\overline{\rho}^4+4G\overline{\rho}^2-2\tilde{B}=0, \tag{22}$$

in which the substitution of the variable

$$\overline{\rho}^2=y \tag{23}$$

leads to the equation

$$6Dy^2+4Gy-2\tilde{B}=0. \tag{24}$$

Solving this equation and separating temperature explicitly, we arrive at the following formula for the average spin moment $\langle\sigma\rangle=\overline{\rho}=\sqrt{y}$:

$$\langle\varphi\rangle=\langle\sigma\rangle^{(0)}|\tau|^{\beta}(1+\langle\sigma\rangle^{(1)}|\tau|^{\Delta_1}). \tag{25}$$

Here $\beta=\nu/2$ is the critical exponent of the average spin moment, and the coefficients of $\langle\sigma\rangle^{(l)}$ are given in Table II.[18]

The curves describing the dependence of $\langle\sigma\rangle$ on τ for various values of b are shown in Fig. 1. Here and below, the curves are plotted for the RG parameter $s=3$.

5. THERMODYNAMIC CHARACTERISTICS OF ISING MODEL AS FUNCTIONS OF TEMPERATURE AND MICROSCOPIC PARAMETERS OF THE SYSTEM

Let us now find complete expressions for thermodynamic functions of an Ising system at $T<T_c$ in the approximation of the ρ^6 model taking into account the first confluent correction (the case $\mathcal{H}=0$).

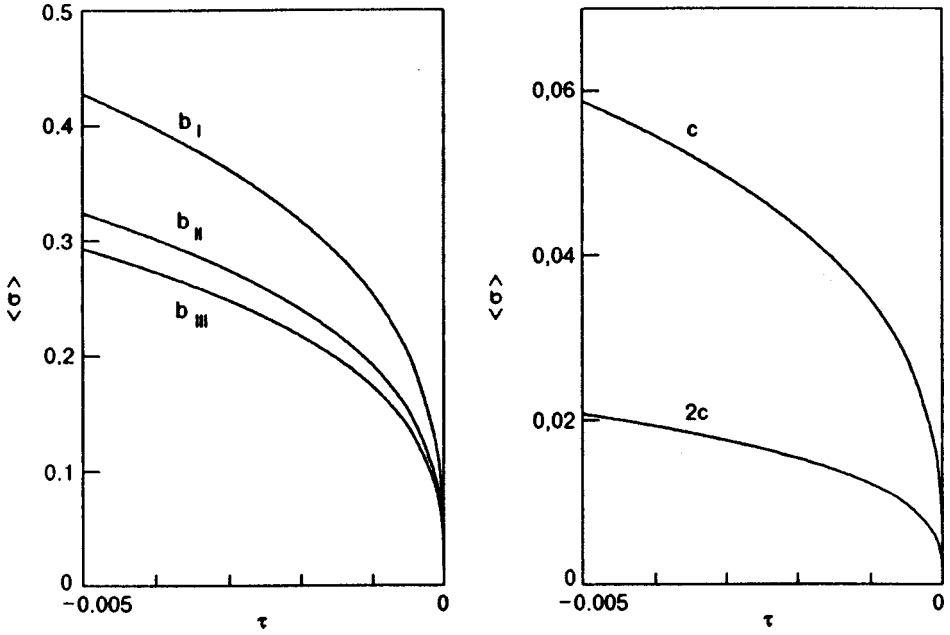

FIG. 1. Temperature dependence of average spin moment of the system in the ρ^6 model approximation for various values of the effective radius b of the potential: $b_I = c/(2\sqrt{3})$; $b_{II}=0{,}3379c$; $b_{III}=0{,}3584c$; and $2c$.

The contributions from the CR and IGR regions to free energy of a $3D$ Ising model near T_c obtained above allow us to write its total free energy (1) in the form

$$F=-kTN'[\gamma_0-\gamma_1|\tau|+\gamma_2|\tau|^2+\gamma_3^{(0)-}|\tau|^{3\nu} + \gamma_3^{(1)-}|\tau|^{3\nu+\Delta_1}]. \quad (26)$$

All the coefficients in expression (26) are functions of microscopic parameters of the system, i.e., the effective radius b of the potential, the Fourier transform $\tilde{\Phi}(0)$ of the potential, and the lattice constant c. The coefficients γ_0, γ_1, and γ_2 can be determined from expressions for corresponding quantities in the high-temperature region (see Refs. 7 and 17). In contrast to $\gamma_3^{(l)-}$ $(l=0,1)$, their values are independent of whether calculations are made for a temperature above or below the phase transition point. The coefficients $\gamma_3^{(l)-}$ have the form of the product of the quantity $\overline{\gamma}_3^{(l)-}$, which is universal relative to microscopic parameters, and the nonuniversal factor $c_\nu^3 c_{\Delta_1}^l$, which is a function of these parameters:

$$\gamma_3^{(l)-}=c_\nu^3 c_{\Delta_1}^l \overline{\gamma}_3^{(l)-}, \quad l=0,1,$$

$$\overline{\gamma}_3^{(l)-}=-\overline{\gamma}_3^{(CR)(l)-}+\overline{\gamma}_{IGR}^{(l)}\overline{\gamma}_{IGR}^{(l)}=\overline{\gamma}_g^{(l)}+\overline{\gamma}_\rho^{(l)}+\overline{\gamma}_3^{(l)\langle\sigma\rangle}. \quad (27)$$

Numerical values of the coefficients $\overline{\gamma}_3^{(l)-}$ are given in Table III.

TABLE III. Values of $\overline{\gamma}_3^{(1)-}$ for some values of s.

s	$\overline{\gamma}_3^{(0)-}$	$\overline{\gamma}_3^{(1)-}$
2.0000	1.7599	−6.7968
2.7349	2.7650	−3.6743
3.0000	3.1073	−3.0714

Proceeding from the expression (26) for free energy F, we can find other thermodynamic functions for $T<T_c$. For example, the following expressions are valid for entropy S, internal energy U, and specific heat C:

$$S=kN'[s^{(0)}-c_0|\tau|-u_3^{(0)-}|\tau|^{1-\alpha}-u_3^{(1)-}|\tau|^{1-\alpha+\Delta_1}],$$

$$U=kTN'[\gamma_1-u_1|\tau|-u_3^{(0)-}|\tau|^{1-\alpha}-u_3^{(1)-}|\tau|^{1-\alpha+\Delta_1}], \quad (28)$$

$$C=kN'[c_0+c_3^{(0)-}|\tau|^{-\alpha}+c_3^{(1)-}|\tau|^{\Delta_1-\alpha}],$$

where $s^{(0)}$, c_0, and u_1 coincide with the corresponding quantities for $T>T_c$,[7,17] while the structure of the remaining coefficients in terms of universality is determined by the relations

TABLE IV. Numerical values of amplitudes A^-, a_c^-, Γ^-, and a_χ^-.

b	$A-$	a_c^-	$\Gamma-$	a_χ^-
		$s=2.0000$		
$b_{\rm I}$	1.9734	7.2567	0.2133	0.1872
$b_{\rm II}$	1.8071	10.5104	0.2262	0.2711
$b_{\rm III}$	1.7436	11.7347	0.2317	0.3027
c	1.2012	21.7395	0.2970	0.5608
$2c$	1.1741	22.2353	0.3015	0.5736
		$s=2.7349$		
$b_{\rm I}$	1.2026	8.1288	0.2341	0.3536
$b_{\rm II}$	1.1027	9.3588	0.2480	0.4071
$b_{\rm III}$	1.0648	9.8206	0.2539	0.4272
c	0.7486	13.5975	0.3211	0.5915
$2c$	0.7328	13.7882	0.3257	0.5998
		$s=3.0000$		
$b_{\rm I}$	1.0331	7.9599	0.2437	0.3884
$b_{\rm II}$	0.9484	8.9081	0.2580	0.4346
$b_{\rm III}$	0.9164	9.2633	0.2640	0.4519
c	0.6506	12.1558	0.3318	0.5931
$2c$	0.6373	12.3022	0.3364	0.6002

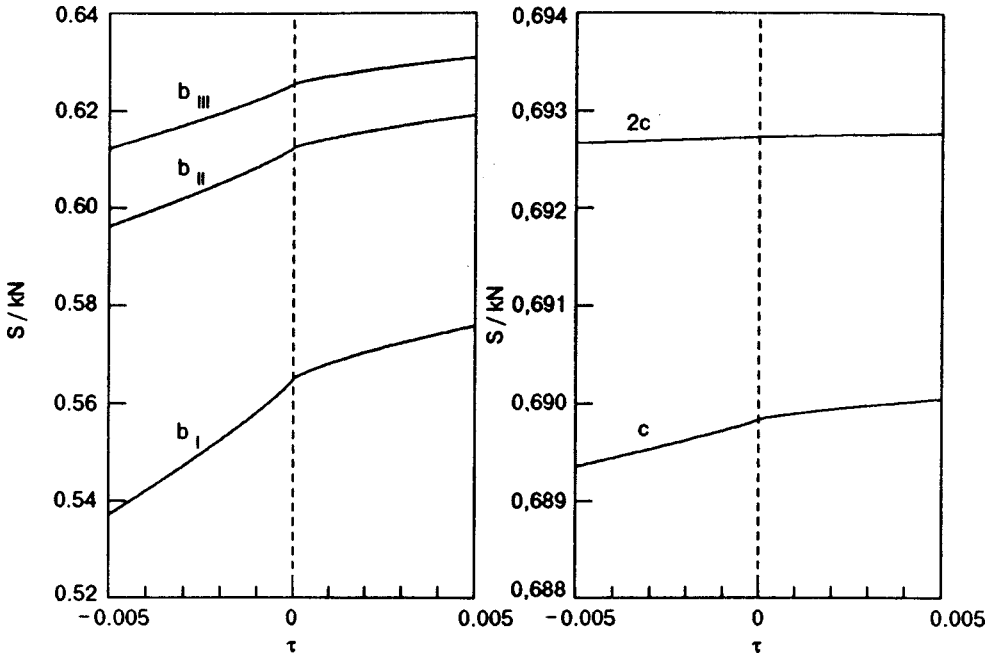

FIG. 2. Dependence of the entropy of the system on τ. Notation is the same as in Fig. 1.

$$u_3^{(l)-}=c_\nu^3 c_{\Delta_1}^l \bar{u}_3^{(l)-}, \quad l=0,1,$$

$$\bar{u}_3^{(0)-}=3\nu\bar{\gamma}_3^{(0)-}, \quad \bar{u}_3^{(1)-}=(3\nu+\Delta_1)\bar{\gamma}_3^{(1)-}, \tag{29}$$

$$\bar{c}_3^{(l)-}=c_\nu^3 c_{\Delta_1}^l \bar{c}_3^{(l)-}, \quad \bar{c}_3^{(0)-}=3\nu(3\nu-1)\bar{\gamma}_3^{(0)-},$$

$$\bar{c}_3^{(1)-}=(3\nu+\Delta_1)(3\nu+\Delta_1-1)\bar{\gamma}_3^{(1)-}.$$

Presenting the specific heat from (28) by the dependence

$$\frac{C}{kN'}=\frac{A^-}{\alpha}|\tau|^{-\alpha}(1+\alpha a_c^-|\tau|^{\Delta_1})+B^-,$$

$$A^-=c_\nu^3\alpha\bar{c}_3^{(0)-}, \quad a_c^-=\frac{c_{\Delta_1}}{\alpha}\frac{\bar{c}_3^{(1)-}}{\bar{c}_3^{(0)-}}, \quad B^-=c_0, \tag{30}$$

similar to the case $T>T_c$, we obtain the following expressions for ratios of the leading critical amplitudes and the amplitudes of corrections to scaling at temperatures above and below the phase transition temperature:

$$\frac{A^+}{A^-}=\frac{\bar{c}_3^{(0)+}}{\bar{c}_3^{(0)-}}, \quad \frac{a_c^+}{a_c^-}=\frac{\bar{c}_3^{(1)+}}{\bar{c}_3^{(1)-}}\frac{\bar{c}_3^{(0)-}}{\bar{c}_3^{(0)+}}. \tag{31}$$

It should be noted that B^- is equal to B^+ calculated for $T>T_c$. The amplitudes A^- and a_c^- are given in Table IV.

Equation (21) makes it possible to calculate the susceptibility of the system per particle, i.e., $\chi=\mu_B(\partial\langle\sigma\rangle/\partial\mathcal{H})$:

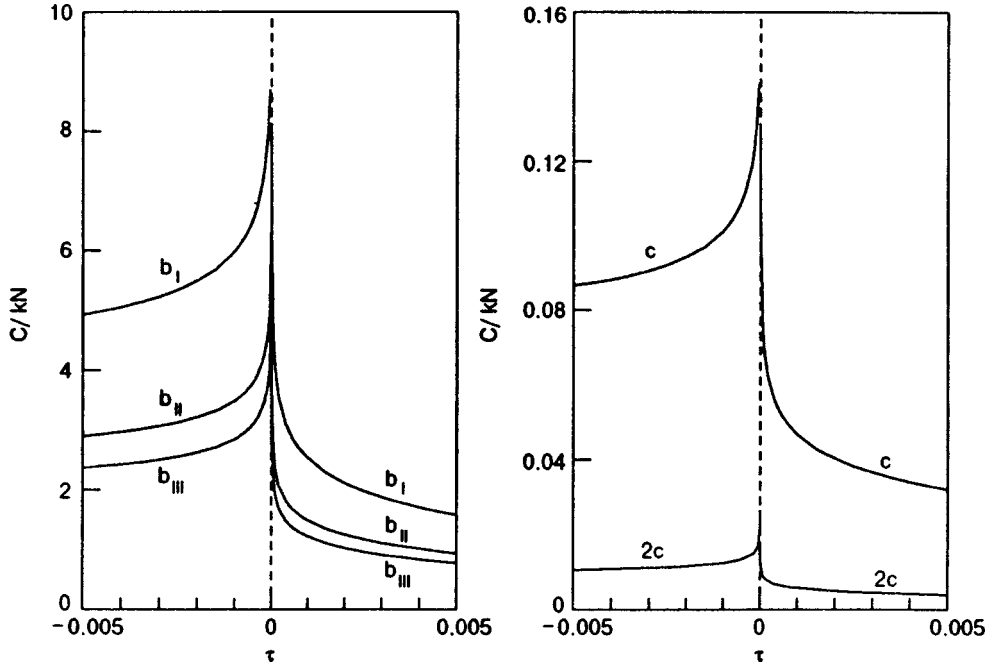

FIG. 3. Specific heat of the spin system for various values of b. Notation is the same as in Fig. 1.

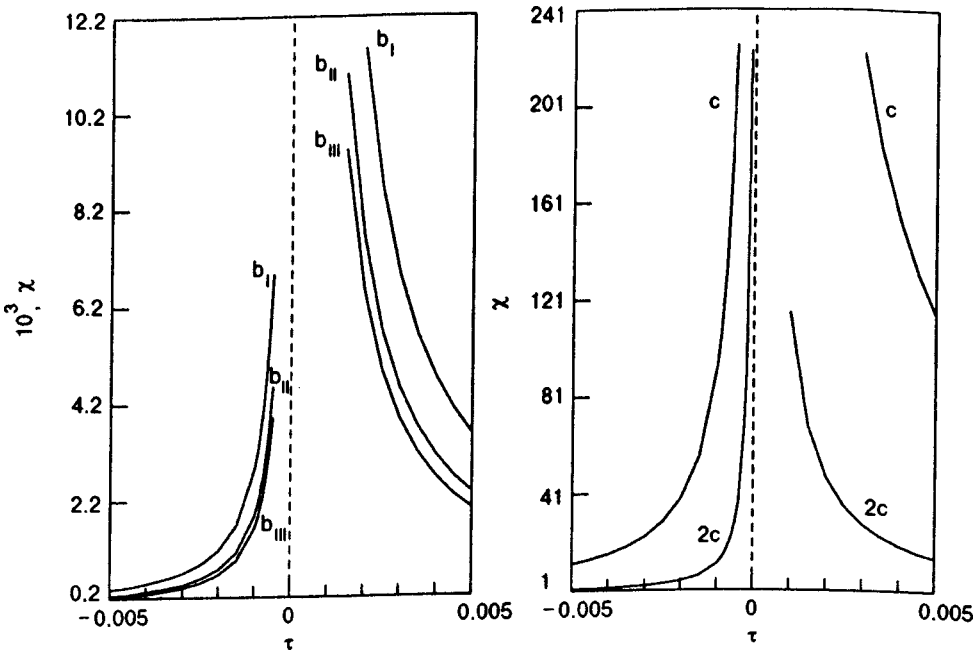

FIG. 4. Temperature dependence of the susceptibility of the system for various values of b. Notation is the same as in Fig. 1.

$$\chi=\Gamma^-|\tau|^{-\gamma}(1+a_\chi^-|\tau|^{\Delta_1})\frac{\mu_B^2}{\tilde{\Phi}(0)}. \tag{32}$$

Here $\gamma=2\nu$ is the critical exponent of susceptibility. The values of amplitudes Γ^- and a_χ^- are given in Table IV.[18]

Using the results of calculations for $T>T_c$[7] as well as the results obtained here, we can plot the graphs of temperature dependences of entropy S/kN, specific heat C/kN, and the susceptibility χ (in the units of μ_B^2/A, $A=\tilde{\Phi}(0)/[8\pi(b/c)^3]$ being the interaction potential constant) near T_c for various values of the effective radius b of the potential (see Figs. 2, 3, and 4). The method of calculation developed here allows us to trace the evolution of thermodynamic characteristics with increasing ratio of the effective radius b of the potential to the lattice constant c. Such an evolution of the free energy F/N of the system (in the units of A) at the phase transition point ($\tau=0$) as well as of the average spin moment $\langle\sigma\rangle$ for $\tau=-10^{-3}$ and the specific heat C/kN of the system for $|\tau|=10^{-3}$ is presented in Figs. 5, 6, and 7.

Thus, the critical behavior of the one-component spin system is described on the basis of sextic density of measure (ρ^6 model). As compared with the quartic approximation (ρ^4 model), the ρ^6 model ensures a more correct quantitative pattern of this description. This follows from the results of our previous calculations (see, for example, Refs. 5 and 6) as well as from the temperature dependences of the average spin moment $\langle\sigma\rangle$ (Fig. 8) and specific heat C/kN of the $3D$ Ising model (Fig. 9). The calculations were made for a simple cubic lattice in zero external field with the interaction between nearest neighbors. In our calculations, we put $b=b_I=c/(2\sqrt{3})$. The ρ^6 model approximation includes the first confluent correction, while the approximation on the basis of the ρ^4 model takes into account the first and second confluent corrections (see Refs. 11–14). The straight line *1*

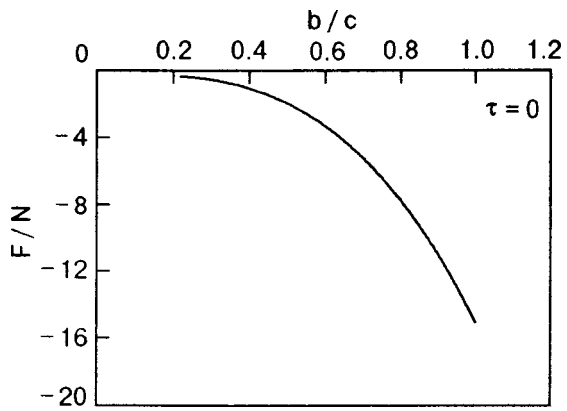

FIG. 5. Dependence of the free energy of the system at the phase transition point ($\tau=0$) on the ratio of the effective radius b of exponentially decreasing interaction potential to the simple cubic lattice constant c.

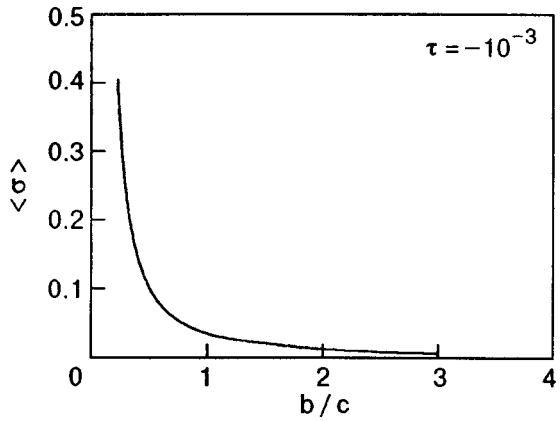

FIG. 6. Behavior of the average spin moment for $\tau=-10^{-3}$ with increasing ratio b/c.

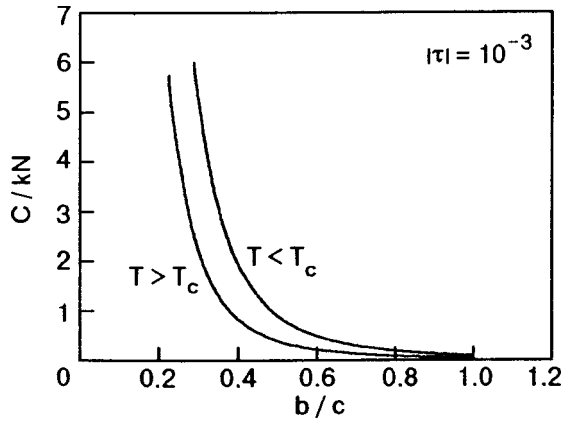

FIG. 7. Evolution of the specific heat of the system for $|\tau|=10^{-3}$ with increasing ratio b/c.

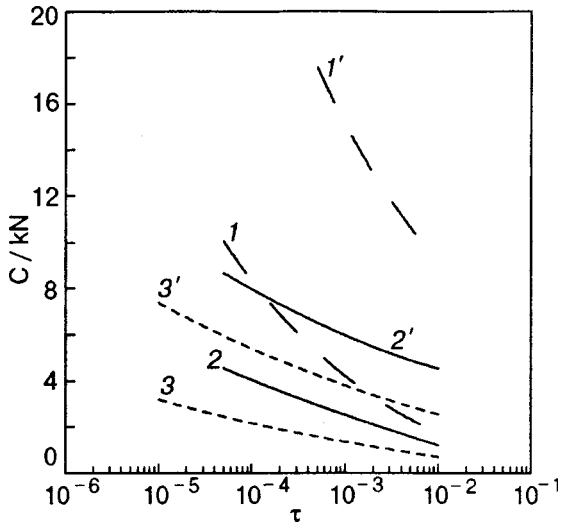

FIG. 9. Dependence of the specific heat of the system on $\tau=|T-T_c|/T_c$. Curves *1*, *2* and *3* correspond to $T>T_c$, curves *1′*, *2′* and *3′* correspond to $T<T_c$, curves *1* and *1′* correspond to the ρ^4 model, curves *2* and *2′* correspond to the ρ^6 model, and curves *3* and *3′* correspond to the results obtained in Ref. 19.

in Fig. 8 for the average spin moment corresponds to the ρ^4 model, line *2* to the ρ^6 model, and line *3* to the results obtain by Liu and Fisher[19] for $\tau=|T-T_c|/T_c$. The high-temperature region in Fig. 9 is presented by the curves *1*, *2* and *3*, while the low-temperature region by the curves *1′*, *2′* and *3′*. The curves *1* and *1′* were obtained on the basis of the ρ^4 model, curves *2* and *2′* in the ρ^6 model approximation, and curves *3* and *3′* correspond to the results obtained by Liu and Fisher.[19] It should be noted that the latter carried out a new numerical analysis of leading critical amplitudes of susceptibility, correlation length, specific heat, and spontaneous magnetization of a 3*D* Ising system, as well as universal relations between these amplitudes.

The CV method makes it possible to carry out the approximate calculation of the partition function of the system and to obtain universal (critical exponents) and nonuniversal quantities (expressions for leading critical amplitudes and the amplitudes of confluent corrections to thermodynamic characteristics) by using a unified approach. The results of calculations for a 3*D* Ising system on the basis of the ρ^4 and ρ^6 models are in accord with the results obtained by other authors. For example,[16] the critical exponents of the correlation length $\nu=0.637$, specific heat $\alpha=0.088$, the average spin moment $\beta=0.319$, the susceptibility $\gamma=1.275$, and the exponent of the first correction to scaling $\Delta_1=0.525$ (ρ^6 model, $s=s^*$), as well as universal ratios of critical amplitudes of specific heat $A^+/A^-=0.435$, susceptibility $\Gamma^+/\Gamma^-=6.967$ and their combination

$$\mathcal{P}=[1-A^+/A^-]/\alpha=3{,}054,$$

$$R_c^+=A^+T^+/[s_0^3(\langle\sigma\rangle^{(0)})^2]=0{,}098(\text{model } \rho^4, s=s^*),$$

where $s_0=\pi\sqrt{2}b/c$, $\langle\sigma\rangle^{(0)}$ is the critical amplitude of the average spin moment (see (25)), are in accord with the values $\nu=0.630$, $\alpha=0.110$, $\beta=0.325$, $\gamma=1.241$, $\Delta_1=0.498$, $A^+/A^-=0.465$, $\Gamma^+/\Gamma^-=5.12$, $\mathcal{P}=3.90$, $R_c^+=0.052$, obtained by using the field-theory approach[20–22] as well as with the values $\nu=0.638$, $\alpha=0.125$, $\beta=0.312$, $\gamma=1.250$, $\Delta_1=0.50$, $A^+/A^-=0.51$, $\Gamma^+/\Gamma^-=5.07$, $R_c^+=0.059$, calculated with the help of high-temperature expansions.[23–27] The methods existing at present make it possible to calculate universal quantities to a quite high degree of accuracy. The advantage of the method under investigation lies in the possibility to obtain and analyze expressions for thermodynamic characteristics as functions of microscopic parameters of the system.

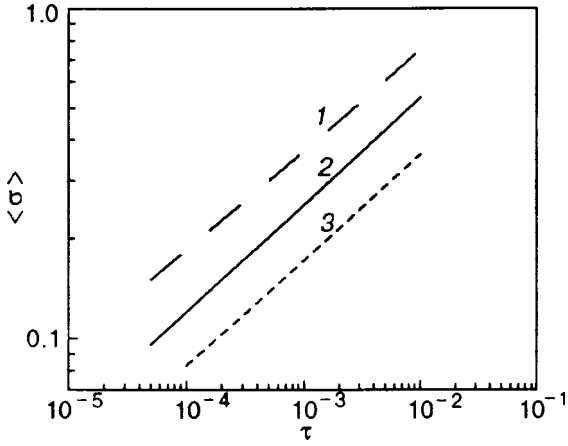

FIG. 8. Temperature dependence of the order parameter of the 3*D* Ising model for a simple cubic lattice. Straight line *1* corresponds to the ρ^4 model, line *2* to the ρ^6 model, and line *3* to the results obtained in Ref. 19.

This research was carried out under partial financial support of the State Foundation of Fundamental Studies at the Ukrainian Ministry of Science (Project No. 2.4/173).

*)E-mail: piv@icmp.lviv.ua

[1] G. A. Baker, Jr., *Quantitative Theory of Critical Phenomena*, Academic Press, Inc., San Diego (1990).
[2] J. J. Binney, N. J. Dowrick, A. J. Fisher, and M. E. J. Newman, *The Theory of Critical Phenomena. An Introduction to the Renormalization Group*, Clarendon Press, Oxford (1992).
[3] D. P. Landau, Physica A **205**, 41 (1994).
[4] C. Domb, *The Critical Point. A Historical Introduction to the Modern Theory of Critical Phenomena*, Taylor and Francis. Ltd., London (1996).

[5] I. R. Yukhnovskii, *Phase Transitions of the Second Order. Collective Variables Method*, World Scientific, Singapore (1987).
[6] V. V. Dukhovii, M. P. Kozlovskii, and I. V. Pylyuk, Teor. Mat. Fiz. **107**, 288 (1996).
[7] I. V. Pylyuk, Fiz. Nizk. Temp. **25**, 1170 (1999) [Low Temp. Phys. **25**, 877 (1999)].
[8] M. P. Kozlovskii, Ya. N. Ilnytskii, and I. V. Pylyuk, Preprint Inst. Theor. Phys., Acad. Sci. Ukr. SSR, ITP-85-107R, Kiev (1985).
[9] M. P. Kozlovskii and I. V. Pylyuk, Preprint Inst. Theor. Phys., Acad. Sci. Ukr. SSR, ITP-89-42R, Kiev (1989).
[10] I. R. Yukhnovskii, M. P. Kozlovskii, and I. V. Pylyuk, Z. Naturforsch., A: Phys. Sci. **46a**, 1 (1991).
[11] I. V. Pylyuk, Preprint Inst. Theor. Phys., Acad. Sci. Ukr. SSR, ITP-90-12R, Kiev (1990).
[12] I. V. Pylyuk and M. P. Kozlovskii, Izv. Akad. Nauk SSSR, Ser. Fiz. **55**, 597 (1991).
[13] M. P. Kozlovskii, I. V. Pylyuk, and I. R. Yukhnovskii, Teor. Mat. Fiz. **87**, 434 (1991).
[14] M. P. Kozlovskii and I. V. Pylyuk, Phys. Status Solidi B **183**, 243 (1994).
[15] M. P. Kozlovskii and I. V. Pylyuk, Preprint Inst. Theor. Phys., Acad. Sci. Ukr. SSR, ITP-90-81R, Kiev (1990).
[16] M. P. Kozlovskii, I. V. Pylyuk, and V. V. Dukhovii, Cond. Matt. Phys. (Lviv) **11**, 17 (1997).
[17] I. V. Pylyuk and M. P. Kozlovskii, Preprint Inst. Cond. Matt. Phys., National Academy of Sciences of the Ukraine, ICMP-97-06U, Lviv (1997).
[18] I. V. Pylyuk and M. P. Kozlovskii, Preprint Inst. Cond. Matt. Phys., National Academy of Sciences of the Ukraine, ICMP-97-07U, Lviv (1997).
[19] A. J. Liu and M. E. Fisher, Physica A **156**, 35 (1989).
[20] J. C. Le Guillou and J. Zinn-Justin, Phys. Rev. B **21**, 3976 (1980).
[21] C. Bagnuls, C. Bervillier, and E. Boccara, Phys. Lett. A **103**, 411 (1984).
[22] M. Barmatz, P. C. Hohenberg, and A. Kornblit, Phys. Rev. B **12**, 1947 (1975).
[23] D. S. Gaunt and M. F. Sykes, J. Phys. A **6**, 1517 (1973).
[24] D. M. Saul, M. Wortis, and D. Jasnov, Phys. Rev. B **11**, 2571 (1975).
[25] W. J. Camp and J. P. Van Dyke, Phys. Rev. B **11**, 2579 (1975).
[26] A. Aharony and P. C. Hohenberg, Phys. Rev. B **13**, 3081 (1976).
[27] W. J. Camp, D. M. Saul, J. P. Van Dyke, and M. Wortis, Phys. Rev. B **14**, 3990 (1976).

Translated by R. S. Wadhwa

Double-peaked character of the temperature dependence of resistance of perovskite manganites for a broadened ferromagnetic transition

A. I. Tovstolytkin,*) A. N. Pogorilyi, and S. M. Kovtun

Institute of Magnetism, National Academy of Sciences of the Ukraine, 252680 Kiev, Ukraine
(Submitted April 9, 1999; revised June 17, 1999)
Fiz. Nizk. Temp. **25**, 1282–1286 (December 1999)

The behavior of a system consisting of a mixture of paramagnetic semiconducting and ferromagnetic metallic phases is examined in the framework of the percolation model. As the temperature decreases below the Curie point, the paramagnetic phase fraction is assumed to decreases according to an exponential law. The evolution of the temperature variation of the resulting resistance is considered as a function of the magnetic transition broadening. An explanation is offered for the low-temperature resistance anomaly observed experimentally in a number of perovskite manganites. © *1999 American Institute of Physics.*
[S1063-777X(99)00612-X]

The interest towards the substituted manganites of the system $R_{1-x}A_xMnO_3$ (where R is a rare-earth element and A=Ba, Sr, Ca, etc.) is aroused by the prospects of their practical application as magnetoresistive materials, as well as by their unique electrical and magnetic properties.[1,2] Compounds with $x=0$ and 1 are antiferromagnetic insulators, but compounds with intermediate composition are ferromagnets with a metallic behavior at temperatures below the Curie point T_C.[3,4] The common features of such materials are the existence of a resistivity peak near T_C and a colossal magnetoresistance (CMR) associated with the suppression of this peak by a magnetic field. Zener[5] explained the ferromagnetism of substituted manganites by introducing the concept of double exchange interaction between Mn^{3+} and Mn^{4+} ions. Later, this concept was generalized and given a mathematical formulation by Anderson and Hasegawa[6] and de Gennes.[7] However, attempts to use this model for explaining a number of effects including CMR were not quite successful.[8,9] The properties of perovskite manganites were explained in Refs. 8, 10, and 11 on the basis of strong electron–phonon and ferromagnetic interactions leading to dynamic phase separation in the form of magnetic polarons. The idea of electron–impurity phase separation and magnetic impurity scattering of charge carriers in degenerate ferromagnetic semiconductors was used in Refs. 9, 12, and 13 to explain CMR, but a complete understanding of the properties of substituted manganites has not been attained so far.

Recently, an extra low-temperature peak was observed (in addition to the peak near the Curie point) on the temperature dependence of R of the electrical resistance in a number of samples belonging to the systems $(La, Ce)MnO_3$ and $(La, Sr)MnO_{3-\delta}$.[14–16] Even before that, Tang *et al.*[17] had observed similar $R(T)$ curves in polycrystalline samples of $(La, A)(Mn, Cu)O_{3-\delta}$ (A=Sr, Ba). Zhang *et al.*[18] attributed the lowtemperature resistivity peak formed as a result of a decrease in the granule size in the perovskite $La_{0.85}Sr_{0.15}MnO_3$ to the tunneling between granules occurring due to different values of the Curie temperature at the granule surface and inside the granules. Steenbeck *et al.*[15] studied films with one grain boundary (on a bicrystalline substrate) and associated the two-peak $R(T)$ dependence with a reduced T_C value in the boundary region. However, such mechanisms cannot explain the behavior of epitaxial films investigated, among others, by Izumi *et al.*[19] However, any explanation was not offered in Ref. 19 for the emergence of the second peak upon a decrease in the film thickness. It should be emphasized in particular that in all the cases described in Refs. 14–19, no magnetic or structural peculiarities which could lead to anomalies in electrical properties were observed below the Curie point. We have used a simple phenomenological model to show that the emergence of a low-temperature anomaly on the $R(T)$ dependence in perovskite manganites may be due to a strong temperature broadening of the ferromagnetic transition.

Recent investigations have shown that paramagnetic and ferromagnetic phases can coexist over a wide temperature range below the Curie point in substituted manganites.[11,14,20,21] Chechersky *et al.*[21] and Simopoulos *et al.*[22] have described the temperature dependence of the fraction of the paramagnetic phase ($T \leqslant T_C$) obtained for some Ca-based manganites experimentally as a result of Mössbauer spectral studies. An analysis of the data presented in these works shows that the magnetic transition may be stretched down to the lowest temperatures (in the samples studied by Chechersky *et al.*,[21] the fraction of the nonmagnetic phase is about 20% even for $T/T_C=0.4$), and a part of the sample may remain paramagnetic even at absolute zero.[17–19] A distinguishing feature of CMR manganites is a strong dependence of their electric properties on the magnetic state: the ferromagnetic phase has the metallic-type conductivity ($dR/dT>0$), while the paramagnetic phase displays the semiconductor-type conductivity.[10,11,21,23] Considering that the dependences $R(T)$ are of opposite sign in the two phases,

the resulting resistance may be quite complex in the regime of coexistence of the two phases, as is indeed observed in some experiments.[14–19]

Let us consider the behavior of a two-phase system consisting of a mixture of paramagnetic and ferromagnetic phases which have different types of conductivity. We denote the resistivity of the material in the two phases by R_p and R_f respectively. We assume that the concentration of each phase (φ_p and φ_f) is a function of temperature, and that both phases coexist in a certain temperature interval below $T_C(\varphi_p+\varphi_f=1)$. Having defined the specific form of the curves $R_p(T)$ and $R_f(T)$, we analyze the evolution of the temperature dependence of the resulting resistance of the system upon a variation of the parameter $\varphi_p(T)$ or $\varphi_f(T)$.

An analysis of extensive experimental material[3,17,24,25] shows that the temperature variation of the resistance of the ferromagnetic phase in each specific case can be described by different functions (from a power function to an exponential function), and it would seem that a universal form of the function $R_f(T)$ does not exist. However, investigations carried out by Snyder *et al.*[23] in samples of bulk poly- and single crystals, as well as in well-annealed polycrystalline thin films of substituted manganites, show that in all the cases, the resistance R_f of the ferromagnetic phase can be presented with a fairly high degree of accuracy in the form

$$R_f=B+Ct^2, \tag{1}$$

which apparently reflects a strong electron correlation in these materials (t is the temperature normalized to T_C, while B and C are constants). A similar expression was obtained by Urushibara *et al.*[3] for single crystals of the system $La_{1-x}Sr_xMnO_3$.

A thorough experimental investigation of the electric properties of films and bulk samples of $La_{0.67}A_{0.33}MnO_3$ (A=Ca, Sr) was carried out by Snyder *et al.*[23,26] above the Curie point over a wide temperature range (up to 1200 K). The authors examined the range of applicability of various models, viz., variable range hopping conductivity, semiconductor-type conductivity, and small polaron hopping conductivity, in adiabatic and nonadiabatic approximations for describing the resistance of the paramagnetic phase of these materials. It was shown that the temperature dependence of R_p can be best described by the formula

$$R_p=At\exp(E/t), \tag{2}$$

corresponding to the small polaron hopping conductivity in the adiabatic approximation (E is the activation energy of a polaron and A is a constant).

Chechersky *et al.*[21] and Simopoulos *et al.*[22] used the Mössbauer spectroscopy technique for measuring the temperature dependence of the volume fraction of the paramagnetic phase φ_p for samples of $La_{1-x}Ca_xMnO_3$ (x=0.2,0.3). Some indirect data, e.g., for samples investigated by Chen and de Lozanne,[27] can be obtained by comparing the temperature dependence of the magnetization of epitaxial and polycrystalline films having the same composition and prepared under identical conditions but on different substrates. Assuming that the fraction of the ferromagnetic phase below T_C is 100% in an epitaxial film, the ratio of magnetization of the investigated samples can be used to estimate the ratio of φ_p and φ_f in the polycrystalline film. A similar procedure can be adopted for samples studied by Izumi *et al.*[19] An analysis carried out by us for $\varphi_p(T)$ curves obtained in Refs. 17–19, 21, 22, and 27 shows that a single formula cannot be found for describing the temperature dependence of ratio of paramagnetic and ferromagnetic phase concentrations. However, we found that the probability of the emergence of low-temperature peak on the $R(T)$ curve increases with an extension of the temperature interval of coexistence of the two phases. The simplest function enabling a variation of the width of such a temperature interval with the help of a single variable is an exponential function. For computations of the fraction φ_p of the paramagnetic phase, we shall assume that

$$\varphi_p=1, \quad (t>1),$$

$$\varphi_p=\exp[(t-1)/d], \quad (t\lesssim 1), \tag{3}$$

where the parameter d characterizes the transition width. It should be remarked that the values of φ_p obtained in Refs. 17, 18, 21, and 27 do not vanish even at the lowest temperatures. Hence the theoretical analysis must cover the case $d<1$ as well as $d\geqslant 1$.

The total resistance R of the system was calculated from the formula which was derived by McLachlan[28] for a two-phase system and which can be transformed as follows:

$$\frac{\varphi_p(R^{1/g}-R_p^{1/g})}{(R^{1/g}+KR_p^{1/g})}+\frac{(1-\varphi_p)(R^{1/g}-R_f^{1/g})}{(R^{1/g}+KR^{1/g})}=0, \tag{4}$$

where

$$K=\frac{\varphi_p^c}{(1-\varphi_p^c)}.$$

In this case, the following condition must be satisfied:

$$R_f\ll R_p. \tag{5}$$

By φ_p^c we mean the critical volume fraction of the high-resistivity (paramagnetic in the present case) phase. The value of g is determined by the morphology of the system and is a function of φ_p^c and the effective demagnetization coefficient L:[28]

$$g=\frac{\varphi_p^c}{(1-L)}.$$

We carried out all the computations by considering the spherically symmetric case and putting $L=1/3$. The critical volume fraction φ_f^c of the metallic phase at which percolation takes place was assumed to be 0.16, which is in accord with the experimental results and the theoretical analysis of the behavior of CMR manganites.[29] The corresponding critical value for the paramagnetic (high-resistivity) phase in this case is equal to $\varphi_p^c=1-\varphi_f^c=0.84$. Such a choice of φ_f^c and L gives $g=1.26$ and $K=5.25$ in Eq. (4).

Figure 1 shows the temperature dependence of the amount of the paramagnetic phase φ_p and the resulting resistance R of a two-phase system calculated by using formu-

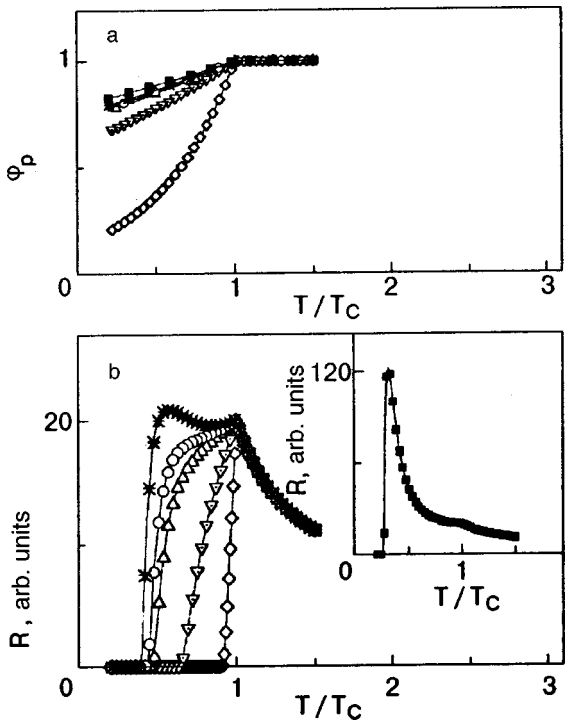

FIG. 1. Temperature dependence of the amount of paramagnetic phase φ_p (a) and electric resistivity R (b) in a two-phase system for different values of the parameter d: 0.5 (◇), 2.0 (∇), 3.0 (Δ), 3.2 (○), 3.45 (*), and 4.2 (■).

las (1)–(4) for different values of the parameter d. Calculations were made for the following values of the coefficients appearing in Eqs. (1) and (2):

$$B=C=10^{-4}, \quad A=1, \; E=3.$$

Such a choice of the coefficients was made, on the one hand, from an analysis carried out in Refs. 14, 23, and 26 and, on the other hand, in view of the constraint imposed by the inequality (5) on functions R_p and R_f.

It can be seen clearly from Fig. 1(b) that an initial increase in d causes a broadening of the resistive transition. However, beginning from $d \cong 3.2$, a second peak is formed on the $R(t)$ dependence at low temperatures. A further increase in the value of d is accompanied by a sharp rise in the low-temperature peak, and only an insignificant singularity, which may be hard to detect experimentally, emerges for $d \geqslant 4.2$ in the vicinity of the Curie point ($t=1$). Great care should be exercised in such cases while interpreting the experimental results and comparing the resistive data with the magnetic data.

It should be noted that the strong temperature broadening of the magnetic transition is a phenomenon encountered quite frequently in substituted manganites. Apparently, this is due to a competition between different types of interaction characterizing these materials,[3,10,11] as well as to a strong dependence of the magnetic properties on the microstructure, mechanical stresses, degree of disorder, and chemical inhomogeneities.[23] It is also worthwhile to note that it may not be quite easy to determine the Curie point correctly under such conditions as was mentioned, for example, by Mitchell *et al.*[30] Strongly broadened transitions were observed experimentally by different methods.[11,14,17,21,30] Regarding the topic of our investigations, the most illustrative results were obtained in Refs. 17, 19, and 27 where a correlation between the magnetic transition broadening and the emergence of the low-temperature resistive anomaly can be traced clearly.

Thus, we have analyzed the electrical properties of a system consisting of paramagnetic and ferromagnetic phases which have different types of conductivity and coexist over a wide temperature interval. It is shown that in spite of the monotonic variation of the magnetic and electric properties of each phase, the resulting resistance may exhibit a number of anomalies in the region of coexistence of phases. The presented data point towards the possibility of realizing such a situation in substituted manganites.

The authors are indebted to A. Ya. Vovk for fruitful discussions on the subject of investigations.

This research was partially supported by the US Civilian Research and Development Foundation (CRDF), Project No. UP1-370.

*)E-mail: atov@imag.kiev.ua

[1] R. von Helmolt, J. Wecker, B. Holzapfel *et al.*, Phys. Rev. Lett. **71**, 2331 (1993).
[2] S. Jin, T. H. Tiefel, M. McCormack *et al.*, Science **264**, 413 (1994).
[3] A. Urushibara, Y. Moritomo, T. Arima *et al.*, Phys. Rev. B **51**, 14103 (1995).
[4] A. A. Mukhin, V. Yu. Ivanov, V. D. Travkin *et al.*, JETP Lett. **68**, 356 (1998).
[5] C. Zener, Phys. Rev. **81**, 440 (1951).
[6] P. W. Anderson and H. Hasegawa, Phys. Rev. **100**, 675 (1955).
[7] P.-G. de Gennes, Phys. Rev. **118**, 141 (1960).
[8] A. J. Millis, P. B. Littlewood, and B. I. Shraiman, Phys. Rev. Lett. **74**, 5144 (1995).
[9] E. L. Nagaev, Usp. Fiz. Nauk **166**, 833 (1996).
[10] M. R. Ibarra and J. M. De Teresa, J. Magn. Magn. Mater. **177–181**, 846 (1998).
[11] W. Archibald, J.-S. Zhou, and J. B. Goodenough, Phys. Rev. B **53**, 14445 (1996).
[12] E. L. Nagaev, Usp. Fiz. Nauk **168**, 917 (1998).
[13] V. N. Krivoruchko, Fiz. Nizk. Temp. **22**, 1047 (1996) [Low Temp. Phys. **22**, 798 (1996)].
[14] P. Mandal and S. Das, Phys. Rev. B **56**, 15073 (1997).
[15] K. Steenbeck, T. Eick, K. Kirsch *et al.*, Appl. Phys. Lett. **73**, 2506 (1998).
[16] A. N. Pogorilyi, N. A. Belous, A. I. Tovstolytkin *et al.*, Fiz. Nizk. Temp. **25**, 97 (1999) [Low Temp. Phys. **25**, 74 (1999)].
[17] Yi Tang, I. Shaltout, R. Braunstein *et al.*, Phys. Status Solidi B **182**, 509 (1994).
[18] N. Zhang, W. Ding, W. Zhong *et al.*, Phys. Rev. B **56**, 8138 (1997).
[19] M. Izumi, Y. Konishi, T. Nishihara *et al.*, Appl. Phys. Lett. **73**, 2497 (1998).
[20] M. K. Gubkin, A. V. Zalesskii, V. G. Krivenko *et al.*, JETP Lett. **60**, 57 (1994).
[21] V. Chechersky, A. Nath, H. Ju, and R. L. Greene, Fiz. Nizk. Temp. **23**, 727 (1997) [Low Temp. Phys. **23**, 536 (1997)].
[22] A. Simopoulos, G. Kallias, E. Devlin *et al.*, J. Magn. Magn. Mater. **177–181**, 860 (1998).
[23] G. J. Snyder, R. Hiskes, S. DiCarolis *et al.*, Phys. Rev. B **53**, 14434 (1996).
[24] M. Rubinstein, D. J. Gillespie, J. E. Snyder, and T. M. Tritt, Phys. Rev. B **56**, 5412 (1997).
[25] S. I. Khartsev, V. N. Krivoruchko, and V. P. Pashchenko, Fiz. Nizk. Temp. **23**, 841 (1997) [Low Temp. Phys. **23**, 631 (1997)].

[26] D. C. Worledge, G. J. Snyder, M. R. Beasley *et al.*, J. Appl. Phys. **80**, 5158 (1996).
[27] C. C. Chen and A. de Lozanne, Appl. Phys. Lett. **73**, 3950 (1998).
[28] D. S. McLachlan, J. Phys. C **20**, 865 (1987).
[29] L. P. Gor'kov, Usp. Fiz. Nauk **168**, 665 (1998).
[30] J. F. Mitchell, D. N. Argyriou, C. D. Potter *et al.*, Phys. Rev. B **54**, 6172 (1996).

Translated by R. S. Wadhwa

Exact instanton solution for quantum tunneling in an uncompensated antiferromagnet

B. A. Ivanov and V. E. Kireev

*Institute of Magnetism, National Academy of Sciences of the Ukraine, 252142 Kiev, Ukraine**

(Submitted April 21, 1999)
Fiz. Nizk. Temp. **25**, 1287–1294 (December 1999)

An exact instanton solution describing macroscopic quantum tunneling for a small antiferromagnetic particle with uncompensated spin and biaxial quadratic anisotropy is constructed. The solution is valid for any relation between anisotropy parameters and relative value of uncompensated spin. The obtained solution is used for calculating the tunneling amplitude taking into account the pre-exponential factor. The amplitude is characterized by a nonanalytic dependence on the ratio of small parameters of the problem, viz., anisotropy in the basal plane and the value of uncompensated spin. © *1999 American Institute of Physics.* [S1063-777X(99)00712-4]

INTRODUCTION

During the last decade, the macroscopic quantum tunneling in magnetic systems has been studied intensely both experimentally and theoretically.[1] Special attention is paid to coherent macroscopic quantum tunneling (CMQT) between states in systems with a discrete degeneracy of the ground state, which are equivalent from the energy point of view, but different physically. This effect can be observed experimentally from the resonant absorption of electromagnetic waves at energy levels split due to tunneling. The interest to this phenomenon is due to the following two factors. First, fine and elegant effects of interference of instanton trajectories emerging in such problems lead to suppression of tunneling for a half-integral spin of the system[2,3] and to oscillatory dependences of tunnel splitting of energy levels on extrinsic parameters.[4,5] Second, the manifestation of CMQT effects is not masked by thermal fluctuations in contrast to the effects of quantum ''escape'' from a metastable to a stable state.

First investigations[6,7] were carried out for small ferromagnetic particles under the assumption that all spins in a particle are parallel (the large spin model). It was found later that antiferromagnets (AFM) are more convenient objects for CMQT studies. According to calculations,[8,9] the energy level splitting in AFM is stronger than in FM, and the effects can be observed at a higher temperature. It is not surprising that CMQT effects were first observed for ferritin particles possessing the antiferromagnetic structure.[10]

It was noted[11–13] that pure AFM, i.e., antiferromagnets with complete compensation of spin, do not exist on the mesoscopic level. At present, ''high-spin'' complexes characterized by the antiferromagnetic interaction in the presence of an uncompensated spin are being considered by many authors. Chiolero and Loss[13] studied tunneling in an uncompensated AFM on the basis of the σ model (which is normally used for pure AFM) generalized to the case of incomplete compensation. These equations are a combination of the Lorentz-invariant σ model and the Landau–Lifshitz equations.[13–15] A peculiar feature of their solutions is that a transition form the antiferromagnetic behavior to ferromagnetic one occurs for a small decompensation (the ratio of the difference in the spins of the sublattices to their sum), which is manifested in the dynamics of nonlinear waves[14] as well as for CMQT.[13] However, Chiolero and Loss[13] analyzed only one limiting case of a strong easy-plane anisotropy. In this case, the equations for FM as well as AFM can be reduced to Lorentz-invariant models for a scalar variable. However, the relation between the anisotropy parameters for high-spin complexes $Mn_{12}Ac$[16] or Fe_8[17] is different, namely, easy-axis anisotropy takes place, and such a simplification is incorrect.

In the present communication, we construct an exact instanton solution for a small antiferromagnetic particle with an uncompensated spin and biaxial quadratic anisotropy. The solution is valid for any relation between anisotropy parameters and the relative value of uncompensated spin. The obtained solution is used for calculating the WKB exponent and the pre-exponential factor (which is determined by the fluctuation determinant) for the tunneling amplitude. It was found that in contrast to Ref. 13, the CMQT amplitude is characterized by a nonanalytic dependence on the parameters of the problem, namely, the relation between anisotropy in the basal plane and the magnitude of the uncompensated spin.

1. MODEL

Let us consider a system of spins in which nearest neighbors are coupled through antiferromagnetic interaction and belong to two magnetic sublattices. In the ground state, the total spins $\mathbf{S}_1$ and $\mathbf{S}_2$ of the sublattices are antiparallel. The total spin $\mathbf{S}=\mathbf{S}_1+\mathbf{S}_2$ differs from zero due to decompensation of the sublattices, $S_1 \neq S_2$. Since we are interested in the case $|S_1-S_2| \ll S_{1,2}$, the dynamics of the system is described in terms of the antiferromagnetism unit vector $\mathbf{l}$, where $\mathbf{l}=(\mathbf{S}_1-\mathbf{S}_2)/|\mathbf{S}_1-\mathbf{S}_2|$, and the total spin is a subordinate variable and is determined by $\mathbf{l}$ and $\dot{\mathbf{l}}$.[14,15]

In order to describe the dynamics of the vector $\mathbf{l}$, we shall proceed from the effective Lagrangian obtained in Refs.

13 and 15. The Euclidean version of the Lagrangian can be presented in the form

$$\mathcal{L}=\frac{\hbar S_{\rm tot}}{\gamma H_e}\left[\frac{1}{2}(\dot\theta^2+\dot\varphi^2\sin^2\theta)-i\omega_n\dot\varphi(1-\cos\theta)\right]+w_a(\theta,\varphi). \tag{1}$$

Here the dot denotes the derivative with respect to the imaginary time τ, θ and φ are the polar coordinates of the unit vector $\mathbf{l}$, $S_{\rm tot}=S_1+S_2$ is the maximum value of the spin of the system, H_e the exchange field, $\gamma=2\mu_B/\hbar$ the gyromagnetic ratio, $\omega_n=\gamma H_e S_{\rm ex}/S_{\rm tot}$ the parameter having the dimensions of frequency and describing decompensation, $S_{\rm ex}=|S_1-S_2|$, and $w_a(\theta,\varphi)$ is the magnetic anisotropy energy whose form is not specified so far.

Lagrangian (1) consists of three terms. They include the kinetic term proportional to $\dot{\mathbf{l}}^2$, which is typical of pure AFM with $S_1=S_2$, the gyroscopic term proportional to the first derivative of the $\mathbf{l}$ vector components with respect to τ and typical of ferromagnets, and anisotropy playing the role of potential energy.

Let us consider possible limiting cases. If $S_1=S_2$, i.e., $\omega_n=0$, we naturally obtain the Lagrangian of the σ model for a pure AFM. A transition to the Lagrangian for a ferromagnet is not a trivial operation. The dynamics of the vector $\mathbf{l}$ approximately corresponds to the dynamics of ferromagnets with increasing ω_n to values of the order of $\gamma(H_e/H_a)^{1/2}$, where H_a is the anisotropy field. Formally, we can obtain from (1) the Lagrangian of a ferromagnet by eliminating the term quadratic in the derivatives, for example, with the help of the substitution $\hbar S_{\rm tot}/\gamma H_e\to C\hbar S_{\rm tot}/\gamma H_e$, $\omega_n\to\omega_n C^{-1}$ and the limiting transition $C\to 0$. To match the constants, we must put $\omega_n=\gamma H_e$. However, such a procedure is not quite correct since it should be borne in mind that the omission of the term proportional to $\dot{\mathbf{l}}^2$ changes the structure of the system Hamiltonian, namely, the dimensionality of the phase space diminishes by a factor of two. In the case of AFM, we can treat the angles θ and φ parmetrizing $\mathbf{l}$ as canonic variables, and the corresponding momenta contain $\dot\theta$ and $\dot\varphi$, while the Hamiltonian variables for a ferromagnet can be expressed only in terms of $\mathbf{l}$. For example, we can choose φ and $\cos\theta$ as a canonic pair. In other words, an uncompensated AFM (as well as pure AFM) is equivalent to a system with two degrees of freedom, while an FM corresponds to a system with one degree of freedom.

In a popular model of strong easy-plane anisotropy, equations of motion give the approximate relation $\theta\simeq\text{const}\,\dot\varphi$. In this case, the Lagrangian acquires the standard form in mechanics, i.e., $M_{\rm eff}(\varphi)\dot\varphi^2/2+W(\varphi)$, where $M_{\rm eff}(\varphi)$ and $W(\varphi)$ are the effective mass and potential determined by the parameters of the system. This approximation was essentially used by Chiolero and Loss[13] for an analysis of instantons in a ferromagnet. In other words, the problem was reduced to a mechanical system with one degree of freedom. It will be proved later that the inclusion of the actual Hamiltonian structure of the equations of motion equivalent to a mechanical system with two degrees of freedom leads to considerable singularities of instanton solutions and important physical effects in CMQT.

An instanton solution is a separatrix trajectory of the dynamic system, connecting a pair of equivalent minima $\mathbf{l}_{\pm}^{(0)}$ of the potential w_a, i.e., the boundary conditions have the form $\mathbf{l}\to\mathbf{l}_{\pm}^{(0)}$ for $\tau\to\pm\infty$. It follows that $\dot{\mathbf{l}}\to 0$ for $\tau\to\pm\infty$. In order to construct an arbitrary solution of the equations of motion for a system with two degrees of freedom, we must know two independent integrals of motion for this system. One of them is an Euclidean analog of the total energy:

$$E=\frac{\hbar S_{\rm tot}}{\gamma H_e}\,\frac{\dot\theta^2+\dot\varphi^2\sin^2\theta}{2}-\omega_a(\theta,\varphi). \tag{2}$$

However, the second integral of motion cannot be indicated easily. It can be constructed in a trivial manner only in the case when anisotropy is purely uniaxial, and w_a depends only of the projection of $\mathbf{l}$ on a certain crystallographic axis $\mathbf{n}$, $w_a=w_a(\mathbf{n}\cdot\mathbf{l})$. In particular, for $\mathbf{l}_{\pm}^{(0)}\|\mathbf{n}$, a purely easy-axis case takes place.

Unfortunately, none of the Noether integrals of motion (the integral of motion associated with the symmetry of w_a in our case) can be used for constructing instanton solutions of the complete system of equations describing the dynamics of the vector $\mathbf{l}$. The situation in our case is actually the same as in an analysis of domain walls in ferromagnets. They are also described by separatrix solutions of the form $\mathbf{l}=\mathbf{l}(\xi)$, where $\xi=x-vt$, x being the coordinate of the wall and v its velocity (see Ref. 18). The only integral of motion connected with the symmetry of anisotropy energy is the projection of $\mathbf{l}$ on the easy axis $\mathbf{n}$, but the motion of the wall is impossible when $\mathbf{n}\cdot\mathbf{l}$ is conserved.

An analysis of dynamic systems with more than one degree of freedom, in particular, the construction of integrable systems, is a classical problem in analytic dynamics. This problem is being studied intensely even now, and a number of important results were obtained in recent years.[19] Among integrable systems, the models of unit vector dynamics are also encountered. By way of an example, we can consider the Neumann classical problem[20] on the motion of a material point over a sphere in the field of a potential which is a quadratic function of Cartesian coordinates. A number of generalizations of this problem have been obtained recently, e.g., a more general form of integrable potentials was constructed,[19] and the effect of gyrotropic terms was also discussed.[21]

In our case, it is important that the system with $w_a=\beta_{ik}l_i l_k$ and a gyrotropic term of the type of the field of a monopole (1) is integrable. Integrable systems of such type with another form of the potential and other gyrotropic terms do not exist to our knowledge. Various forms of the second integral of motion are given in Refs. 21 and 22. The integrability of model (1) also follows from the exact integrability of the Landau–Lifshitz equations for the magnetization of a one-dimensional ferromagnet, which was established by Sklyanin.[23] Indeed, the Lagrangian for a ferromagnet can be reduced to (1) by the wave ansatz $\xi=x-vt$ after a certain change in notation.

2. STRUCTURE OF INSTANTON SOLUTION

We shall consider the case of second-order rhombic anisotropy, which is integrable (see above). We choose w_a in the form

$$w_a=\frac{\hbar S_{\rm tot}}{2\gamma H_e}(\omega_z^2\cos^2\theta+\omega_y^2\sin^2\theta\sin^2\varphi) \tag{3}$$

and assume that $0<\omega_y\leqslant\omega_z$. The frequencies ω_y and ω_z are proportional to the roots of widely used anisotropy fields H_{az} and H_{ay}, i.e., $w_{z,y}=\gamma(H_eH_{ax,y})^{1/2}$. With such a choice of the form of w_a and the relation between the constant, Ox is an easy axis, Oy an intermediate axis, and Oz a difficult axis. The potential w_a has two symmetric minima for $\theta=\pi/2$ ($\varphi=0$ and $\varphi=\pi$) between which tunneling can take place.

Since the system of equations is integrable, we can analyze any of its solutions, for example, by separating variables in the corresponding Hamilton–Jacobi equation. In particular, we can construct in this way the instantons periodic in τ, which are required for describing tunneling at a finite temperature.[24,25] Moreover, the possibility of separating variables in the Hamilton–Jacobi equation indicates that variables can also be separated in the Schrödinger equation obtained by canonic quantization of the variables θ and φ. This approach was used for system with one degree of freedom.[26,27]

However, in order to construct a simple instanton solution, it is sufficient to use a property of the corresponding solution of the problem in real time. It is known that in this solution the motion takes place in a planar cross section of the unit sphere. It was found that the generalization of this property can be carried out for imaginary time also.

For this purpose, we rotate $\mathbf{l}$ about the easy axis Ox through an angle α:

$$\begin{aligned}&\cos\theta\to\cos\theta\cos\alpha+\sin\theta\sin\varphi\sin\alpha,\\&\sin\theta\cos\varphi\to-\cos\theta\sin\alpha+\sin\theta\sin\varphi\cos\alpha\end{aligned} \tag{4}$$

and transform the Lagrangian. Rotation (4) leaves the kinetic term invariant, while the gyroscopic term acquires a correction in the form of the total derivative with respect to τ, which is insignificant for equations of motion, but is important for calculating action from the obtained trajectories. After the transformation (4), the equations of motion acquire the form

$$\begin{aligned}&-\ddot\theta+\dot\varphi^2\sin\theta\cos\theta-i\omega_n\dot\varphi\sin\theta+\sin\theta\cos\theta[(\omega_z^2\sin^2\alpha\\&\quad+\omega_y^2\cos^2\alpha)\sin\varphi-(\omega_z^2\cos^2\alpha+\omega_y^2\sin^2\alpha)]\\&\quad+(\cos^2\theta-\sin^2\theta)(\omega_z^2-\omega_y^2)\cos\alpha\sin\alpha\sin\varphi=0,\\&-\ddot\varphi\sin^2\theta-2\dot\theta\dot\varphi\sin\theta\cos\theta+i\omega_n\dot\theta\sin\theta\\&\quad+(\omega_z^2\sin^2\alpha+\omega_y^2\cos^2\alpha)\sin^2\theta\sin\varphi\cos\varphi\\&\quad+(\omega_z^2-\omega_y^2)\sin\alpha\cos\alpha\sin\theta\cos\theta\cos\varphi=0.\end{aligned} \tag{5}$$

We choose the boundary conditions in the form $\mathbf{l}_-=\mathbf{e}_x$ and $\mathbf{l}_+=-\mathbf{e}_x$, i.e., $\theta(\pm\infty)=\pi/2$; $\varphi(-\infty)=0$, $\varphi(+\infty)=\pi$. We put $\theta=\pi/2$ in this system, which does not contradict the boundary conditions, and obtain the following redefined system of two equations in the dynamic variable φ:

$$\begin{aligned}&i\omega_n\dot\varphi=-(\omega_z^2-\omega_y^2)\sin\alpha\cos\alpha\sin\varphi,\\&\ddot\varphi=(\omega_z^2\sin^2\alpha+\omega_y^2\cos^2\alpha)\sin\varphi\cos\varphi.\end{aligned} \tag{6}$$

It can easily be seen that these equations can be made compatible by an appropriate choice of the parameter α.

Let us first consider a degenerate case, For a pure AFM with $\omega_n=0$ and $\omega_z\neq\omega_y$, the first equation is transformed into an identity if $\alpha=\pi k/2$, where k is an integer. The second equation gives an instanton solution of the standard form $\sin\varphi=\pm\cosh^{-1}\omega(\tau-\tau_0)$ with $\omega=\omega_y$ or ω_z depending on whether the value of k is even or odd respectively. The former case corresponds to instantons with $\mathbf{l}$ rotated through the intermediate axis, and the latter to rotation through the difficult axis. It can easily be verified that a pair of instantons with π multiple to α has a smaller value of the real component $\mathrm{Re}\,\mathcal{A}_{\rm Eu}=2\omega_y\hbar S_{\rm tot}/\gamma H_e$, of the Euclidean action than a pair of instantons of the second type.

In the case under investigation with $\omega_n\neq0$, solutions exist only for $\omega_z\neq\omega_y$, i.e., in the presence of anisotropy in the basal plane. We obtain the compatibility equation for the redefined system (6) in the form

$$i(\omega_z^2-\omega_y^2)\sin\alpha\cos\alpha=(\omega_z^2\sin^2\alpha+\omega_y^2\cos^2\alpha)^{1/2}, \tag{7}$$

which shows that α is a complex number, i.e.,

$$\alpha=\frac{\pi k}{2}+\frac{i}{2}\,\mathrm{arccosh}\,\frac{[(\omega_z^2+\omega_y^2+\omega_n^2)^2-4\omega_y^2\omega_z^2]^{1/2}-\omega_n^2}{\omega_z^2-\omega_y^2}, \tag{8}$$

and transformation (4) is a composition of ordinary and hyperbolic rotations. As in the case $\omega_n\neq0$, four instantons exist in this case. Even k correspond to a pair of instantons for which the plane of rotation of $\mathbf{l}$ contains the intermediate axis, while odd k correspond to rotations through the difficult axis. Instanton solutions have the form

$$\varphi=\pm2\arctan e^{\Omega(\tau-\tau_0)}, \tag{9}$$

where τ_0 is an arbitrary constant and

$$\Omega=\frac{1}{2}[\sqrt{\omega_n^2+(\omega_z+\omega_z)^2}\pm\sqrt{\omega_n^2+(\omega_z-\omega_y)^2}]. \tag{10}$$

The minus sign corresponds to an instanton with the rotation of $\mathbf{l}$ through the intermediate axis and the plus sign, through the difficult axis. Direct calculations show that instantons passing through the intermediate axis have a smaller real component of action than the instantons passing through the difficult axis for any relation between ω_n, ω_y, and ω_z. The latter instantons do not give even a local minimum of $\mathrm{Re}\,\mathcal{A}_{\rm Eu}$. It will be proved below in Sec. 4 that the operator of second variation of action for instantons with the rotation of $\mathbf{l}$ through he difficult axis has a negative eigenvalue. Thus, we must consider only two instantons with rotation in the plane passing through the intermediate axis. Hence we shall assume that formula (10) has the minus sign on the right-hand side.

The real component of Euclidean action for these instantons has the form of the sum of two terms

$$\mathrm{Re}\,\mathcal{A}_{\mathrm{Eu}}=2\,\frac{\hbar S_{\mathrm{tot}}}{\gamma H_e}\,\Omega+\hbar S_{\mathrm{ex}}\ln\frac{\sqrt{\omega_z^2-\Omega^2}+\sqrt{\omega_y^2-\Omega^2}}{\sqrt{\omega_z^2-\omega_y^2}}. \tag{11}$$

The first term is proportional to the number of spins and coincides with the corresponding expression for a pure AFM. The second term emerges from the gyroscopic term in the Lagrangian. It is proportional to the excess spin and can be associated with ferromagnetic properties of the system. The logarithm appearing in this term is just the imaginary component of the angle of rotation α from (8).

Naturally, the familiar results can be obtained from the general formula (11) as limiting cases. For example, for $S_2 \to 0$, $S_{\mathrm{ex}}=S$, $\omega_n=\gamma H_e$, $\Omega \ll \omega_y, \omega_z$ we obtain the well-known expression for ferromagnets:[7]

$$\mathrm{Re}\,\mathcal{A}_{\mathrm{Eu}}=\hbar S\ln\frac{\omega_z+\omega_y}{\omega_z-\omega_y}, \tag{12}$$

or

$$\exp(-\mathrm{Re}\,\mathcal{A}_{\mathrm{Eu}}/\hbar)=\left|\frac{\omega_z+\omega_y}{\omega_z-\omega_y}\right|^S,$$

for $\omega_y=\omega_z$, tunneling is naturally impossible. The limiting case of a strong easy-plane anisotropy considered by Chiolero and Loss[13] for uncompensated AFM can be obtained from (11) in the limit $\omega_n, \omega_y \ll \omega_z$. In this case, we have

$$\mathrm{Re}\,\mathcal{A}_{\mathrm{Eu}}=2\,\frac{\hbar S_{\mathrm{tot}}}{\gamma H_e}\,\omega_y\left(1+\frac{1}{2}\,\frac{\omega_n^2}{\omega_z^2}\right), \tag{13}$$

which is a typical result for a system with one degree of freedom, in which the effective mass contains a contribution from the terms of ferromagnetic and antiferromagnetic origin.[13]

Peculiarities of an uncompensated AFM as a system with two degrees of freedom is manifested most clearly for magnets with nearly easy-axis or rhombic anisotropy, when $\omega_y \sim \omega_z$. We introduce $\Delta\omega=\omega_z-\omega_y$ as a characteristic of anisotropy in the basal plane. It will be shown that in this case the tunneling characteristics are determined by relations between the parameters ω_n, $\Delta\omega$, and $\overline{\omega}=(\omega_y+\omega_z)/2$. In the general case, formula (11) is quite cumbersome, and we shall consider it for the most typical case $\Delta\omega \ll \Delta\omega, \omega_n$, when

$$\mathrm{Re}\,\mathcal{A}_{\mathrm{Eu}}=\frac{\hbar S_{\mathrm{tot}}}{\gamma H_e}\left[\sqrt{4\overline{\omega}^2+\omega_n^2}-\omega_n+\omega_n\ln\frac{\omega_n\sqrt{4\overline{\omega}^2+\omega_n^2}-\omega_n^2}{\overline{\omega}\Delta\omega}\right]. \tag{14}$$

It can easily be seen that the ferromagnetic behavior (divergence of $\mathrm{Re}\,\mathcal{A}_{\mathrm{Eu}}$ for $\omega_y \to \omega_z$) can be manifested for quite small values of ω_n also if only $\omega_n \gg \Delta\omega$. For $\omega_n \ll \overline{\omega}$, expression (14) is simplified and assumes the form

$$\mathrm{Re}\,\mathcal{A}_{\mathrm{Eu}}=\frac{\hbar S_{\mathrm{tot}}}{\gamma H_e}\left(2\,\overline{\omega}+\omega_n\ln\frac{\omega_n}{\Delta\omega}\right). \tag{15}$$

This expression is nonanalytic in the parameter $\omega_n/\Delta\omega$, which can be significant for an analysis of high-spin molecules of the $Mn_{12}Ac$ type. It will be proved in the next section that even more significant peculiarities appear in an analysis of the pre-exponential factor in the amplitude of tunneling.

3. CALCULATION OF TUNNELING PROBABILITY

It was proved in the previous section that there exist two pairs of solutions of the equations of motion (5), but only one of them corresponds to the minimum of the real component of Euclidean action. Following the method of steepest descent, we must use only this pair for calculating the amplitude of the tunneling transition. In the approximation of low instanton density and in the main approximation in the parameter $\exp(-\mathrm{Re}\,\mathcal{A}_{\mathrm{Eu}}/\hbar)$, we can write the following expression for the physically observable quantity, viz., the splitting of the ground state:[28]

$$\Delta_0=2|\cos\pi S_{\mathrm{tot}}|D\exp(-\mathcal{A}_{\mathrm{Eu}}/\hbar). \tag{16}$$

The factor $|\cos\pi S_{\mathrm{tot}}|$ emerges due to interference of a pair of instantons for which the values of action are complex conjugate.[2,3] It describes the suppression of tunneling for a half-integral spin and does not affect Δ_0 for an integral S_{tot}. The quantity $\exp(-\mathrm{Re}\,\mathcal{A}_{\mathrm{Eu}}/\hbar)$ is the transparency of a barrier in the semiclassical approximation. The factor D is a pre-exponential factor associated with small fluctuations about the instanton solution:

$$D=\int \mathcal{D}[\vartheta]\mathcal{D}[\mu]\exp\left(-\frac{1}{2}\,\frac{\delta^2\mathcal{A}_{\mathrm{Eu}}}{\hbar}\right), \tag{17}$$

where

$$\delta^2\mathcal{A}_{\mathrm{Eu}}=\frac{\hbar S_{\mathrm{tot}}}{\gamma H_e}\,\Omega\int dx(\vartheta,\mu)A^{(2)}\left(\frac{\vartheta}{\mu}\right) \tag{18}$$

and

$$A^{(2)}=\begin{pmatrix}-\partial_x^2+1+\varepsilon-2\cosh^{-2}x & -i\nu(\partial_x+\tanh x)\\ i\nu(\partial_x-\tanh x) & -\partial_x^2+1-2\cosh^{-2}x\end{pmatrix}. \tag{19}$$

In formula (18), we have introduced the dimensionless variable $x=\Omega\tau$. Here $\vartheta=\theta-\theta_0$ and $\mu=(\varphi-\varphi_0)\sin\theta_0$ are the transverse and longitudinal deviations from the instanton trajectory $\theta_0(\tau), \varphi_0(\tau)$. It is more convenient to introduce the variable μ than to use $\varphi-\varphi_0$ since it allows us to write the measure for functional integration in the form which does not contain $\sin\theta$ ($\mathcal{D}[\vartheta]\mathcal{D}[\mu]$) and to obtain the Schrödinger operators in $A^{(2)}$; $\delta^2\mathcal{A}_{\mathrm{Eu}}$ is the second variation of action calculated for the instanton solution. The action can be calculated in the easiest form by linearizing the equations of motion (5). The nondiagonal structure of $A^{(2)}$ corresponds to two interacting field degrees of freedom, which complicates the calculation of D considerably as compared to the standard case.

The operator $A^{(2)}$ contains two dimensionless parameters $\nu=\omega_n/\Omega$ and $\varepsilon=[(\omega_z^2+\omega_y^2)/\Omega^2]-2$. For ε, we obtain the following expression:

$$\varepsilon=2\,\frac{\pm[(\omega_z^2+\omega_y^2+\omega_n^2)^2-4\omega_z^2\omega_y^2]^{1/2}-\omega_n^2}{\omega_z^2+\omega_y^2+\omega_n^2\mp[(\omega_z^2+\omega_y^2-\omega_n^2)^2-4\omega_z^2\omega_y^2]^{1/2}}. \tag{20}$$

The plus and minus signs correspond to instantons with rotation of **l** through the intermediate and difficult axes respectively. In the former case, $\varepsilon \geqslant 0$, while in the latter case $\varepsilon \leqslant 0$; the equality $\varepsilon = 0$ is possible only for $\omega_n = 0$ and $\omega_y = \omega_z$. It should be noted that for a pure AFM, $\varepsilon = \omega_y^2/\omega_z^2 - 1$, i.e., is determined only by anisotropy in the basal plane, and $\varepsilon \to 0$ for $\omega_y \to \omega_z$ (easy-axis limit). The presence of decompensation transforms the limiting value of ε for $\omega_y \to \omega_z$ into

$$\varepsilon_0 = \frac{\omega_n^2}{\omega_y^2} + \frac{\omega_n}{\omega_y}\sqrt{4 + \omega_n^2/\omega_y^2}, \tag{21}$$

i.e., this parameter remains finite for $\omega_y \to \omega_z$. In the easy-axis (or rhombic) case under investigation ($\omega_y \sim \omega_z$) with a weak decompensation ($\omega_n \ll \omega_y, \omega_z$), the quantities $\nu \simeq \omega_n/\omega_y$ and ε are small parameters.

In order to calculate D, we must carry out functional integration with respect to $\mathcal{D}[\vartheta]$ and $\mathcal{D}[\mu]$. This can be done by transforming $A^{(2)}$ to the diagonal form $A^2 = \Sigma_n \lambda_n \eta_n^2$ through a unitary transformation, i.e., finding in fact the eigenvalues λ_n of the operator (19). Further, we can write $\mathcal{D}[\vartheta]\mathcal{D}[\mu] = \Pi_n d\eta_n$ and carry out Gaussian integration with respect to η_n. This gives $D = (\Pi_n' \lambda_n)^{-1/2}$, where Π' indicates that the product is formed over all eigenvalues except zero values. It is well known that the zero mode $\lambda = 0$ leads to the emergence of the factor $\Omega(\mathrm{Re}\,\mathcal{A}_{\mathrm{Eu}}/2\pi\hbar)^{1/2}$ in D. It should be noted that it is proportional to the square root of the number of spins, while Π_n' does not contain such an extensive quantity. The spectrum of $A^{(2)}$ can contain discrete modes with eigenvalues λ_1. These modes are responsible for the factors $\lambda_1^{-1/2}$ in D.

Let us now determine the eigenvalues. It can easily be verified that (19) has a zero eigenvalue corresponding to the eigenvector $\mu = \cosh^{-1} x$, $\vartheta = 0$. It can easily be seen that another zero mode does not exist except the nonphysical case $\nu = 0$, $\varepsilon = 0$ (pure AFM with an isotropic easy plane). However, for $\omega_n = 0$, there exists another discrete energy level with $\lambda_1 = \varepsilon$, i.e., the problem has one more small eigenvalue. For $\omega_n \neq 0$ and $\nu \ll 1$, an exact solution does not exist, and hence we shall find λ_1 with the help of the theory of perturbation in the small parameter ν. Choosing the zeroth approximation in the form $\mu^{(0)} = 0$, $\vartheta^{(0)} = \cosh^{-1} x$, $\lambda_1^{(0)} = \varepsilon$, we can easily write $\lambda_1 = \varepsilon + \nu^2$ in the main approximation in λ and ν.

The continuous spectrum has two branches each of which is degenerate in the sign of k with the dispersion relation

$$\lambda(k) = 1 + k^2 + \frac{\varepsilon}{2} \pm \sqrt{(\varepsilon/2)^2 - \nu^2(1 + k^2)}. \tag{22}$$

For $k^2 > (\varepsilon/2\nu)^2 - 1$, these branches are complex conjugate to λ. The complex nature of λ does not give an imaginary contribution to D since complex conjugate to λ can be combined into real-valued pairs $\Pi_k'[\lambda(k)\lambda^*(k)]^{-1/2}$ while evaluating D.

Details of calculations of the contribution from the continuous spectrum to the pre-exponential factor D can be found in the review by Vainshtein *et al.*[28] We shall give only the final form of the dispersion relation of type (22):

$$D_{\mathrm{cont}} = \exp\left\{\frac{1}{4\pi}\int_{-\infty}^{+\infty} dk\,\frac{d\delta(k)}{dk}\ln[\lambda(k)\lambda^*(k)]\right\}. \tag{23}$$

Here $\delta(k)$ is the phase shift of eigenfunctions η_{k_n} of the operator $A^{(2)}$, which can be determined from the asymptotic expressions $\eta_k \propto \exp(ikx \pm i\delta(k)/2)$ for $x \to \pm\infty$. Its derivative $d\delta(k)/dk$ gives the change in the density of states of the continuous spectrum as compared to the homogeneous density of states. We shall use the value of $\delta(k)$ obtained in the main approximation in ν^2, namely, $\delta(k) = 2\arctan k$, which gives

$$D_{\mathrm{cont}} = 4(1 + \sqrt{1 + \varepsilon + \nu^2})^2. \tag{24}$$

For the easy-axis case under investigation, $\varepsilon \sim \nu \sim \omega_n/\omega_y$, and we can neglect ν^2 as compared to ε in the pre-exponential factor. However, we must retain in $\mathrm{Re}\,\mathcal{A}_{\mathrm{Eu}}$ the term containing ω_n/ω_y due to the large value of the logarithm in it. Finally, the splitting of the energy level in the ground state can be presented in the form

$$\Delta_0 = 8\omega_y \frac{(1 + \sqrt{1 + \varepsilon})^2}{\sqrt{\varepsilon}}\left(\frac{\mathrm{Re}\,\mathcal{A}_{\mathrm{Eu}}}{2\pi\hbar}\right)^{1/2} |\cos \pi S_{\mathrm{tot}}|\, e^{-\mathrm{Re}\,\mathcal{A}_{\mathrm{Eu}}}. \tag{25}$$

Thus, the above-mentioned peculiarity of the problem, namely, the fact that we are dealing with a mechanical system with two degrees of freedom, is manifested noticeably in the pre-exponential factor also and leads to the emergence of the factor $\varepsilon^{-1/2}$ in the tunneling probability.

CONCLUSION

The above analysis has proved that peculiar properties of model (1) as an analog of a mechanical system with two degrees of freedom are important for uniaxial or rhombic anisotropy with a weak anisotropy in the basal plane. As the anisotropy parameter ε decreases, the exponential factor suppresses tunneling, but the emergence of factor $\varepsilon^{-1/2}$ in the tunneling probability increases anisotropy as compared to the standard case. Obviously, tunnel splitting for $\varepsilon \to 0$ tends to zero, but these factors must be taken into account for small but finite values of ε and ν.

In first publications on macroscopic tunneling, the limit of strong easy-plane anisotropy for aniferromagnets with weak decompensation was considered as a typical example of systems in which tunneling effects are observed for particles containing as many as possible spins. This condition corresponds, for example, to ferritin which is a classical object in the physics of macroscopic tunneling. However, the main attention in recent years is paid to new objects, viz., high-spin complexes containing tens (and not thousands as in the case of ferritin) of spins and characterized by a wide spectrum of the values of parameters (in fact, any preset spectrum). In such objects, tunneling can be realized under nonoptimal conditions also, e.g., in the presence of uniaxial anisotropy. In this case the conventional approach reducing

the problem (in a certain approximation) to a system with one degree of freedom is inapplicable, and theory of the type of that developed by us here should be used.

The authors are grateful to V. G. Bar'yakhtar and A. K. Kolezhuk for fruitful discussions.

This research was partially supported the Ukrainian Foundation of Fundamental Studies, Grant No. 2.4.27.

*E-mail: vbaryakhtar@bitp.kiev.ua

[1] E. M. Chudnovsky and J. Tejada, *Macroscopic Quantum Tunneling of the Magnetic Moment*, Cambridge University Press, London (1998).
[2] D. Loss, D. P. DiVincenzo, and G. Grinstein, Phys. Rev. Lett. **69**, 3232 (1992).
[3] J. von Delft and C. L. Henley, Phys. Rev. Lett. **69**, 3236 (1992).
[4] V. Yu. Galyshev and A. F. Popkov, Europhys. Lett. **29**, 327 (1995); Zh. Éksp. Teor. Fiz. **108**, 1755 (1995) [JETP **81**, 962 (1995)].
[5] B. A. Ivanov and V. E. Kireev, JETP Lett. **69**, 398 (1999).
[6] E. M. Chudnovsky, Zh. Éksp. Teor. Fiz. **50**, 1035 (1979) [Sov. Phys. JETP **23**, 521 (1979)].
[7] E. M. Chudnovsky and L. Gunther, Phys. Rev. Lett. **60**, 661 (1988); Phys. Rev. **B37**, 9455 (1998).
[8] B. Barbara and E. M. Chudnovsky, Phys. Lett. A **145**, 205 (1990).
[9] I. V. Krive and O. B. Zaslavskii, J. Phys.: Condens. Matter **2**, 9457 (1990).
[10] D. D. Awschalom, J. F. Smyth, G. Grinstein, and D. Loss, Phys. Rev. Lett. **68**, 3092 (1992).
[11] E. M. Chudnovsky, J. Magn. Magn. Mater. **140–144**, 1821 (1995).
[12] J. M. Duan and A. Garg, J. Phys.: Condens. Matter **7**, 2171 (1995).
[13] A. Chiolero and D. Loss, Phys. Rev. B **56**, 738 (1997).
[14] B. A. Ivanov and A. L. Sukstanskii, Zh. Éksp. Teor. Fiz. **84**, 370 (1983) [Sov. Phys. JETP **57**, 214 (1983)].
[15] B. A. Ivanov and A. L. Sukstanskii, Solid State Commun. **50**, 523 (1984).
[16] J. A. Friedman, M. P. Sarachik, J. Tejada, and R. Ziolo, Phys. Rev. Lett. **76**, 3830 (1996).
[17] C. Sangregorio, T. Ohm, C. Paulsen *et al.*, Phys. Rev. Lett. **78**, 4645 (1997).
[18] V. G. Bar'yakhtar and B. A. Ivanov, in *Solitons and Thermodynamics of Low-Dimensional Magnets* (ed. by I. M. Khalatnikov), Sov. Sci. Rev. **16**, 1 (1992).
[19] A. I. Perelomov, *Integrable Systems in Classical Mechanics and Lie Algebra* [in Russian], Nauka, Moscow (1990).
[20] C. Neumann, J. Reine Angew. Math. **56**, 46 (1859).
[21] V. M. Eleonskii and N. E. Kulagin, Zh. Éksp. Teor. Fiz. **84**, 616 (1983) [Sov. Phys. JETP **57**, 356 (1983)].
[22] V. M. Eleonskii, N. N. Kirova, and N. E. Kulagin, Zh. Éksp. Teor. Fiz. **77**, 409 (1979) [Sov. Phys. JETP **50**, 209 (1979)].
[23] E. K. Sklyanin, Preprint LOMI E-3-79, Leningrad (1979).
[24] E. M. Chudnovsky, Phys. Rev. A **46**, 8011 (1998).
[25] E. M. Chudnovsky and D. A. Garanin, Phys. Rev. Lett. **79**, 4469 (1997).
[26] V. A. Kalatsky, E. Müller-Hartman, V. L. Pokrovsky, and F. S. Uhrig, Phys. Rev. Lett. **80**, 1304 (1998).
[27] J.-Q. Liang, H. J. W. Muller-Kirsten, A. V. Shurgaia, and F. Zimmerschied, Phys. Lett. A **237**, 169 (1998).
[28] A. I. Vainshtein, V. I. Zakharov, V. A. Novikov, and M. A. Shifman, Usp. Fiz. Nauk **136**, 553 (1982) [Sov. Phys. Usp. **25**, 195 (1982)].

Translated by R. S. Wadhwa

Dynamics of domain walls and solitons in easy-plane magnets with weak exchange interaction

M. V. Gvozdikova

Kharkov State University, 310077 Kharkov, Ukraine

A. S. Kovalev

*B. Verkin Institute for Low Temperature Physics and Engineering, National Academy of Sciences of the Ukraine, 310164 Kharkov, Ukraine**)

(Submitted May 12, 1999)
Fiz. Nizk. Temp. **25**, 1295–1303 (December 1999)

Internal spin dynamics of collinear domain walls and collinear soliton-like localized states in easy plane magnets is investigated. The dependence of internal mode frequencies of these excitations on the exchange interaction is determined using the essentially discrete Takeno–Homma model for low values of this interaction. © *1999 American Institute of Physics.* [S1063-777X(99)00812-9]

INTRODUCTION

Theoretical investigations of nonlinear excitations in magnets are confined, as a rule, to the simplest case of magnets with an isotropic exchange interaction exceeding considerably the single-ion magnetic anisotropy.[1,2] In the $1D$ case, this sometimes leads to completely integrable models for which all soliton and many-soliton solutions are well known. However, the exchange interaction in the direction perpendicular to the layers in layered compounds synthesized recently[3–6] can be anomalously weak (of the order of or even much smaller than the magnetic anisotropy energy) in view of a large separation between magnetic layers intercalated by organic layers. Moreover, this exchange interaction in compounds like $(CH_2)_n(NH_3)_2MnCl_4$, $(C_nH_{2u+1}NH_3)_2MnCl_4$[3,4] and $(NH_3)_2(CH_2)_nCuCl_4$[5,6] can be varied purposefully by changing the number n of organic groups in intercalants. The remaining characteristics of compounds (strong interaction within a layer and one-ion anisotropy) remain unchanged. This makes it possible to study the changes in the structure and dynamics of magnets as a function of the parameters of the substance and not of parameters of excitations. Even the first experimental results of investigations of quasi-two-dimensional magnets proved that the resonance properties of such compounds change significantly in the range of anomalously weak exchange interaction, for example, additional absorption peaks appear in the gap of the spectrum of linear waves.[4,7] To explain this phenomenon, Goncharuk *et al.*[8] investigated theoretically the internal modes in collinear domain walls (DW) and specific localized collinear spin configurations. The collinear structure of DW in a ferromagnet with a strong single-ion anisotropy was considered for the first time by Van den Broek and Zijlstra[9] in the classical approximation and by Ostrovskii and Loktev[10,11] in the quantum approximation. Ostrovskii and Loktev[10,11] were the first to pay attention to the importance of inclusion of single-ion anisotropy in the dynamics of localized excitations in magnets (see also Ref. 12). Later, this problem as well as the transformation of collinear phases of DW and localized spin configurations into canted phases were discussed by us earlier in detail from the position of ''soliton science.'' [13,14] Theoretical analysis of the DW and soliton dynamics in compounds with a weak exchange interaction[8–10] was carried out for magnets with easy-axis single-ion anisotropy. The obtained results can be applied to easy-axis layers antiferromagnets.[3,4]

On the other hand, copper-based layered compounds studied experimentally[5,6] possess one-ion anisotropy of the easy-plane type with a weak additional anisotropy in the easy plane, and the theoretical results[8,13,14] cannot be applied to these compounds directly. In contrast to easy-plane one-ion anisotropy for which ferro- and antiferromagnets are described by essentially different dynamic equations, ferro- and antiferromagnets in the easy-plane case are described in the main approximation by identical second-order equations in time with a single angular variable.[1,2]

Stepanov *et al.*[5,6] studied resonance properties of metal-organic compounds $(NH_3)_2(CH_2)_nCuCl_4$ with the index $n=2,3,4$, which are easy-plane antiferromagnets with an easy-plane one-ion anisotropy $\beta^z \sim 2$ kOe and a weak anisotropy $\beta^x \sim 0.14$ kOe in the easy plane. These parameters are independent of the number n. However, the energy of exchange interaction between planes depends on this parameter strongly: $J \sim 500$, 40, and 4 kOe for $n=2,3$, and 4 respectively. (The energy of exchange interaction in magnetic planes has the value ~ 1000 kOe and is independent of their separation, viz., the number n). As the number n increases by unity, the exchange interaction between the layers decreases by an order of magnitude, and the system becomes more and more discrete in the direction perpendicular to the layers. It is convenient to characterize this discreteness by the parameter $\lambda_0 = J/\beta^z \sim 250,20$, and 2 for $n=2,3$, and 4 respectively. We shall use below the simplified Takeno–Homma model valid for $J \ll \beta^z$. This model becomes essentially discrete only for $J \sim \beta^x$. For this reason, another discretness parameter $\lambda = J/\beta^x$ associated with weak anisotropy

in the easy plane is more important. For experimentally studied compounds, this parameter is equal to 3600, 280, and 30 for $n=2,3$, and 4 respectively. In order to satisfy the inequality $\lambda \lesssim 1$, experiments with compounds characterized by the index $n=5(\lambda \simeq 3)$ and $n=6(\lambda \simeq 0.3)$ are required. Thus, the results obtained below are of predictive nature. We shall study internal modes of DW and soliton-like configurations (360° DW) in a magnet with an easy-plane single-ion anisotropy and a weak exchange interaction in the Takeno–Homma model.

MODEL

We proceed from the one-dimensional Heisenberg Hamiltonian with an isotropic (in magnetic respect) exchange interaction and biaxial single-ion anisotropy (below, n labels magnetic layers, and all static and dynamic states are regarded as homogeneous in the planes of these layers):

$$H=-\sum_n J\mathbf{S}_n\mathbf{S}_{n+1}+\frac{1}{2}\sum_n [\beta^z(S_n^z)^2-\beta^x(S_n^x)^2], \tag{1}$$

where $\mathbf{S}_n$ is the spin at a lattice site, and $\beta^z,\beta^x>0$, which corresponds to the easy-plane anisotropy along the z-axis and additional easy-axis anisotropy along the x-axis in the xy plane. In a magnet with an ''easy plane'' in the ground state, spins are oriented in the xy plane (although such a relation between the sign of β and the type of the ground state can change when anisotropy of the exchange interaction is taken into consideration).

In order to describe magnetization dynamics in the classical model for a biaxial magnet with a strong easy-plane anisotropy and a weak anisotropy in the easy plane, we shall use the Landau–Lifshitz equations for a nondissipative medium,[1,2] which have the following form for Hamiltonian (1):

$$\hbar\frac{d}{dt}\mathbf{S}_n=[\mathbf{S}_n\times\hat{J}(\mathbf{S}_{n+1}+\mathbf{S}_{n-1})]-\beta^z[\mathbf{S}_n\times\mathbf{e}_z](\mathbf{S}_n\mathbf{e}_z)+\beta^x[\mathbf{S}_n\times\mathbf{e}_z](\mathbf{S}_n\mathbf{e}_z), \tag{2}$$

where $\hat{J}$ is the diagonal matrix of the form $J=\mathrm{diag}(J,J,J)$, and $\mathbf{e}_z$ and $\mathbf{e}_x$ are unit vectors along the corresponding axes. This equation must be supplemented by the condition of conservation of the classical spin magnitude (length of magnetization vector). Consequently, the vector equation (2) can be reduced to two scalar first-order equations or a single equation in the case of a complex field. Introducing the complex variable $\Psi_n=S_n^x+iS_n^y$ (Ψ_n and Ψ_n^* are classical analogs of the creation and annihilation operators for magnons), we can write the Landau–Lifshitz equations (2) in the form

$$i\hbar\frac{d}{dt}\Psi_n=J\Psi_n(S_{n+1}^z+S_{n-1}^z)-JS_n^z(\Psi_{n+1}+\Psi_{n-1})-\beta^z\Psi_nS_n^z-\frac{\beta^x}{2}S_n^z(\Psi_n+\Psi_n^*), \tag{3}$$

where the third spin component is $S_n^z=\sqrt{S_0^2-|\Psi_n|^2}$.

The dynamics of a magnet has a more visual form in terms of the angular variables θ_n,φ_n in a polar system of coordinates associated with the prefered axis z, in which

$$S=S_0(\sin\theta_n\cos\varphi_n,\sin\theta_n\sin\varphi_n,\cos\theta_n):\hbar\frac{d}{dt}\theta_n$$
$$=-S_0J[\sin\theta_{n+1}\sin(\varphi_{n+1}-\varphi_n)+\sin\theta_{n-1}\sin(\varphi_{n-1}-\varphi_n)]+\beta^xS_0\sin\theta_n\sin\varphi_n\cos\varphi_n, \tag{4}$$

$$\hbar\sin\theta_n\frac{d}{dt}\varphi_n=S_0J\cos\theta_n[\sin\theta_{n+1}\cos(\varphi_{n+1}-\varphi_n)+\sin\theta_{n-1}\cos(\varphi_{n-1}-\varphi_n)]$$
$$-S_0J^z\sin\theta_n(\cos\theta_{n+1}+\cos\theta_{n-1})+S_0\beta^z\cos\theta_n\sin\theta_n+S_0\beta^x\cos\theta_n\sin\theta_n\cos^2\theta_n. \tag{5}$$

For magnets with an anomalously weak exchange interaction ($J\ll\beta^z$) and a strong one-ion easy-plane anisotropy ($\beta^z\gg\beta^x$), almost all spins lie in the easy plane: $\chi_n=\pi/2-\theta_n\ll 1$, and it follows from (5) that $\chi\approx\hbar(S_0\beta^z)d\varphi_n/dt$. In this case, Eq. (4) can be reduced to a scalar equation describing the Takeno–Homma model:[15,16]

$$\frac{[HM]^2}{S_0^2\beta^z}\frac{d^2}{dt^2}\varphi_n+J[\sin(\varphi_n-\varphi_{n-1})+\sin(\varphi_n-\varphi_{n+1})]+\beta^x\sin\varphi_n\cos\varphi_n=0. \tag{6}$$

In the case of antiferromagnets, the equation for the quantities ψ_n will obviously coincide with Eq. (6) upon the simultaneous substitution $J\to -J$ and $\varphi_n=(\pi/2)(1-(-1)^n)+\psi_n$, and all the results of the Takeno–Homma model for ferromagnets can be extended without any change to antiferromagnets.

In the long-wave limit, when the inequalities $\beta^x\ll J\ll\beta^z$ (and naturally $\beta^x\ll\beta^z\ll J$) are satisfied simultaneously, the Takeno–Homma model is reduced to the well-known sine-Gordon equation (SGE):[17]

$$\frac{1}{\omega_0^2}\frac{\partial^2\varphi}{\partial t^2}-l^2\frac{\partial^2\varphi}{\partial x^2}+\sin\varphi\cos\varphi=0, \tag{7}$$

where the homogeneous resonance frequency is $\omega_0=S_0\sqrt{\beta^z/\beta^x}/\hbar$, and the so-called magnetic length is $l=\sqrt{J/\beta^x}$. Henceforth, time will be measured in the units of $1/\omega_0$, and we shall use the discreteness parameter $\lambda=l^2$ instead of magnetic length l. The solutions φ_0 and φ_s of the SGE for domain walls and solitons respectively are well known:[17]

$$\varphi_0=2\arctan(\exp(x/l)), \tag{8}$$

$$\varphi_s=2\arctan\left[\frac{\sqrt{1-\omega^2}\sin\omega t}{\omega\cosh(\sqrt{1-\omega^2}x/l)}\right]. \tag{9}$$

In this approximation, the DW (8) does not possess intrinsic dynamics (internal modes are absent). Soliton (9) is a dynamic object, and its localization is accompanied by internal oscillations with frequency ω which can vary in the interval

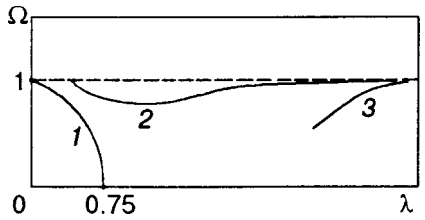

FIG. 1. Schematic dependence of internal mode frequency on discreteness parameter λ for a collinear domain wall (kink) in an easy-plane ferromagnet in the Takeno-Homma model (curve *1*). Curve *3* was obtained by Fei Zhang[18] in the Takeno–Homma model for a noncollinear kink with large values of λ. Curve *2* was obtained by Braun *et al.*[19] for the discrete SG model.

$0<\omega<1$ for a fixed value of the discreteness parameter (magnetic length l). Different values of frequency correspond to different values of soliton energy $E=4S_0\times\sqrt{J/\beta^x}\sqrt{1-\omega^2}$ and different number $N=4S_0\times\sqrt{J/\beta^z}\arccos\omega$ of elementary excitations coupled in it (see Ref. 13).

COLLINEAR STRUCTURE OF DOMAIN WALL AND ITS INTERNAL MODE

Returning to the discrete description of an easy-plane ferromagnet with a weak intraplanar anisotropy in the Takeno–Homma model, we write Eqs. (6) in the dimensionless form, measuring time in the units of $1/\omega_0$ and using the parameter $\lambda=J/\beta^x$ to characterize the extent of discreteness of the system:

$$\frac{d^2\varphi_n}{dt^2}+\lambda[\sin(\varphi_n-\varphi_{n+1})+\sin(\varphi_n-\varphi_{n-1})]+\sin\varphi_n\cos\varphi_n=0. \tag{10}$$

This equation was studied in detail both analytically and numerically.[15,16,18] However, the authors of these publications chose larger values of the parameter λ for numerical calculations and failed to observe qualitative changes in the structure and dynamics of localized nonlinear excitations occurring for $\lambda\simeq 1$ and upon a transition of localized excitation to a collinear structure.

First of all, we consider a stationary domain wall and the possibility of the existence of internal mode for such a wall. It was pointed out by us earlier[13] that this mode is absent in an easy-axis ferromagnet in the long-wave limit, but it appears when the discreteness of exchange interaction is taken into account.

In the framework of long-wave SGE, an internal mode of the DW type (8) is not observed either, but it is present when the discreteness of interactions between particles is taken into account in the linear approximation,[19] i.e., when exchange terms in Eq. (10) are linearized. In this case, the detachment of the internal mode from the frequency $\Omega=\omega/\omega_0=1$ of homogeneous ferromagnetic resonance is quite small and attains its maximum value of only ~ 0.05 for $\lambda\sim 1$, then decreasing to zero again for $\lambda\to 0$ (curve *2* in Fig. 1). However, the inclusion of nonlinearity of exchange interaction in the discrete case leads to a considerable change in the results. It was shown numerically by Fei Zhang[18] that the frequency of DW internal mode decreases significantly even for $\lambda=4$ and attains the value $\Omega\cong 0.8$ (see curve *3* in Fig. 1). Unfortunately, Fei Zhang[18] did not continue numerical calculations to the critical value $\lambda_0=0.75$ at which the DW goes over to a collinear form.

We take into account the fact that the Heisenberg exchange interaction in the discrete case which is essentially nonlinear and periodic in the angle between the nearest spins.

For small values of exchange interaction ($\lambda<0.75$), the domain wall is in the collinear state, and the ground state of the spin configuration with the domain wall …↑↑↑↓↓↓… corresponds to the following values of angles:

$$\varphi_n=0,\quad n\leqslant 0,$$
$$\varphi_n=\pi,\quad n>0, \tag{11}$$

We linearize the system of equations (10) in the vicinity of the ground state (11) by introducing the small corrections $\psi_n\ll 1$:

$$\varphi_n=\psi_n,\quad n\leqslant 0,$$
$$\varphi_n=\pi+\psi_n,\quad n>0, \tag{12}$$

The system of linear equations for the quantities ψ_n assumes the form

$$\begin{aligned}
&\frac{d^2\psi_n}{dt^2}+\lambda[2\psi_n-\psi_{n+1}-\psi_{n-1}]+\psi_n=0,\ \ n\leqslant -1,\\
&\frac{d^2}{dt^2}+\lambda[\psi_1-\psi_{-1}]+\psi_0=0,\\
&\frac{d^2\psi_1}{dt^2}+\lambda[\psi_0-\psi_2]+\psi_1=0,\\
&\frac{d^2\psi_n}{dt^2}+\lambda[2\psi_n-\psi_{n+1}-\psi_{n-1}]+\psi_n=0,\ \ n\geqslant 2.
\end{aligned} \tag{13}$$

We seek the solution for small corrections in the form $\psi_n=v_n\exp(i\Omega t)$ and obtain the following system of algebraic equations for the amplitudes v_n:

$$\begin{aligned}
&(2\lambda+1-\Omega^2)v_n-\lambda(v_{n+1}+v_{n-1})=0,\ \ n\leqslant -1,\\
&(1-\Omega^2)v_0+\lambda(v_1-v_{-1})=0,\\
&(1-\Omega^2)v_1-\lambda(v_0-v_2)=0,\\
&(2\lambda+1-\Omega^2)v_n-\lambda(v_{n+1}+v_{n-1})=0,\ \ n\geqslant 2.
\end{aligned} \tag{14}$$

The solutions of this system, which decrease at infinity and describe possible internal modes, can be sought in the form

$$v_n=A\exp(-\kappa n),n>0,$$
$$v_n=B\exp(\kappa n),\quad n\leqslant 0. \tag{15}$$

From Equations. (15) for $n\leqslant -1$ and $n\geqslant 2$, we can find the relation between the parameters κ,Ω, and λ:

$$[1-\Omega^2]+\lambda[2-2\cosh(\kappa)]=0. \tag{16}$$

Equations (14) for $n=0,1$ lead to an additional relation between κ,Ω, and λ:

$$1-\Omega^2-\lambda[\exp(-\kappa)\pm 1]=0 \tag{17}$$

as well as the relation between the amplitudes A and B:

$$A=B[1-(1-\Omega^2)(1/\lambda)\exp(\kappa)]. \tag{18}$$

The minus sign in expression (17) corresponds to a symmetric solution with $\Omega=1,\kappa=0$, and $A=B$, i.e., a homogeneous noncollinear oscillation with the frequency corresponding to the edge of the spectrum of linear spin waves in a spin chain without a DW. Thus, a homogeneous oscillation of the spin system in the Takeno-Homma model does not ''feel'' the presence of a DW in it. A symmetric solution usually corresponds to the oscillation of the center of the DW in the Peierls relief, but no such excitations are observed in a collinear DW.

The plus sign in expression (17) corresponds to an antisymmetric solution for the internal mode of the DW with the following dependence of the frequency of this mode on the discreteness parameter and the following form of a decrease of the internal mode field:

$$\Omega^2=1-4\lambda/3, \quad \kappa=\ln 3. \tag{19}$$

The distribution of amplitudes of spin oscillations near the center of the DW in the internal mode has the form

$$\ldots,\frac{v_0}{27},\frac{v_0}{9},\frac{v_0}{3},v_0,-v_0,-\frac{v_0}{3},-\frac{v_0}{9},-\frac{v_0}{27},\ldots. \tag{20}$$

Thus, the domain wall has an antisymmetric internal mode corresponding to a periodic variation of the DW width with time. The dependence $\Omega(\lambda)$ is shown in Fig. 1 (curve *1*). The internal mode emerges as a result of bifurcation for the critical value $\lambda_0=0.75$ of exchange interaction and exists for $\lambda<\lambda_0$. This critical value of the discreteness parameter coincides with the value of critical parameter obtained by Goncharuk *et al.*[8] for an easy-axis ferromagnet. However, the internal mode for an easy-plane ferromagnet is spatially antisymmetric, while in the easy-axis case such a symmetry was absent in view of different time dependences of the corresponding dynamic equations.

For $\lambda>\lambda_0$, the domain wall goes over from the collinear to a canted structure with $\varphi\neq 0,\pi$ and with its own dependence of internal mode on the exchange interaction constant (discreteness parameter), which is transformed in the long-wave limit into the dependence obtained Fei Zhang[18] (curve *3* in Fig. 1). This question requires an additional analysis. It was proved by us earlier[13,14] that the dynamics of localized excitations in essentially discrete nonlinear systems is close qualitatively to that of corresponding finite-dimensional dynamic models describing spin chains of finite length in the DW or soliton configuration.

Let us consider a chain of four spins in the DW configuration $\uparrow\uparrow\downarrow\downarrow$, for which $\psi_1=\psi_2=\psi_0=\psi_{-1}=0$ in the collinear phase in the static configuration, and boundary spins are free, i.e., equation for a boundary spin has the form

$$\frac{d^2\psi}{dt^2}+\lambda\sin(\psi_2-\psi_1)+\sin\psi_2\cos\psi_2=0. \tag{21}$$

The collinear structure of the spin complex under investigation exists only for the values $\lambda<\lambda_0=1/\sqrt{2}$ of discreteness parameter. It should be noted that the critical value of the parameter λ in the four-spin complex is quite close to that for an infinite spin chain ($\lambda_0=0.75$). The eigenfrequency spectrum for a finite-length chain contains four modes. In the collinear phase, the system of dynamic equations linearized in ψ_n has solutions of the form $\psi_n\sim\sin\Omega t$ with the following dependences of frequencies on the discreteness parameter for the above-mentioned four modes (a,b,c,d):

$$\begin{aligned}
&(a):\psi_{-1}=-\psi_0=-\psi_1=\psi_2,\ \ \Omega^2=1+2\lambda,\\
&(b):-(\sqrt{2}-1)\psi_{-1}=\psi_0=-\psi_1=(\sqrt{2}-1)\psi_2,\\
&\Omega^2=1+\sqrt{2}\lambda,\\
&(c):\psi_{-1}=\psi_0=\psi_1=\psi_2,\ \ \Omega^2=1,\\
&(d):(\sqrt{2}+1)\psi_{-1}=\psi_0=-\psi_1=-(\sqrt{2}+1)\psi_2,\\
&\Omega^2=1-\sqrt{2}\lambda.
\end{aligned} \tag{22}$$

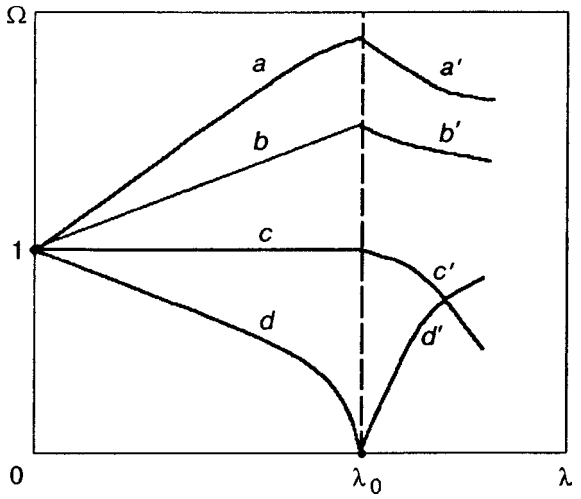

FIG. 2. Eigenfrequency spectrum for a finite-length chain in the Takeno–Homma model (4 spins): a and c are symmetric and b and d are antisymmetric modes of the collinear structure; a' and c' are symmetric and b' and d' are antisymmetric modes of a canted phase of the domain wall.

The obtained dependences $\Omega(\lambda)$ are presented as curves a,b,c and d in Fig. 2. The symmetric mode c and the antisymmetric mode d are most interesting. As in the case of an infinite chain, the c-mode has a homogeneous resonance frequency in a system without a domain wall ($\Omega=1$). The antisymmetric d-mode is an analog of the internal mode of a collinear kink considered above: the spins adjoining the ''domain wall'' oscillate in it with a considerably larger amplitude than for spins at the periphery ($\psi_2/\psi_1\approx 0.4$, while in an infinite chain we have $\psi_2/\psi_1\approx 0.33$).

It is interesting to compare the spectrum of internal modes (22) of a spin complex with a DW with the spectrum of internal modes of such a complex in the ground state with parallel spins $\uparrow\uparrow\uparrow\uparrow$. It can easily be proved that the symmetric modes a and c have identical forms and can be described by formulas (22) for cases (a) and (c). The antisymmetric modes b and d change significantly in the ground state of the four-spin complex:

$$(\tilde{b}):-(\sqrt{2}+1)\psi_{-1}=\psi_0=-\psi_1=(\sqrt{2}+1)\psi_2,$$

$$\Omega^2=1+\lambda(2+\sqrt{2}),$$

$$(\tilde{d}):(\sqrt{2}\text{-}1)\psi_{-1}=\psi_0=-\psi_1=-(\sqrt{2}-1)\psi_2,$$

$$\Omega^2=1+\lambda(2-\sqrt{2}). \tag{23}$$

Thus, the first antisymmetric mode of the spectrum of the spin complex in the ground state is transformed into the antisymmetric internal mode of the DW.

The advantage of the analysis of a finite-dimensional spin chain is that the problem for four spins can be solved analytically in explicit form for a canted DW with $\lambda>\lambda_0$ also. In the static case, we can easily find the following dependence of internal structure of a canted DW on the discreteness parameter from Eqs. (13) and (21):

$$-\psi_{-1}=\psi_2 =\frac{1}{2}\arcsin\left\{2\lambda\left[\frac{(1-2\lambda^2)(1-4\lambda+2\lambda^2)}{(1-2\lambda)(1-2\lambda-4\lambda^2)}\right]^{1/2}\right\}, \tag{24}$$

$$-\psi_0=\psi_1=\psi_2+\arcsin\left(\frac{1}{2\lambda}\sin 2\psi_2\right). \tag{25}$$

Expression (24) shows that the solution for the canted phase exists only in the range $\lambda_0<\lambda<\lambda_1=1+\sqrt{2}$ of the order parameter. However, the model system under investigation correctly describes the initial infinite spin chain only for small deviations of discreteness parameter from its critical value λ_0.

Linearizing the dynamic equations (10) and (21) in small spin deviations from the static configuration (24) and (25), we can easily find the transformation of frequency dependences of all modes of a finite-dimensional system in the region of a canted DW:

$$\Omega^2_{a,c}=\frac{1}{2}[2\lambda\cos(\psi_2-\psi_1)+\cos 2\psi_1+\cos 2\psi_2 \pm\sqrt{4\lambda^2\cos^2(\psi_2-\psi_1)+(\cos 2\psi_1-\cos 2\psi_2)^2}], \tag{26}$$

$$\Omega^2_{b,d}=\frac{1}{2}[2\lambda\cos(\psi_2-\psi_1)+\cos 2\psi_2-(2\lambda-1)\cos 2\psi_1 \pm\sqrt{4\lambda^2\cos^2(\psi_2-\psi_1)+(\cos 2\psi_2+(2\lambda-1)\cos 2\psi_1)^2}], \tag{27}$$

where $\psi_1(\lambda)$ and $\psi_2(\lambda)$ are defined by (24) and (25). The plots of the corresponding dependences are shown in Fig. 2 (curves a',b',c' and d') for values of λ in the vicinity of λ_0.

It can be seen from Fig. 2 that the antisymmetric mode d' exists in the canted phase also, where its frequency increases according to the root law $\Omega^2\propto 2\sqrt{2}(\lambda-\lambda_0)$ as for an easy-axis ferromagnet.[13] We can propose that a similar mode also exists in an infinite spin chain. Its frequency dependence must begin at the point $\Omega=0,\lambda=\lambda_0$ (0.75) in Fig. 1 and attains dependence *3* obtained by Fei Zhang[18] in the long-wave limit for large values of λ. Besides, it can be seen from Fig. 2 that the nontrivial localized symmetric mode c' appears in the canted phase of the DW. In the vicinity of the critical point $\lambda=\lambda_0$, its frequency decreases linearly from the value $\Omega=1$: $\Omega\approx 1-(4-3\sqrt{2})(\lambda-\lambda_0)$. In an infinite chain, the frequency of this mode describing the oscillations of the center of the DW in the limit $\lambda\gg\lambda_0$ tends to zero, and the dependence $\Omega(\lambda)$ for this oscillatory mode must coincide with that obtained by Bogdan *et al.*[20]

SOLITON-LIKE COLLINEAR SPIN STRUCTURE

Let us consider a more complicated spin configuration of the type …↑↑↑↓↑↑↑… with one inverted spin. In the long-wave description, such a state could exist only in the dynamic case and corresponded to a magnetic soliton. When discrete exchange interaction is taken into account, the static state of this type corresponding to a 360° collinear domain wall (referred to as ''soliton'' for brevity) can also exist.

For small values of exchange interaction, the ground state of the system corresponds to the following distribution of spin orientation angles in the easy plane:

$$\varphi_n=0, \quad n\leqslant -1,$$
$$\varphi_0=\pi, \tag{28}$$
$$\varphi_n=2\pi, \quad n\geqslant 1.$$

We introduce small corrections $\psi_n\ll 1$ to the ground state and obtain from (10) the following system of linear algebraic equations for solutions of the form $\psi_n=v_n\exp(i\Omega t)$:

$$\begin{aligned}&(2\lambda+1-\Omega^2)v_n-\lambda(v_{n+1}+v_{n-1})=0, \ |n|\geqslant 2,\\ &(1-\Omega^2)v_1+\lambda(v_0-v_2)=0,\\ &(-2\lambda+1-\Omega^2)v_0+\lambda(v_1+v_{-1})=0,\\ &(1-\Omega^2)v_{-1}+\lambda(v_0-v_{-2})=0.\end{aligned} \tag{29}$$

As in the previous case, it is natural to seek localized solutions for internal modes of the spin configuration under investigation in the form

$$\begin{aligned}&v_n=A\exp(-\kappa n), n\geqslant 1,\\ &v_0=C,\\ &v_n=B\exp(\kappa n), \ \ n\leqslant -1.\end{aligned} \tag{30}$$

From equations (29) for $n\leqslant -2$ and $n\geqslant 2$, we obtain relation (16) between the parameters κ,Ω,λ, while the equations for v_{-1},v_0, and v_1 leads to the relation between A,B, and C and the additional relation between κ,Ω,λ:

$$\frac{C}{A}=\frac{C}{B}=\exp(-\kappa)\left[\exp(-\kappa)-\frac{1-\Omega^2}{\lambda}\right]; \tag{31}$$

$$\left[\exp(-\kappa)-\frac{1-\Omega^2}{\lambda}\right] \times\left\{\left[\exp(-\kappa)-\frac{1-\Omega^2}{\lambda}\right]\left(2-\frac{1-\Omega^2}{\lambda}\right)-2\right\}=0. \tag{32}$$

In expression (32), one solution for which $1-\Omega^2=\lambda\exp(-\kappa)$ splits immediately. This solution corresponds to an antisymmetric mode with $A=B$, $C=0$, whose amplitude attenuates with increasing distance from the center of a ''soli-

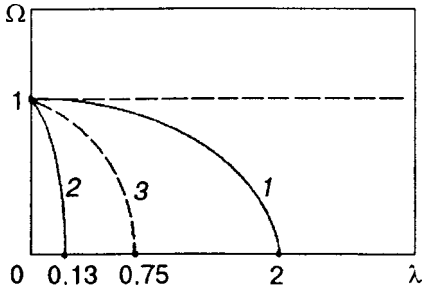

FIG. 3. Frequency dependence of internal modes of a localized collinear structure with an inverted spin in a layer of an easy-plane ferromagnet: curve *1* is the antisymmetric mode and curve *2* is the symmetric mode. The dependence $\Omega(\lambda)$ for the internal mode of a collinear DW (curve *3*) is shown for comparison.

tion'' with the spatial damping decrement $\kappa=\ln 2$. The dependence of the frequency of this mode on the magnitude of exchange interaction (discreteness parameter λ) has the form

$$\Omega^2=1-\lambda/2, \tag{33}$$

and the mode emerges as a result of bifurcation and exists for $\lambda\leqslant 2$ (curve *1* in Fig. 3). The distribution of spin oscillation amplitudes in this mode has the form $\ldots\uparrow 0\downarrow\ldots$, where dots denote spins oscillating with small amplitudes, and the symbol 0 corresponds to a stationary central inverted spin.

Using relation (16), eliminating the parameter κ from (32), and introducing the quantity $Z=1-\Omega^2$, we can easily write the expression in the braces in (32) in the form

$$Z(2Z^2-7\lambda Z+4\lambda^2)=0. \tag{34}$$

Thus, three additional solutions of the system under investigation also exist. The first solution $Z=0$ corresponds to the edge of the spectrum of spin waves with $\Omega=1$, $\kappa=0$, $A=B=C$. As in the case of a 180° domain wall, a soliton (360° domain wall) in this model does not interact with homogeneous oscillations of the edge of the continuous spectrum. The second solution with the dependence $\Omega^2=1-\lambda(7-\sqrt{17})/4$ does not satisfy our assumption on the localization of the oscillation. In this solution, $\kappa=\ln[(5-\sqrt{17})/2]<0$, and its amplitude increases with the distance from the soliton center. Finally, a solution for localized symmetric oscillations with the following dependence of the frequency of this internal mode on the discreteness parameter

$$\Omega^2=1-\lambda(7+\sqrt{17})/4, \tag{35}$$

and the following relation between the amplitudes of spin oscillations in the localized state

$$A=B, C=-A\frac{\sqrt{17}-3}{2}. \tag{36}$$

also exists.

The amplitudes of oscillations in this solution exhibit rapid spatial attenuation with increasing distance from the soliton center ($\kappa=\ln[(5-\sqrt{17})/2]$), and three central spins oscillate in actual practice. The dependence (35) shown in Fig. 3 by curve *2* terminates for the value $\lambda=(7-\sqrt{17})/8\approx 0.13$. Curve *3* in this figure shows the dependence $\Omega(\lambda)$ for a collinear 180° domain wall in Fig. 1. For a fixed value of exchange interaction in the range of small parameters λ, the frequency of the symmetric internal mode lies below the frequency of the antisymmetric mode. Since the solution for a 360° domain wall can be interpreted as the state of two adjacent 180° domain walls, symmetric and antisymmetric internal modes having a configuration with an inverted spin emerge as a result of detachment of the internal mode frequency of a 180° domain wall in the system of two such walls.

The interpretation of nonlinear dynamic states in the case of an easy-plane ferromagnet is more complicated than in the case of an easy-axis ferromagnet considered earlier,[14] and it remains unclear how the dependence for a soliton solution in the case of a strong exchange interaction ''matches'' to the frequency dependence for internal modes of soliton-like states for small values of λ in the region of transient values of exchange integral.

Nevertheless, we can give a number of arguments showing that the internal modes emerging for small values of exchange interaction in this case differ qualitatively in origin from soliton solutions for large values of exchange. It is known from the theory of dynamic solitons[17] that soliton solutions for finite-dimensional systems ''split'' from spatially homogeneous excitations of the system and have the same symmetry, i.e., the phases of oscillations of particles (or spins as in our case) in a soliton are the same along the entire chain.

Let us consider the phases of spin oscillations in the internal modes studied above. We shall comment the situation with a 360° domain wall for a simple finite-dimensional system consisting of three spins with numbers $n=-1,0,1$ for which deviations from the ground state are permitted. The spectrum of intrinsic linear excitations of the form $\varphi_n=v_n\exp(i\Omega t)$ for the ground state of this system with parallel spins consists of three modes with $\Omega^2=1(\nu_0=\nu_1=\nu_{-1})$, $\Omega^2=1+\lambda(\nu_0=0, \nu_1=-\nu_{-1})$ and $\Omega^2=1+3\lambda(\nu_0=-2\nu_1=-2\nu_{-1})$.

On the other hand, in a configuration of the type of the 360° domain wall considered above, i.e., for the ground state $\varphi_0=\pi, \varphi_1=\varphi_{-1}=0$, the spectrum of small oscillations relative to this state is formed by the following internal modes: $\Omega^2=1(\nu_0=\nu_1=\nu_{-1})$, $\Omega^2=1-\lambda(\nu_0=0, \nu_1=-\nu_{-1})$ and $\Omega^2=1-3\lambda(\nu_0=-2\nu_1=-2\nu_{-1})$. The last two modes are equivalent to the antisymmetric and symmetric modes of the infinite spin chain with an inverted spin considered above.

These two ''internal'' modes coincide in symmetry with the modes from the spectrum of linear excitations of the ground state. In the case of an inhomogeneous ground state, these modes are transformed from two lower-lying modes following the homogeneous mode and having different symmetries. Since the soliton mode must split from the homogeneous mode and possess a different symmetry, this is a new type of localized excitations emerging for small values of exchange interaction. It should be noted that in the case of an easy-plane ferromagnet, a soliton excitation in the long-wave limit corresponds to the oscillation of the central spin about

the position $\varphi_0 = 0$, while oscillations of the central spin in the obtained internal modes occur about the value of $\varphi_0 = \pi$.

Thus, we have analyzed the dynamics of localized nonlinear excitations of the type of collinear 180° and 360° domain walls for ferro- and antiferromagnets with a strong easy-plane single-ion anisotropy and a weak additional anisotropy in this plane on the basis of the classical Takeno–Homma discrete model. Internal modes of these states are determined as well as their frequency dependence on the magnitude of exchange interaction (discreteness parameter).

The authors are grateful to M. M. Bogdan for fruitful discussions and valuable remarks concerning the text.

This research was carried out under the support of the International Science Foundation (ISEP Grant No. QSU082087).

*)E-mail: kovalev@ilt.kharkov.ua

[1] A. M. Kosevich, B. A. Ivanov, and A. S. Kovalev, *Nonlinear Magnetization Waves. Dynamic and Topological Solitons* [in Russian], Naukova Dumka, Kiev (1983).
[2] A. M. Kosevich, B. A. Ivanov, and A. S. Kovalev, Phys. Rep. **194**, 117 (1990).
[3] A. A. Stepanov, V. A. Pashchenko, and M. I. Kobets, Fiz. Nizk. Temp. **14**, 550 (1988) [Sov. J. Low Temp. Phys. **14**, 304 (1988)].
[4] A. A. Stepanov, V. A. Pashchenko, and M. I. Kobets, Fiz. Nizk. Temp. **14**, 1212 (1988) [Sov. J. Low Temp. Phys. **14**, 669 (1988)].
[5] A. A. Stepanov, M. I. Kobets, and V. A. Pashchenko, Fiz. Nizk. Temp. **20**, 267 (1994) [Low Temp. Phys. **20**, 211 (1994)].
[6] A. A. Stepanov, M. I. Kobets, and V. A. Pashchenko, Fiz. Nizk. Temp. **21**, 1084 (1995) [Low Temp. Phys. **21**, 834 (1995)].
[7] A. A. Stepanov and D. A. Yablonskii, Fiz. Nizk. Temp. **15**, 215 (1989) [Sov. J. Low Temp. Phys. **15**, 122 (1989)].
[8] A. N. Goncharuk, A. A. Stepanov, and D. A. Yablonskii, Fiz. Tverd. Tela (Leningrad) **31**, 132 (1989) [Sov. Phys. Solid State **31**, 2099 (1989)].
[9] J. J. Van den Broek and H. Zijlstra, IEEE Trans. Magn. **7**, 226 (1971).
[10] V. S. Ostrovskii, Pis'ma Zh. Éksp. Teor. Fiz. **42**, 143 (1985) [JETP Lett. **42**, 175 (1985)].
[11] V. M. Loktev and V. S. Ostrovskii, Fiz. Tverd. Tela (Leningrad) **27**, 3026 (1985) [Sov. Phys. Solid State **27**, 1816 (1985)].
[12] V. M. Loktev and V. S. Ostrovskii, Fiz. Nizk. Temp. **20**, 983 (1994) [Low Temp. Phys. **20**, 775 (1994)].
[13] M. V. Gvozdikova, A. S. Kovalev, and Yu. S. Kivshar, Fiz. Nizk. Temp. **24**, 635 (1998) [Low Temp. Phys. **24**, (1998)].
[14] M. V. Gvozdikova and A. S. Kovalev, Fiz. Nizk. Temp. **24**, 1077 (1998) [Low Temp. Phys. **24**, 808 (1998)].
[15] S. Takeno and S. Homma, J. Phys. Soc. Jpn. **56**, 457 (1987).
[16] S. Homma, Prog. Theor. Phys. **77**, 1090 (1987).
[17] A. M. Kosevich and A. S. Kovalev, *Introduction to Nonlinear Physical Mechanics* [in Russian], Naukova Dumka, Kiev (1990).
[18] Fei Zhang, Physica D **D110**, 51 (1997).
[19] O. M. Braun, Yu. S. Kivshar, and M. Peyrard, Phys. Rev. E **56**, 6050 (1997).
[20] M. M. Bogdan, A. M. Kosevich, and V. O. Voronov, in *Solitons and Applications* (ed. by V. G. Makhankov, V. K. Fedyanin, and O. K. Pashaev), World Scientific, Singapore (1990).

Translated by R. S. Wadhwa

ELECTRONIC PROPERTIES OF METALS AND ALLOYS

Phenomenological model for Casimir attraction of a metal film

V. N. Dubrava and V. A. Yampol'skiĭ

Institute for Radiophysics and Electronics, National Academy of Sciences of the Ukraine, 310085 Kharkov, Ukraine[*)]

(Submitted May 26, 1999; revised July 9, 1999)
Fiz. Nizk. Temp. **25**, 1304–1312 (December 1999)

The force of surface interaction (Casimir effect) between a bulk conductor and a metal film deposited on a dielectric substrate is studied by the method of quantum field theory. The film thickness is assumed to be much smaller than the skin depth at characteristic frequencies of fluctuation fields. The equations for one-particle Green's function of the electromagnetic field in the metal film are solved on the basis of a simple phenomenological model. Namely, complex macroscopic electrodynamic properties of the film are described by introducing the surface permittivity determined by the conductivity $\langle\sigma\rangle$ averaged over sample thickness. The dependence of the Casimir attractive force on the specularity parameter ρ characterizing the interaction of conduction electrons with the film surface is predicted. The results of investigations demonstrate that the electronic and surface properties of metal films can in principle be studied experimentally by measuring the force of their Casimir attraction. [S1063-777X(99)00912-3]

1. INTRODUCTION

According to the definition given by its author,[1] the Casimir effect is an ''observable nonclassical force of electromagnetic attraction between two parallel perfectly conducting plates.'' This force per unit area is defined as

$$F_0 = -\frac{\partial \mathcal{E}}{\partial a} = -\frac{\pi^2}{240}\frac{\hbar c}{a^4}. \tag{1}$$

Here $\mathcal{E}$ is the energy of interaction, $\hbar$ Planck's constant, c the velocity of light, and a the separation between the plates. Casimir interpreted the emergence of the force F_0 as the result of a peculiar liberation of energy E of electromagnetic vacuum during its partial filling with a material medium.

The Casimir force also emerges in a more general case of interaction between plane-parallel dielectric media[2] and can be interpreted in the sense of the Van der Waals (molecular) attraction. This specific type of the Van der Waals interaction is of fluctuational electromagnetic origin and is associated with spontaneous polarization of dielectrics. Depending on temperature, either quantum-mechanical or thermal mechanisms of polarization dominate in the medium. The criterion is the ratio of the characteristic frequency ω_c of ''radiation'' to the parameter $kT/\hbar$. For

$$kT \ll \hbar\omega_c \tag{2}$$

the interaction between two media occurs through the vacuum electromagnetic field. The Casimir result (1) can be obtained under the low-temperature condition (2) if the permittivity ϵ of bodies tends to infinity.

For real conductors, we have

$$\epsilon = 1 + \frac{i\sigma(\omega)}{\omega}, \tag{3}$$

where $\sigma(\omega)$ is the conductivity. Simple analysis shows that for

$$\omega_c \ll \omega_p \tag{4}$$

(ω_p is the plasma frequency), the frequency dispersion in conductivity is manifested only in corrections to force (1) in view of the large electrical conductivity of metals. The relative value of these corrections has the scale[3]

$$\Delta F/F_0 \sim Z \ll 1, \tag{5}$$

where $Z = 1/\sqrt{\epsilon(i\omega_c)}$ is the surface impedance of the metal at the characteristic frequency $\omega_c \sim c/a \ll \omega_p$.[1)] It should be noted that under the conditions (2) and (4), the Casimir force is described by formula (1) in the main approximation irrespective of the type of the conductor. For example, it is insensitive to the electron spectrum anisotropy. The decisive circumstance in this case is that expression (1) is the consequence of vanishing of the electric component of the fluctuational field at the boundaries of conductors.

If we consider the interaction between thin films of thickness d much smaller than the characteristic skin depth δ, inequality (5) is violated even for a large electrical conductivity σ. In this case, we go over from the asymptotic form (1) obtained in the limit $d \gg \delta$ to a new expression for the Casimir force which[4] is a function of not only the size of the film, but also its electronic characteristics, viz., plasma frequency ω_p and electron relaxation frequency ν.

It should be emphasized that the sensitivity of the Casimir force to collective peculiarities of the metal is natu-

rally not exhausted by the above-mentioned functional dependence on plasma frequency and electron relaxation frequency, which should be referred to as bulk characteristics of the electron subsystem. Another important peculiarity of any conducting medium is the type of electron–surface scattering playing a fundamental role in the electrodynamics of conductors for $d \ll l$ ($l = v_F/(\nu - i\omega)$ is the effective electron mean free path and v_F the Fermi velocity).

This research is mainly devoted to an analysis of the role of surface properties of a metal film in the formation of the Casimir force. The results of this analysis demonstrate that it is possible in principle to study experimentally the ''roughness'' parameter of the metal film boundary through precision measurements of the force of its Casimir attraction.

In Sec. 2, the technique for calculating the Casimir force proposed by Lifshitz and Pitaevskii[1] is developed and a simplified expression for the free energy of two interacting plane-parallel macroscopic bodies with arbitrary dielectric permittivities is derived.

In the next sections, the attractive force exerted by a bulk conductor on a thin metal film deposited on a dielectric substrate with a low optical density is investigated. In Sec. 3, the problem is formulated and basic inequalities under which the effect of temperature in the Casimir force can be neglected and individual peculiarities of conducting media should be taken into account. Section 4 is devoted to the solution of electrodynamic equations for Green's function of the electromagnetic field. The response of vacuum to a thin metal film is described by introducing into the field equations of the surface permittivity associated with the conductivity of the metal film averaged over the sample thickness. In Sec. 5, several asymptotics are obtained for the energy of interaction of a bulk conductor with a thin metal film for specular and diffuse boundaries under the frequency conditions of the normal and ''infrared'' skin effects. Besides, we analyze the role of dielectric properties of the substrate which also participate in the Casimir interaction and find the conditions under which the resultant Casimir force in the main approximation is determined by the electron parameters of the metal.

2. FREE ENERGY IN THE CASIMIR EFFECT

The Van der Waals contribution to the free energy of an inhomogeneous condensed medium with a local complex permittivity $\epsilon(\mathbf{r}|\omega)$ is given by the formula[2]

$$\delta\mathcal{F} = -kT \sum_{n=0}^{\infty}{}' \omega_n^2 \int dr \mathcal{D}_{ii}(\mathbf{r},\mathbf{r}|\omega_n)\,\delta\epsilon(\mathbf{r}|i\omega_n), \tag{6}$$

where $\mathcal{D}_{ik}(\mathbf{r},\mathbf{r}'|\omega_n)$ is the temperature Green's function of electromagnetic field, $\omega_n = 2\pi nkT$, and the prime on the sum symbol indicates that the term with $n=0$ is taken with half the weight; here and below, $\hbar = c = 1$.

Formula (6) can be presented in compact form:

$$\delta\mathcal{F} = -kT \sum_{n=0}^{\infty}{}' \omega_n^2 \mathrm{Tr}_{(r)} \mathcal{D}(\omega_n)\,\delta\epsilon(\omega_n). \tag{7}$$

Here $\mathcal{D}(\omega_n)$ is Green's operator with the matrix elements $\mathcal{D}_{ik}(\mathbf{r},\mathbf{r}'|\omega_n)$; $\epsilon(\omega_n)$ is the diagonal operator of permittivity, and the operation Tr is interpreted in the functional sense, i.e.,

$$\mathrm{Tr}_{(\mathbf{r})} F = \int d\mathbf{r}\,\mathrm{tr}[F(\mathbf{r},\mathbf{r})] \tag{8}$$

(tr[…] is the ordinary trace).

The explicit form of the Greenian $\mathcal{D}$ in the ''radiation'' gauge is determined by the solution of the linear equation

$$K\mathcal{D} = -1, \tag{9}$$

in which the differential operator K has the kernel

$$K_{il}(\mathbf{r},\mathbf{r}'|\omega_n) = [\epsilon(\mathbf{r}|i\omega_n)\omega_n^2\delta_{il} + \mathrm{rot}_{im}\mathrm{rot}_{ml}]\,\delta(\mathbf{r}-\mathbf{r}').$$

Using (9), we can easily see that the total change in the free energy $\mathcal{F}$ upon a change in permittivity ϵ is

$$\mathcal{F} = kT \sum_{n=0}^{\infty}{}' \omega_n^2 \mathrm{Tr}_{(\mathbf{r})}[\log K(\omega_n)]. \tag{10}$$

For two independent e- and m-polarizations of the electromagnetic field,[5] we have

$$K_e = \omega_n^2\epsilon - \nabla^2;$$

$$K_m = \omega_n^2 - \left(\nabla, \frac{1}{\epsilon}\nabla\right). \tag{11}$$

Disregarding the infinitely large additive constant, we can write

$$\log K = -\int_0^{\infty} dm^2 \frac{1}{m^2 + K},$$

where the auxiliary variable m has the meaning of effective mass. Thus, according to (10), we have

$$\mathcal{F} = -kT \sum_{n=0}^{\infty} \sum_{n=0}^{\infty}{}' dm^2 \mathrm{Tr}_{(\mathbf{r})} \mathcal{G}(\omega_n). \tag{12}$$

Here $\mathcal{G} = (m^2 + K)^{-1}$ is Green's function with the matrix elements $\mathcal{G}(\mathbf{r},\mathbf{r}'|\omega_n)$ satisfying the equation

$$(m^2 + K)\mathcal{G}(\mathbf{r},\mathbf{r}'|\omega_n) = \delta(\mathbf{r}-\mathbf{r}'). \tag{13}$$

In order to simplify the general formula (12), we use symmetry considerations. For this purpose, we choose the system of coordinates so that the x-axis is perpendicular to the plane of interacting plates. Then it follows from isotropy and translation invariance of the system in the y, x plane that

$$\mathcal{G} = \mathcal{G}(|\rho - \rho'|),$$

where $\rho = (y,z)$ is the two-dimensional radius vector. Expanding $\mathcal{G}$ into a two-dimensional Fourier integral, we obtain on the basis of formula (8)

$$\mathrm{Tr}_{(\mathbf{r})}\mathcal{G} = \mathrm{Tr}_x \int \frac{d\mathbf{p}\,d\mathbf{q}}{(2\pi)^2} g(x,x'|q^2,\omega_n).$$

Ultimately, expression (12) for the Van der Waals contribution to the free energy of the system of two plane-parallel media can be written in the form

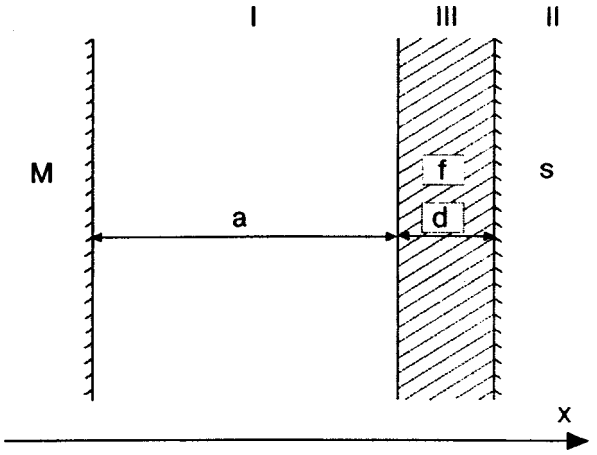

FIG. 1. Geometry of the problem: bulk metal (M), metal film (f), and dielectric substrate (s).

$$\mathcal{F}=-\frac{kT}{(2\pi)^2}S\sum_{n=0}^{\infty}{}'\int_0^\infty dm^2\int_{-\infty}^{\infty}d\mathbf{q}(\mathrm{Tr}_x g), \tag{14}$$

where S is the area of the plates.

Under the low-temperature conditions (2), the sum in Eq. (14) can be replaced by the integral. The obtained expression defines the energy E of the vacuum electromagnetic field in the presence of a stationary system of bodies, i.e.,

$$\frac{E_{(e,m)}}{S}=-\frac{1}{8\pi^2}\int_0^\infty dm^2dq^2d\zeta\int_{-\infty}^{\infty}dx g_{(e,m)}(x,x), \tag{15}$$

where Green's functions $g_{(e,m)}(x,x')$ for two independent e- and m-polarizations of electromagnetic field, which are known in electrodynamics as E- and H-waves, can be determined as solutions of the differential equations

$$\left(m^2+q^2+\zeta^2\epsilon(x)-\frac{\partial^2}{\partial x^2}\right)g_e(x,x')=\delta(x-x'),$$
$$\left(m^2+\frac{q^2}{\epsilon(x)}+\zeta^2-\frac{\partial}{\partial x}\frac{1}{\epsilon(x)}\frac{\partial}{\partial x}\right)g_m(x,x')=\delta(x-x'), \tag{16}$$

where $\epsilon(x)$ is the permittivity of the system of bodies under investigation as a function of the coordinate x.

3. GEOMETRY OF THE PROBLEM AND BASIC INEQUALITIES

Let us consider a static system comprising a bulk conductor M and a thin metal film f (region III) of thickness d on a dielectric substrate s (region II) having the permittivity $\epsilon_\infty=\text{const}$. The size of the gap (region I) between the film f and the bulk metal M is denoted by a (see Fig. 1). Under the condition of optical transparency of the film–substrate system, we can separate in the asymptotics for the Casimir energy $\mathcal{E}$ two additive contribution $\mathcal{E}_{M-f}$ and $\mathcal{E}_{M-s}$ attributed to the interaction of the bulk conductor with the metal film and with the dielectric substrate:

$$\mathcal{E}=\mathcal{E}_{M-f}+\mathcal{E}_{M-s}. \tag{17}$$

This actually means that the presence of the metal film does not affect the Casimir interaction between the conductor and the dielectric substrate in the main order, and the introduction of the dielectric in turn does not affect the interaction between the conductor and the metal film. Thus, while determining $\mathcal{E}_{M-f}$, we can neglect the effect of the substrate, i.e., assume that $\epsilon_\infty=1$, and while calculating $\mathcal{E}_{M-s}$, we can disregard the effect of the film, i.e., put $d=0$. The differences that can emerge in this case as compared to the exact solution of the problem have a higher order of smallness than the terms in (17).

Apart from optical transparency, we shall also assume that the conditions of the low–temperature approximation (2) are satisfied, which means that we can neglect thermal fluctuations of electromagnetic field, as well as inequality (4) equivalent to the condition of vanishing of displacement current in Maxwell's equations.

4. DETERMINATION OF GREEN'S FUNCTION OF ELECTROMAGNETIC FIELD

While analyzing the contribution to the Casimir energy from the e- and m-polarized fluctuational electromagnetic field, we must solve Eqs. (16) together with the boundary conditions of continuity for g and its normal derivative (for E-waves) and the quantity g'/ϵ (for H-waves) at the points of discontinuity of $\epsilon(x)$. It is well known that Green's function g in each of the regions I–III can be expressed in terms of two linearly independent fundamental solutions u_- and u_+ satisfying a homogeneous equations and defined on the left and right boundaries of the region under investigation:

$$g(x,x')=\frac{1}{W}\begin{cases}u_-(x)u_+(x'), & x<x',\\ u_-(x')u_+(x), & x'<x,\end{cases}$$

where $W=u_-(x)u'_+(x)-u'_-(x)u_+(x)$ is the Wronskian.

An analysis shows that in the case of optical transparency of the metal film, a decisive contribution to the Casimir energy comes from fluctuations of the m-polarized electromagnetic field. For this reason, we write only the fundamental solutions of the second equation from system (16), i.e. we are interested in:

$$\begin{cases}u_-=\cosh k(x-d)-\epsilon kd\sinh ka\cosh k(x-a-d),\\ u_+=\cosh k(x-D).\end{cases} \tag{18}$$

Here D is an infinitely large distance at which a perfectly reflecting mirror is arranged (its introduction is necessary if we assume that the system is closed), the surface dielectric permittivity ϵ is defined as

$$\epsilon=1+\frac{\langle\sigma(i\zeta)\rangle}{\zeta},$$

$\langle\sigma\rangle$ is the conductivity of the metal film averaged over its thickness, and $k=(\zeta^2+q^2+m^2)^{1/2}$. Besides, we assume that the inequality $d\epsilon^{1/2}/\zeta\ll 1$ is satisfied.

The system of fundamental solutions in region I can be obtained from Eq. (18) by replacing ''right'' by ''left'' relative to the film f, i.e.,

$$u_-\leftrightarrow u_+,\quad D-x\to x,\quad a\to D-a-d.$$

We do not write fundamental solutions in region III since the value of the integral over the interval $a<x<a+d$ in Eq. (15) is much smaller than the value of integrals over the vacuum regions I and II.

We can now easily find, on the basis of Eq. (18), an expression for Green's function of the m-component of the fluctuational electromagnetic field. The result of its integration for coinciding arguments can be written in the form

$$\int_0^D dx g_m(x,x)=\frac{\partial}{\partial m^2}\ln W_m, \tag{19}$$

where

$$W_m=k[\sinh k(D-d)+\epsilon kd\sinh ka\sinh k(D-d-a)] \tag{20}$$

is the Wronskian having the meaning of the dispersion equation for eigenmodes of the system under investigation at an imaginary frequency.

5. CALCULATION OF CASIMIR ENERGY

Substitutingb Eq. (19) into (15) and carrying out elementary integration with respect to the variable m^2, we obtain

$$\frac{E}{S}=\frac{1}{8\pi^2}\int_0^\infty dq^2 d\zeta \ln k[\sinh k(D-d)+\epsilon kd\sinh(ka)\sinh k(D-d-a)]. \tag{21}$$

Direct evaluation of integral (21) leads to an infinitely large value of E. The divergence of the energy E of vacuum in Eq. (21) is primarily due to the high intensity of vacuum fluctuations for small wavelengths. But since the observable value in the Casimir effect is the attractive force F and not the energy E, the energy of interaction $\mathcal{E}$ is defined to within an arbitrary term E_0 independent of a, which vanishes after differentiation:

$$E(a)=\mathcal{E}(a)+E_0.$$

It was found that the divergence in Eq. (21) is just due to the nonobservable energy component E_0. An analysis of formula (21) shows that its origin is associated with the infinitely large energy of zero-point oscillations, which is proportional to the volume DS occupied by the electromagnetic system as well as to the ''surface'' energy (proportional to S) emerging due to transparency of the film boundaries. The subtraction of infinitely large contributions to $E(a)$ corresponding to them is equivalent to the choice of $E_0=E(a\to\infty)$. Consequently, the finite component $\mathcal{E}(a)$ in the energy of electromagnetic vacuum we are interested in is defined as

$$\mathcal{E}(a)=E(a)-E(a\to\infty), \tag{22}$$

where the quantity $E(a\to\infty)$ denotes the asymptotic form of E for $a\to\infty$. On the basis of Eq. (22), we can conclude that the quantum-electrodynamic meaning of the Casimir energy lies in partial liberation of the energy of vacuum as a result of introduction of material bodies into it.

Using Eqs. (21) and (22), we obtain the final result for the energy of Casimir interaction between a bulk conductor and a thin metal film:

$$\mathcal{E}_{M-f}=\frac{1}{8\pi^2}\int_0^\infty dq^2\int d\zeta\ln\left[1-\frac{\epsilon kd}{2+\epsilon kd}\exp(-2ka)\right]. \tag{23}$$

While evaluating the double integral in Eq. (23), we must specify the dependence of $\langle\sigma\rangle$ on the surface and volume (ω_p,ν) characteristics of the electron subsystem. In the framework of the classical approach, electron scattering by the metal surface is described by the boundary condition for the electron distribution function. In the simplest model,[6] the surface properties are characterized by the specular parameter ρ which is equal to the relative number of electrons reflected specularly at the sample boundary. In the isotropic case, the electrical conductivity $\langle\sigma\rangle$ of a thin metal film with a specularly reflecting $(\rho=1)$ and diffuse $(\rho=0)$ boundary is defined by the following asymptotic expressions:[6]

$$\langle\sigma\rangle=\begin{cases}\sigma_L, & \rho=1\\ \sigma_F=(3d\sigma_L/4l)\ln(l/d), & \rho=0,\end{cases} \tag{24}$$

in which $\sigma_L=\omega_p^2/(\nu-i\omega)$ is the conductivity of the bulk sample and σ_F the Fuchs conductivity.

Formula (24) is valid in the so-called Knudsen limit $d\ll l$. In this case, the conductivity of a film with diffuse boundaries is due to a small group of transient electrons moving almost parallel to the plate surface and experiencing no collisions with the boundaries during the mean free time. The relative number of transient electrons is equal to d/l in the order of magnitude.

For $d\gg l$, when the effects connected with surface scattering of electrons are masked by bulk collisions, the conductivity in the main approximation is insensitive to the type of the electron–surface interaction, i.e.,

$$\langle\sigma\rangle=\sigma_L.$$

Using Eq. (24), we obtain analytic expressions for the Casimir energy (23).

1. *Specular boundary* $(\rho=1)$. In this simple case, we reproduce the results obtained earlier in Ref. 7:

$$\mathcal{E}_{M-f}^{(\rho=1)}=-0.70\hbar\omega_p\frac{\sqrt{ad}}{\pi(4a)^3},$$

$$\nu\ll\omega_p\sqrt{d/a}\ll\omega_p,\quad c/a, \tag{25}$$

$$\mathcal{E}_{M-f}^{(\rho=1)}=-\frac{\hbar\sigma_0}{2\pi^2}\frac{d}{(2a)^3}\ln\left(\frac{\nu}{\omega_p}\sqrt{a/d}\right),$$

$$\omega_p\sqrt{d/a}\ll\nu\ll\omega_p,\quad c/a. \tag{26}$$

Pay attention to the fact that for samples with specular boundaries, the conditions corresponding to the normal $(\omega_0\ll\nu)$ and infrared $(\nu\ll\omega_0)$ skin effects can be realized in the Casimir effect depending on the relation between the relaxation frequency ν and $\omega_0=\omega_p\sqrt{d/a}$. For $\nu\ll\omega_0$, the quantity $\mathcal{E}_{M-f}$ has the same functional dependence on the parameters of the problem as for the Casimir energy in a system of two thin metal films of the same thickness.[4] This is due to the fact that the main contribution to the Casimir interaction in both cases comes from the frequency $\omega_c\sim\omega_0$. In the frequency range corresponding to the normal skin effect, the

decisive contribution comes from the frequency interval (ω_0, ν). Consequently, the value of $\mathcal{E}_{M-f}$ turns out to be larger than the corresponding asymptotic forms from Ref. 4 by a factor equal to the logarithm of the parameter $(\nu/\omega_p)\sqrt{a/d} \gg 1$.

2. *Diffuse boundary* $(\rho=0)$. In the case of diffuse reflection of electrons at the metal film boundary, the Casimir energy cannot be calculated with an asymptotic accuracy. This is mainly due to the emergence of the Fuchs logarithm $\ln(l/d)$ in Eq. (24) for the average conductivity $\langle\sigma\rangle$. It should be noted, however, that the Knudsen limit $l \gg d$ is violated for relatively large characteristic frequencies. This restricts considerably the range of applicability of formula (23) for the Casimir energy as a function of the Fuchs conductivity σ_F (24). We can avoid artificial restriction imposed on characteristic frequencies by dividing the integral with respect to ζ in Eq. (23) into two parts:

$$\int_0^\infty d\zeta = \int_0^{\omega_K} d\zeta(\sigma=\sigma_F) + \int_{\omega_K}^\infty d\zeta(\sigma=\sigma_L), \tag{27}$$

where ω_K is the characteristic frequency for which the Knudsen approximation is formally violated. Such a mathematical approach is valid rigorously only if the integration domain in the neighborhood of the point ω_K makes a small contribution to the values of both integrals. This condition can be violated in the frequency range corresponding to the normal skin effect since the characteristic frequencies in the low-frequency limit assume values from a finite interval. Consequently, the application of formula (27) in the general case requires additional mathematic substantiation.

In order to avoid difficulties associated with the application of the Fuchs conductivity σ_F, we use the general expression for the average conductivity of a metal film of arbitrary thickness with a diffuse boundary,

$$\langle\sigma\rangle = \frac{3}{2}\sigma_0 \int_0^1 dn(1-n^2)\left[1-\frac{1}{d}\left(1-\exp\left(-\frac{d}{\ln}\right)\right)\right] \tag{28}$$

and the approximate formula for the energy of Casimir interaction:

$$\mathcal{E}_{M-f}^{(\rho=0)} = -\frac{1}{8\pi^2(2a)^3} \times \int_0^\infty dx\, x^2 \exp(-x) \int_{p_c}^1 \frac{dp}{p}\langle\sigma(p,x)\rangle d + \ldots, \tag{29}$$

which is valid (to within an insignificant numerical factor of the order of unity) for $p_c \ll 1$. In this formula, the lower integration limit p_c can be determined from the condition

$$p \sim \langle\sigma(p)\rangle d.$$

Formula (29) is fundamental for taking into account collective properties of the electron subsystem in the Casimir force and can be obtained from Eq. (23) after the substitution of variables

$$q = \omega\sqrt{1/p^2-1}, \quad \zeta = \frac{x}{2a}p$$

and the expansion of the logarithm into a power series.

Under the conditions of the infrared skin effect, when

$$\nu a \ll p_c,$$

we assume that $d/l = \Delta x p/2$, where $\Delta = d/v_F a$ is an arbitrary parameter. Substituting Eqs. (28) into (29) and integrating with respect to the variable x, we obtain the following simplified expression for the Casimir energy:

$$\mathcal{E}_{M-f}^{(\rho=0)} = -\frac{3A^2}{8\pi^2(2a)^3}\int_{p_c}^1 \frac{dp}{p^2}\int_0^1 dn(1-n^2)\frac{1}{1+2n/\Delta p}, \tag{30}$$

where $A^2 = da\omega_p^2$.

For comparatively small distances (or large characteristic frequencies), when $\Delta \gg 1$, the ''infrared'' Casimir effect acquires two characteristic frequency regions depending on the value of the dimensionless parameter $p_c\Delta$. For $p_c\Delta \gg 1$, we have $p_c \sim A \ll 1$, and the leading term in the asymptotic form of the Casimir energy assumes, in accordance with Eq. (30), the form

$$\mathcal{E}_{M-f}^{(\rho=0)} \simeq -\hbar\omega_p \frac{\sqrt{ad}}{\pi(4a)^3},$$

$$\nu\frac{l_0}{d} \ll \omega_p\sqrt{d/a} \ll c/a, \quad \omega_p, \tag{31}$$

where $l_0 = v_F/\nu$ is the electron mean free path. For $p_c\Delta \ll 1$, we have $p_c \sim A^2\Delta \ll 1$, and

$$\mathcal{E}_{M-f}^{(\rho=0)} = -\frac{3\hbar\omega_p}{(8\pi a)^2}\frac{d^2\omega_p}{av_F}\ln^2\left(\frac{d\omega_p}{v_F}\sqrt{d/a}\right),$$

$$\nu\sqrt{l_0/d} \ll \omega_p\sqrt{d/a} \ll \nu\frac{l_0}{d} \ll \frac{c}{a}, \quad \omega_p. \tag{32}$$

Finally, under the conditions of normal skin effect, when

$$\omega_p\sqrt{d/a} \ll \nu\sqrt{l_0/d} \ll \nu\frac{l_0}{d} \ll \frac{c}{a}, \quad \omega_p,$$

the asymptotics of the Casimir energy can be estimated on the basis of formula (26) if we substitute the static Fuchs conductivity $\sigma_F = (3d\sigma_0/4l_0)\ln(l_0/d)$ for the Lorentz conductivity σ_0:

$$\mathcal{E}_{M-f}^{(\rho=0)} \approx \frac{\hbar\sigma_F}{2\pi^2}\frac{d}{(2a)^3}\ln\left(\frac{d\sigma_F}{a\nu}\right). \tag{33}$$

An analysis shows that for a film with a diffuse boundary and thickness

$$\delta_0\frac{v_F}{c} \ll d \ll \delta_0\sqrt{v_F/c} \tag{34}$$

($\delta_0 = c/\omega_p$ is the field penetration depth in the infrared skin effect) for

$$d \ll a \ll d\frac{c}{U_F}, \tag{35}$$

Eqs. (31)–(33) realize sequentially the functional dependence of the Casimir interaction energy on the distance between the bulk metal and the film. Under the conditions (34)

and (35), the film thickness d can be varied from 10^{-5} to 10^{-6} cm. In this case, the admissible values of distance a belong to the interval $10^{-2}-10^{-6}$ cm.

If $d \ll \delta_0 v_F/c$, the asymptotic formula (31) becomes invalid since the inequality $\omega_c \ll \omega_p$ is violated. In this case, while determining electromagnetic Green's functions, we must assume

$$\epsilon = \epsilon_0 - \frac{\omega_p^2}{\omega^2},$$

and the contribution from the permittivity ϵ_0 of the ion core ''suppresses'' possible electron effects in the Casimir force, i.e., the situation is similar to the interaction between two bulk conductors. The same applies to the asymptotic formulas (32) and (33) for $d \gg \delta_0 \sqrt{v_F/c}$.

Concluding the section, we note that radical transition from one asymptotic form to another is observed in the range of distances

$$a \sim a_0 = d^3 \omega_p^2 / v_F^2, \tag{36}$$

for which the type of the functional dependence of the Casimir energy $\mathcal{E}(a)$ changes.

In view of the absence of frequency dependence in ϵ_∞, the energy $\mathcal{E}_{M-s}$ of the Casimir interaction of the conductor with the dielectric substrate must have the same functional dependence on the distance as for the energy of interaction between bulk metals (see expression (1) for force). In the case of a low optical transparency of the dielectric, i.e., for

$$\epsilon_\infty - 1 \ll 1 \tag{37}$$

we obtain

$$\mathcal{E}_{M-s} = -\frac{\epsilon_\infty - 1}{(2\pi)^2} \frac{\hbar c}{(2a)^3}. \tag{38}$$

According to Eq. (17), the contribution of the $M-s$ interaction to the total energy $\mathcal{E}$ is smaller than the energy of the $M-f$ interaction if the optical density parameter of the dielectric substrate satisfies the inequality

$$c(\epsilon_\infty - 1)/a \ll \omega_c. \tag{39}$$

In this case, dispersion properties of the film f play a leading role in the Casimir force.

6. CONCLUSION

We have obtained the most general asymptotic expressions for the Casimir energy in the case of interaction of a bulk conductors with a thin film of isotropic metal, in which collective properties of the electron subsystem are taken into account in the main approximation. The role of the effects of surface electron relaxation in the formation of the Casimir force is demonstrated in the model of specularity parameter. It is found that the Casimir force becomes sensitive to the electron characteristics of the metal film with a diffuse boundary for a film thickness $d \ll \delta_0 \sqrt{v_F/c}$. For films with a specular boundary, the critical values of d are much smaller:[4] $d \ll \delta_0 \nu/\omega_p$.

The calculation of the Casimir energy for a film with a diffuse boundary proved that when the inequality (34) is satisfied, the influence of the size effect in the conductivity of the metal film on the magnitude of the Casimir force is significant only in the range of intermediate (Eqs. (32) and (33)) distances, namely, in the frequency range corresponding to the normal skin effect. For smaller distances (or higher characteristic frequencies), surface effects in the electron conductivity are suppressed by bulk effects connected directly with the high frequency of the fluctuational electromagnetic field. Under these conditions, the asymptotic form (31) of the Casimir energy coincides with expression (25) obtained for a film with a specularly reflecting boundary.

Under the conditions of normal skin effect, the approximate formula for the Casimir energy can be written in the form

$$\mathcal{E}_{M-f}^{(\rho=0)} \propto \hbar \sigma_F \frac{d}{a^3}.$$

In this situation, it is possible to neglect frequency dispersion in conductivity, and hence the functional dependence of $\mathcal{E}_{M-f}^{(\rho=0)}$ on distance a remains the same as for a system of interacting perfect conductors.

Thus, the surface effects in the electrical conductivity of a metal film in the model of specular parameter affect only the magnitude of the Casimir interaction (1). Besides, the bulk properties of the electron subsystem also affect the functional dependence of the force of Casimir attraction on distance (Eq. (31)). In this case, the point $\hat{a}$ of transition from one region of the asymptotic form to another is closely related to the nature of electron–surface scattering. In the model of specular parameter, $\hat{a} \sim a_0$ (36) if $\rho = 0$ and $\hat{a} \sim (l_0/d)^2 a_0$ for $\rho = 1$. This means that for films with the known electron parameters ω_p, ν, and v_F, we can judge about the roughness of a metal surface from the experimentally observed value of $\hat{a}$.

All the results are obtained here for isotropic conductors. Casimir interaction for films of anisotropic metals requires a special analysis and discussion. First of all, in real experiments we must take into account the fact that apart from the Casimir attraction in the anisotropic case, a torque rotating the film emerges in the system. The direction of this torque depends on mutual orientation of the normal to the surface and crystallographic axes. Besides, all asymptotic formulas for the Casimir force change. It can be stated, however, that even in the anisotropic situation the Casimir force (as well as the conductivity of films) is sensitive to the type of electron–surface scattering.

In several recent publications (see, for example, Refs. 8 and 9), the Casimir attraction is studied experimentally. In spite of incredible complexity of such experiments, we still hope that the results of our research will find their place among studies of this interesting macroscopic phenomenon in near future.

The authors express their gratitude to Prof. V. D. Natsik for fruitful discussions.

*)E-mail: yam@ire.kharkov.ua

[1)]Here and below, we shall use the Heaviside system of electromagnetic units, in which the definition of surface impedance differs from the conventional definition in the absence of the factor $4\pi/c$.

[1]H. B. G. Casimir, Konink. Nederl. Acad. Weten., Proc. Sec. Sci. **51**, 793 (1948).
[2]E. M. Lifshitz and L. P. Pitaevskii, *Statistical Physics*, Part 2, Pergamon, Oxford (1960).
[3]V. M. Mostepanenko and N. N. Trunov, *The Casimir Effect and Its Applications*, Clarendon, London (1997).
[4]V. N. Dubrava, V. A. Yampol'skii, and O. I. Lyubimov, Radiofizika i Elektronika **4**, 70 (1999). [Engl. Transl.: Telecommunications and Radio Engineering, to be published.].
[5]J. Schwinger, Proc. Natl. Acad. Sci. USA **89**, 4091 (1992).
[6]K. Fuchs, Proc. Cambridge Philos. Soc. **34**, 100 (1938).
[7]V. N. Dubrava, V. A. Yampol'skii, and O. I. Lyubimov, Dop. Natz. Akad. Nauk Ukr. (2000), in press.
[8]R. Onofrio, Phys. Lett. A **A198**, 365 (1995).
[9]S. K. Lamoreaux, Phys. Rev. Lett. **78**, 5 (1997).

Translated by R. S. Wadhwa

LOW-DIMENSIONAL AND DISORDERED SYSTEMS

Characteristic energy losses of electrons in a two-dimensional electron gas in a magnetic field

A. M. Ermolaev and Babak Haghighi

Kharkov State University, 310077 Kharkov, Ukraine
(Submitted March 4, 1999; revised May 12, 1999)
Fiz. Nizk. Temp. **25**, 1313–1319 (December 1999)

The electron energy loss function is calculated in the random phase approximation for a two-dimensional electron gas in a quantizing magnetic field. Local states of electrons at impurity atoms are taken into consideration. The energy losses due to one-particle and collective excitations of two-dimensional electrons are determined. The activation of electrons localized at impurities leads to the emergence of steps on the dependence of loss function on the energy of an incident electron. Cerenkov losses associated with emission of magnetoplasmons appear starting from a threshold velocity of the electron. When the velocity exceeds the threshold value significantly, the losses are due only to spontaneous emission of magnetoplasmons. The corresponding loss function decreases in inverse proportion to the electron velocity. © *1999 American Institute of Physics.* [S1063-777X(99)01012-9]

INTRODUCTION

It was proved by us earlier[1] that electron trapping at isolated impurity atoms affects significantly the properties of magnetoplasma waves in a two-dimensional electron gas. Local energy levels of $2D$ electrons[2–5] alternating with Landau levels are manifested in two ways. On the one hand, new resonances of electromagnetic radiation absorption in a two-dimensional conductor, which are associated with electron transitions between Landau levels and local levels, are generated. They are accompanied by the emergence of new branches in the magnetoplasma wave spectrum. On the other hand, the interaction of cyclotron motion with the motion of electrons localized at impurities leads to the cross bifurcation of the dispersion curve of magnetoplasmons, which is similar to that observed in the spectrum of a crystal lattice with quasilocal vibrations of impurity atoms.[6] Such a bifurcation was observed experimentally[7] during measurements of the magnetic field dependence of absorption of radiation transmitted through the inversion layer at the interface between silicon and silicon dioxide. Ando[8] explained the bifurcation by the inclusion of a nonlocal correction to the conductivity of $2D$ electrons, which has a resonance at the double cyclotron frequency. However, more detailed analysis of this phenomenon by using other methods of probing magnetoplasma waves in a $2D$ electron gas is required to explain the bifurcation comprehensively.

The bifurcation of the dispersion curve for magnetoplasmons can be observed during measurements of characteristic electron energy losses in a $2D$ electron gas in a magnetic field. This method is being used successfully for studying elementary excitations in plasmas,[9,10] solids, and quantum liquids.[11,12]

We shall prove here that local states affect the spectrum of electron energy losses in a $2D$ electron gas in a magnetic field. In zero magnetic field and in the absence of electron trapping, this problem was solved by Bret and Deutsch,[13] while local states in zero magnetic field were taken into account by us earlier.[14]

1. ELECTRON ENERGY LOSS FUNCTION IN A $2D$ ELECTRON GAS IN A QUANTIZING MAGNETIC FIELD

Let us suppose that an electron gas is in the plane $z=0$ at the boundary between two half-spaces with permittivities ε_1 and ε_2. The magnetic field $\mathbf{H}$ is perpendicular to this plane. We denote by $|\alpha\rangle$ the stationary state of the $2D$ electron gas and by $|\chi\sigma\rangle$ the state of an incident electron in a magnetic field. Here $\chi=(n,p_y)$ are orbital quantum numbers of the electron and σ is the spin quantum number. The matrix elements of the Hamiltonian V of the Coulomb interaction of a test electron moving in the plane $z=0$ with the $2D$ electron gas are given by[10,14]

$$\langle \alpha'\chi'\sigma'|V|\alpha\chi\sigma\rangle=\bar{e}^2\delta_{\sigma'\sigma}\int\frac{d^2q}{2\pi q}I_{\chi'\chi}(\mathbf{q})\langle\alpha'|n(\mathbf{q})|\alpha\rangle, \tag{1}$$

where $\bar{e}=e[2/(\varepsilon_1+\varepsilon_2)]^{1/2}$, e is the electron charge and $I_{\chi'\chi}(\mathbf{q})=\langle\chi'|e^{iqr}|\chi\rangle$ are the matrix elements of a plane wave in the Landau basis, and $n(\mathbf{q})$ is the Fourier component of the $2D$ electron density operator. The probability of the transition $|\alpha\chi\sigma\rangle\rightarrow\rightarrow|\alpha'\chi'\sigma'\rangle$ per unit time, averaged over α,p_y, and σ and summed over α', p_y', and σ' is given by

$$W_{n'n}=2\pi\bar{e}^4n_e\int d^2qq^{-2}C_{n'n}\left(\frac{q^2l^2}{2}\right)S(\mathbf{q},\omega), \tag{2}$$

where n_e is the electron number density, l the magnetic length,

$$C_{n'n}(x)=\frac{n_1!}{n_2!}x^{n_2-n_1}\mathrm{e}^{-x}[L_{n_1}^{n_2-n_1}(x)]^2, \tag{3}$$

$n_1=\min(n,n')$; $n_2=\max(n,n')$; $L_{n_2}^{n_1}$ are generalized Laguerre polynomials,

$$S(\mathbf{q},\omega)=\frac{1}{n_e}\sum_{\alpha\alpha'} w_\alpha|\langle\alpha'|n(-\mathbf{q})|\alpha\rangle|^2\delta(\omega+E_\alpha-E_{\alpha'})$$

is the dynamic structural factor of a $2D$ electron gas in a magnetic field, $\omega=\varepsilon_\chi-\varepsilon_{\chi'}$ the energy loss during the scattering of an incident electron, E_α the energy of an electron gas in the $|\alpha\rangle$ state, and w_α the Gibbs distribution function. Here and below, the quantum-mechanical constant and the area occupied by the electron gas are assumed to be equal to unity. The difference between the cyclotron frequency and the frequency corresponding to spin splitting of electron energy levels is disregarded.

The transition probability (2) is connected with the imaginary component of the polarization operator Π of a $2D$ electron gas. We shall use the expression for this operator obtained in the random phase approximation.[10,14] It contains the polarization operator P of a $2D$ electron gas in the field of impurity atoms in the presence of a magnetic field. In the linear approximation in the number density n_i of impurity atoms, it is defined as $P=P_0+\delta P$, where P_0 is the polarization operator of $2D$ electrons in a magnetic field and

$$\begin{aligned}\delta P(q,\omega)=&\frac{m\omega_c n_i}{2\pi}\sum_{nn'k\sigma}C_{n'n}\left(\frac{q^2l^2}{2}\right)\frac{r_{k\sigma}}{(\varepsilon_{n'}-\varepsilon_k^l)^2}\\&\times[f(\varepsilon_{k\sigma}^l)-f(\varepsilon_{n\sigma})][(\varepsilon_k^l-\varepsilon_n+\omega+i0)^{-1}\\&+(\varepsilon_k^l-\varepsilon_n-\omega-i0)^{-1}]\end{aligned} \tag{4}$$

is the contribution of local levels. Here m is the electron effective mass, ω_c the cyclotron frequency, $\varepsilon_{n\sigma}$ and $\varepsilon_{k\sigma}^l$ are the positions of the nth Landau level and the kth local level, $r_{k\sigma}$ is the residue of the amplitude of electron scattering by an impurity atom at the pole $\varepsilon_{k\sigma}^l$,[1] and f the Fermi function.

If the velocity of an incident electron exceeds $(\omega_c/m)^{1/2}$, we can neglect the influence of the magnetic field on its motion. In this case, the transition probability (2) and the energy lost by an electron per unit time are defined as

$$W_{\mathbf{p}'\mathbf{p}}=8\pi^2\overline{e}^4q^{-2}(n_\omega+1)\left[-\mathrm{Im}\prod(\mathbf{q},\omega)\right], \tag{5}$$

$$Q=\int\frac{d^2p'}{(2\pi)^2}(\varepsilon_p-\varepsilon_{p'})W_{\mathbf{p}'\mathbf{p}}, \tag{6}$$

where $\mathbf{q}=\mathbf{p}-\mathbf{p}'$ and $\omega=\varepsilon_p-\varepsilon_{p'}$ are the momentum and energy losses for the incident electron during scattering, and n_ω is Planck's function. Magnetic field appears in the expressions (5) and (6) for scattering probability and loss function only in the polarization operator.

In the absence of impurity atoms, the energy loss function for a test particle in a $2D$ electron gas is given by

$$\begin{aligned}Q_0=&\pi m\overline{e}^4\omega_c\sum_{n'}\omega(n_\omega+1)\sum_{n_1n_2}[F(\varepsilon_{n_1})-F(\varepsilon_{n_2})]\\&\times\delta(\omega+\varepsilon_{n_1}-\varepsilon_{n_2})\int_0^\infty\frac{dx}{x}C_{n'n}(x)C_{n_2n_1}(x).\end{aligned} \tag{7}$$

Here $\omega=\omega_c(n-n')$; $F(\varepsilon_n)=\Sigma_\sigma f(\varepsilon_{n\sigma})$. If we disregard the effect of ''twisting,''[9,10] i.e., the influence of the magnetic field on the incident electron, formulas (5)–(7) give

$$\begin{aligned}Q_0=&m^2\overline{e}^4\omega_c\sum_{nn'}\theta(\varepsilon+\omega)\omega(n_{-\omega}+1)[F(\varepsilon_{n'})-F(\varepsilon_n)]\\&\times\int_0^{2\pi}d\varphi q^{-2}C_{n'n}\left(\frac{q^2l^2}{2}\right),\end{aligned} \tag{8}$$

where ε is the energy of the incident electron,

$$q^2=4m\left\{\varepsilon+\frac{\omega}{2}-[\varepsilon(\varepsilon+\omega)]^{1/2}\cos\varphi\right\};$$

φ is the scattering angle in the plane $z=0$, and θ the Heaviside function. For small electron momentum losses ($ql\ll1$), we can use the representation of the function (3) in the form of a series. In this case, the main contribution to the loss function (8) is

$$Q_0=\begin{cases}2\pi^2\overline{e}^4n_e, & \varepsilon>\omega_c,\\ 2\pi^2\overline{e}^4n_en_{\omega_c}, & \varepsilon<\omega_c.\end{cases} \tag{9}$$

When $\varepsilon>\omega_c$, the electron energy losses (9) are due to transitions $n\to n+1$ of $2D$ electrons between adjacent Landau levels. If, however, $\varepsilon<\omega_c$, the energy of an incident particle increases due to transitions $n\to n-1$. Such transitions are absent in a degenerate electron gas.

Electron energy losses are associated with one-particle as well as collective excitations of a $2D$ electron gas. Let us consider them separately.

2. ONE-PARTICLE EXCITATIONS

Analyzing the contribution of one-particle excitations to the loss function, we shall disregard the Coulomb excitation in a $2D$ electron gas. In this case, $\Pi=P$, and the loss function contains the contribution δQ due to activation of electrons trapped at impurities. This contribution is given by

$$\begin{aligned}\delta Q=&m\overline{e}^4\omega_cn_i\sum_{n'}\omega(n_\omega+1)\int\frac{d^2}{q^2}C_{n'n}\left(\frac{q^2l^2}{2}\right)\\&\times\sum_{n_1n_2k\sigma}C_{n_1n_2}\left(\frac{q^2l^2}{2}\right)\frac{r_{k\sigma}}{(\varepsilon_{n_2}-\varepsilon_k^l)^2}\{[f(\varepsilon_{k\sigma}^l)\\&-f(\varepsilon_{k\sigma}^l+\omega)]\delta(\varepsilon_k^l-\varepsilon_{n_1}+\omega)+[f(\varepsilon_{k\sigma}^l-\omega)\\&-f(\varepsilon_{k\sigma}^l)]\delta(\varepsilon_k^l-\varepsilon_{n_1}-\omega)\}.\end{aligned} \tag{10}$$

The first term in this formula is connected with transitions of trapped electrons to Landau levels, while the second is associated with transitions from Landau levels to local levels. In the approximation under investigation, the transition probability (2) has δ-shaped peaks at frequencies $|\varepsilon_n$

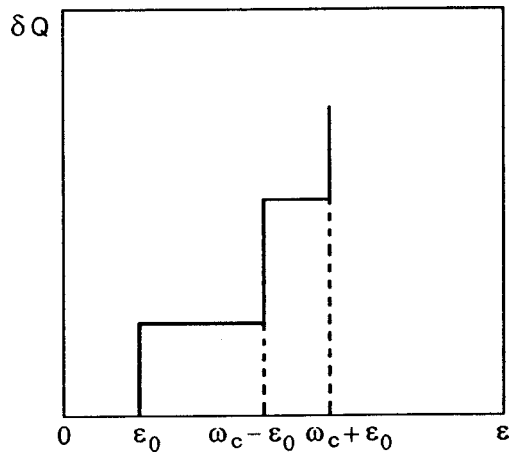

FIG. 1. Schematic dependence of the loss function δQ (11) due to one-particle excitations of localized electrons on the electron energy ε.

$-\varepsilon_k^l|$. The inclusion of a finite width of the levels participating in transitions leads to blurring of these peaks.

If we disregard the effect of ''twisting,'' the energy loss (10) becomes

$$\delta Q=\pi\overline{e}^4 l^{-2} r n_i \sum_{s=0}^{\infty} \theta(\varepsilon-\omega_s)\omega_s^{-2}(n_{\omega_s}+1) \times \sum_{k\sigma} [f(\varepsilon_{k\sigma}^l)-f(\varepsilon_{(k+s)\sigma})]+\pi\overline{e}^4 l^{-2} r n_i \times \sum_{p=1}^{\infty} \theta(\varepsilon-\omega_p)\omega_p^{-2}(n_{\omega_p}+1) \times \sum_{k\sigma} [f(\varepsilon_{(k-p)\sigma})-f(\varepsilon_{k\sigma}^l)], \quad (11)$$

where $\omega_s=s\omega_c+\varepsilon_0$ are frequencies of transitions of trapped electrons to Landau levels, $\omega_p=p\omega_c-\varepsilon_0$ the frequencies of electron transitions from Landau levels to local levels, and ε_0 the separation between a Landau level an a local level split from it. In this expression, we disregard the dependence of ε_0 and the residue r on the number of a Landau level. If $\varepsilon_0 \ll \omega_c$, the residue is[1] $r=2\pi(l\varepsilon_0)^2$. The symbol Σ_k in formula (11) indicates summation over the numbers of local levels participating in transitions at a given frequency. The difference between Fermi functions takes into account the Pauli exclusion principle. At low temperatures, the energy loss (11) as a function of energy of an incident electron is a step curve shown schematically in Fig. 1. The step boundaries are resonant frequencies ω_s and ω_p. The height of the first step between ε_0 and $\omega_1=\omega_c-\varepsilon_0$ at zero temperature is $\pi e^{-4} r n_i/(l\varepsilon_0)^2$. The ratio of this quantity to (9) is n_i/n_e.

3. COLLECTIVE EXCITATIONS

Characteristic electron energy losses in a $2D$ electron gas are due to the excitation of magnetoplasma waves. In Ref. 1, the dispersion equation for magnetoplasmons was solved numerically. The inclusion of contribution (4) to the polarization operator associated with electron trapping complicates the dispersion equation and leads to the emergence of new roots. They correspond to new branches in the spectrum of magnetoplasma waves attenuating weakly in transmission bands close to the resonant frequencies ω_s and ω_p.[1]

Let us consider a neighborhood of the frequency $\omega_r=\omega_c+\varepsilon_0$ of transitions of trapped electrons to a Landau level. Retaining in (4) only the resonant term in the vicinity of this frequency, we obtain

$$\delta P=\frac{n_i a}{m l^2 \omega_r}\frac{1}{\omega-\omega_r+i\nu_0}, \quad (12)$$

where a is the oscillator force of the resonant transition and ν_0 the width of the local level. If $ql \ll 1$, we have

$$a=\frac{m}{2\pi\omega_r}\sum_{k\sigma} r_{k\sigma}[f(\varepsilon_{k\sigma}^l)-f(\varepsilon_{(k+1)\sigma})]. \quad (13)$$

If the chemical potential of electrons lies between the levels ε_{N-} and $\varepsilon_{(N+1)-}^l$ (the subscripts ''+'' and ''−'' indicate the electron spin orientation), the sum (13) is left with only one term with $k=N$, where N is the number of the local level participating in transitions. Taking into account contribution (12) in the dispersion equation, we obtain the following cubic equation for the magnetoplasmon spectrum:

$$x^3-(1+b)x^2-\left(\frac{\omega_q}{\omega_r}\right)^2 x+\left(\frac{\omega_q}{\omega_r}\right)^2+b\left(\frac{\omega_c}{\omega_r}\right)^2=0, \quad (14)$$

where

$$x=\frac{\omega}{\omega_r}, \quad b=a\frac{n_i}{n_e}\left(\frac{\omega_{q0}}{ql\omega_r}\right)^2, \quad \omega_q=(\omega_c^2+\omega_{q0}^2)^{1/2},$$

and ω_{q0} is the frequency of a $2D$ plasmon in the absence of localization in zero magnetic field.[15] Positive roots of Eq. (14) are given by

$$x_\pm=y_\pm+\frac{1}{3}(1+b), \quad (15)$$

where

$$y_+=-2R\cos\frac{\varphi}{3}, \quad y_-=-2R\cos\frac{\pi+\varphi}{3},$$

$$R=-\frac{1}{3}\left[(1+b)^2+3\left(\frac{\omega_q}{\omega_r}\right)^2\right]^{1/2}, \quad \cos\varphi=\frac{g}{2R^3},$$

$$g=-\frac{2}{27}(1+b)^3+b\left[\left(\frac{\omega_c}{\omega_r}\right)^2-\frac{1}{3}\left(\frac{\omega_q}{\omega_r}\right)^2\right]+\frac{2}{3}\left(\frac{\omega_q}{\omega_r}\right)^2.$$

The dispersion curve ω_q of a magnetoplasmon is intersected by the straight line $\omega=\omega_r$ at the point

$$q_0=\frac{m}{2\pi\overline{e}^2 n_e}(\omega_r^2-\omega_c^2).$$

Electron trapping leads to cross bifurcation of the dispersion curve into two branches $\omega_\pm=\omega_r x_\pm$. The branch ω_+ lies above ω_q, while ω_- is below ω_q. As $a\to 0$, the root ω_+ approaches ω_r and ω_- tends to ω_q. The damping decrement for these branches is

$$\gamma_\pm=\nu\left[1+b\left(\frac{\omega_r}{\omega_{q0}}\right)^2\frac{(\omega_\pm^2-\omega_c^2)^2}{\omega_r\omega_\pm}\frac{\nu_0/\nu}{(\omega_\pm-\omega_r)^2\nu_0^2}\right], \quad (16)$$

where ν is the frequency of electron collisions due to potential scattering by impurity atoms only. The decrement has a Lorentzian peak at the resonant frequency. The width of this peak coincides with the width of the local level.

For numerical estimates, we shall use the values of parameters typical of a weakly doped inversion layer at the interface between silicon and silicon dioxide:[15] $m=10^{-28}$ g, $n_e=10^{12}\,\mathrm{cm}^{-2}$, $\varepsilon_1+\varepsilon_2=15$, $n_i/n_e=10^{-3}$, $\varepsilon_0/\omega_c=0{,}1$. Then in a magnetic field of induction 1 T we obtain $\omega_r=1.8\cdot10^{12}\,\mathrm{s}^{-}$, $q_0=2.8\times10^2\,\mathrm{cm}^{-1}$, and the separation between the branches $\omega_\pm$ at the point q_0 is $\omega_+-\omega_-=8.8\cdot10^{13}\,\mathrm{s}^{-1}$.

The energy lost by an electron per unit time due to Cherenkov radiation of magnetoplasmons is given by

$$Q_e=\frac{1}{2\pi}\sum_{n'}\omega(n_\omega+1)\int d^2qC_{n'n}\left(\frac{q^2l^2}{2}\right)\times\left|\left[\frac{\partial}{\partial\omega}\mathrm{Re}\,P(q,\omega)\right]_{\omega=\omega_q}\right|^{-1}\delta(\omega-\omega_q),\tag{17}$$

where ω_q is the magnetoplasma wave spectrum and $\omega=\varepsilon_n-\varepsilon_{n'}$. If we neglect the ''twisting'' effect, formula (17) assumes the form

$$Q_e=\frac{1}{2\pi}\int d^2p'\omega(n_\omega+1)\times\left|\left[\frac{\partial}{\partial\omega}\mathrm{Re}\,P(q,\omega)\right]_{\omega=\omega_q}\right|^{-1}\delta(\omega-\omega_q),\tag{18}$$

where $\mathbf{q}=\mathbf{p}-\mathbf{p}'$ and $\omega=\varepsilon_p-\varepsilon_{p'}$. Confining our analysis to the leading contribution P_0 in the denominator of formula (18), we obtain

$$Q_e=\frac{m}{4\pi n_e}\int_0^\infty d\omega\omega(n_\omega+1)\int_0^\infty\frac{dq}{q\omega_q}(\omega_q^2-\omega_c^2)^2\times\delta(\omega-\omega_q)\int_0^{2\pi}d\varphi\,\delta(\Omega_+-qv\cos\varphi).\tag{19}$$

Here $\Omega_\pm=\omega\pm\varepsilon_q$; $\varepsilon_q=q^2/2m$; v is the velocity of an incident electron. In the absence of impurity atoms, this formula leads to

$$Q_e=\frac{2\overline{e^2}}{v}\int_{\omega_c}^\infty d\omega\omega(n_\omega+1)\,\theta\left(1-\frac{\Omega_+}{qv}\right)\left[1-\left(\frac{\Omega_+}{qv}\right)^2\right]^{-1/2},\tag{20}$$

where $q=\dfrac{m}{2\pi\overline{e^2}n_e}(\omega^2-\omega_c^2)$.

The increment of the electron energy due to absorption of magnetoplasmons is

$$Q_a=\frac{2\overline{e^2}}{v}\int_{\omega_c}^\infty d\omega\omega n_\omega\theta\left(1-\left|\frac{\Omega_-}{qv}\right|\right)\left[1-\left(\frac{\Omega_-}{qv}\right)^2\right]^{-1/2}.\tag{21}$$

This contribution is absent at zero temperature.

If

$$v>v_0=\frac{\omega_c^2}{2\pi\overline{e^2}n_e}\left[\frac{3}{\omega_c^2}(\pi\overline{e^2}n_em^{-1/2})^{4/3}-1\right],\tag{22}$$

the inequality $\Omega_+<qv$ is satisfied in the interval (ω_-,ω_+), where $\omega_\pm$ are the largest roots of the fourth-degree algebraic equation $\Omega_+=qv$. The cyclotron frequency should not exceed ω_+. In this case, formula (20) leads to

$$Q_e=8\pi\overline{e^4}n_e\theta(v-v_0)\int_{\omega_m}^{\omega_+}d\omega\omega(\omega^2-\omega_c^2)(n_\omega+1)\times\left[-\prod_{k=1}^{8}(\omega-\omega_k)\right]^{-1/2},\tag{23}$$

where ω_k are the roots of the equations $\Omega_+=\pm qv$, and ω_m is the larger of the frequencies ω_c and ω_-.

In the limiting case $v\gg v_0$, formula (23) assumes the form

$$Q_e=4\pi\overline{e^4}n_e\int_0^1dx\,\frac{n_x+1}{(1-x^2)^{1/2}},\tag{24}$$

where

$$n_x=\{\exp[\beta\omega_c(1+(\omega_0^2/\omega_c^2)x)^{1/2}]-1\}^{-1};$$

$\omega_0=(4\pi\overline{e^2}n_ev)^{1/2}$ and β is the inverse temperature. The first term in (24) is associated with induced emission and the second with spontaneous emission of $2D$ magnetoplasmons by fast electrons. If $H\to0$ and $\beta\to\infty$, formula (24) leads to the expression $Q_e=2\pi^2\overline{e^4}n_e$ derived earlier.[13] It follows hence that the electron energy loss per unit path length is proportional to the electron velocity.

In zero magnetic field, the threshold velocity (22) is $v_0=(3/2)(\pi\overline{e^2}n_e)^{1/3}m^{-2/3}$. In this case, one of the roots of the equation $\Omega_+=\pm qv$ is equal to zero. The remaining roots satisfy a cubic equation and are given by

$$\omega_1=-\frac{2\omega_0}{\sqrt3}\cos\frac{\varphi_1}{3},\quad\omega_2=-\frac{2\omega_0}{\sqrt3}\cos\left(\frac{\varphi_1}{3}+\frac{2\pi}{3}\right),$$
$$\omega_3=-\frac{2\omega_0}{\sqrt3}\cos\left(\frac{\varphi_1}{3}+\frac{4\pi}{3}\right),\quad\omega_4=-\frac{2\omega_0}{\sqrt3}\sinh\frac{\varphi_2}{3},\tag{25}$$
$$\omega_5=\frac{\omega_0}{\sqrt3}\left(\sinh\frac{\varphi_2}{3}+i\sqrt3\cosh\frac{\varphi_2}{3}\right),$$
$$\omega_6=\frac{\omega_0}{\sqrt3}\left(\sinh\frac{\varphi_2}{3}-i\sqrt3\cosh\frac{\varphi_2}{3}\right),$$

where

$$\cos\varphi_1=\sinh\varphi_2=\frac{3^{3/2}\overline{e}(\pi n_e)^{1/2}}{2mv^{3/2}}.$$

In the limit $v\gg v_0$, the values of φ_1 and φ_2 are small, and the roots (25) are approximately equal to $0{,}0,\pm\omega_0$, and $\pm i\omega_0$. Substituting these values of the roots into (23), we obtain the familiar expression for the loss function.[13]

For any velocity v of an incident electron, the inequality $|\Omega_-|<qv$ is satisfied in the interval (ω_-,ω_+), where $\omega_\pm$

are positive roots of the equation $|\Omega_-|=qv$. The increment of the electron energy (21) due to absorption of magnetoplasmons is given by

$$Q_a=8\pi\bar{e}^4 n_e\int_{x_m}^{x_+}dx x(x^2-1)n_x\left[-\prod_{k=1}^{8}(x-x_k)\right]^{-1/2}, \tag{26}$$

where $x=\omega/\omega_c$, $x_\pm=\omega_\pm/\omega_c$, $x_m=\omega_m/\omega_c$, ω_m is the larger frequency from ω_- and ω_c, and x_k are the roots of the equations

$$(x^2-1)^2\pm\frac{q_0^v}{\Omega_0}(x^2-1)-\frac{\omega_c}{\Omega_0}x=0,$$

$$q_0=\frac{m\omega_c^2}{2\pi\bar{e}^2 n_e},\quad \Omega_0=\frac{q_0^2}{2m},\quad n_x=[\exp(\beta\omega_c x)-1]^{-1}.$$

For a high velocity of the incident electron, the roots x_k are equal to ±1, $\pm(1+q_0v/\Omega_0)^{1/2}$, ±1, $\pm i(q_0v/\Omega_0-1)^{1/2}$. In this limit, expression (26) coincides with the first term in (24). This means that energy losses for fast electrons are due only to spontaneous emission of magnetoplasmons.

In zero magnetic field, formula (26) gives

$$Q_a=8\pi\bar{e}^4 n_e\int_{y_-}^{y_+}dy y(y^2-1)n_y\left[-\prod_{k=1}^{6}(y-y_k)\right]^{-1/2},$$

were

$$y=\frac{\omega}{\omega_0},\quad n_y=[\exp(\beta\omega_0 y)-1]^{-1},$$

$$y_-=\frac{2}{\sqrt{3}}\sinh\varphi,\quad y_+=\begin{cases}\dfrac{2}{\sqrt{3}}\cosh\dfrac{\varphi_1}{3}, & v<v_0\\[2ex] \dfrac{2}{\sqrt{3}}\cos\dfrac{\varphi_2}{3}, & v>v_0\end{cases},$$

$$\sinh\varphi=\cosh\varphi_1=\cos\varphi_2=\frac{3^{3/2}\omega_0}{4mv^2},$$

and y_k are the roots of the cubic equations

$$y^3\pm y-\frac{\omega_0}{2mv^2}=0.$$

If $v\gg v_0$, the last term in these equations can be omitted. This gives

$$Q_a=\frac{8\pi\bar{e}^4 n_e}{(\beta\omega_0)^2}\int_0^{\beta\omega_0}dx\frac{x}{e^x-1}\left[1-\left(\frac{x}{\beta\omega_0}\right)^4\right]^{-1/2}. \tag{27}$$

At low temperatures ($\beta\omega_0\gg1$), this expression is transformed to

$$Q_a=\frac{4\pi^3\bar{e}^4 n_e}{3(\beta\omega_0)^2}.$$

If, however, $\beta\omega_0\ll1$, formula (27) leads to

$$Q_a=\frac{\sqrt{2\pi}\bar{e}^4 n_e}{\beta\omega_0}\left[\Gamma\left(\frac{1}{4}\right)\right]^2.$$

As the temperature increases, expression (27) increases monotonically.

CONCLUSIONS

The problem on energy losses for charged particles in plasmas in a magnetic field was solved by Akhiezer.[10] Bert and Deutsch[13] applied the method developed in Ref. 10 for calculating the energy loss function for particles in a $2D$ electron gas. In our previous publication,[14] we considered the effect of electron trapping in the field of impurity atoms on the loss function in two-dimensional conductors in zero magnetic field. The calculation of the loss function taking into account electron trapping and a quantizing magnetic field is a natural continuation of these publications.

Local energy levels of electrons in a $2D$ electron gas in a magnetic field affect the spectrum and attenuation of magnetoplasma waves considerably. They are responsible for the existence of two branches in the wave spectrum and lead to the cross bifurcation of the dispersion curve of magnetoplasmons into two branches. These peculiarities of the spectrum of magnetoplasma waves in a $2D$ electron gas can be observed in experiments on the measurement of characteristic losses of electron energy.

The electron energy losses are mainly due to two factors, viz., the one-particle excitations of electrons and the Cherenkov radiation of magnetoplasmons. We have proved that the loss function contains the terms associated with activation of electrons trapped at impurities by the field of an incident electron. This leads to the emergence of steps on the curve describing the dependence of loss function on the energy of the incident electron. The boundaries of steps are frequencies of electron transitions between Landau levels and local levels. The height of the steps depends on temperature, concentration of impurity atoms, and magnetic field strength.

Energy losses for Cherenkov radiation of magnetoplasmons appear starting from a certain threshold velocity of electrons depending on the density of electron gas and magnetic field strength. The absorption of magnetoplasmons has no threshold. When the velocity of an incident electron exceeds the threshold velocity, the losses for induced emission and absorption of magnetoplasmons are compensated, and only the contribution from spontaneous emission is left. The energy loss per unit electron path length decreases in inverse proportion to the electron velocity. The observation of the peculiarities of loss functions makes it possible to obtain information on the spectrum of electron impurity states in a $2D$ electron gas in a magnetic field as well as the spectrum and attenuation of magnetoplasma waves.

[1] N. V. Gleizer, A. M. Ermolaev, and Babak Haghighi, Fiz. Nizk. Temp. **23**, 1223 (1997) [Low Temp. Phys. **23**, 917 (1997)].
[2] I. M. Lifshits, S. A. Gredeskul, and L. A. Pastur, *Introduction to the Theory of Disordered Systems* [in Russian], Nauka, Moscow (1982).
[3] A. M. Kosevich and L. V. Tanatarov, Fiz. Tverd. Tela (Leningrad) **6**, 3423 (1964) [Sov. Phys. Solid State **6**, 2738 (1964)].
[4] E. P. Bataka and A. M. Ermolaev, Izv. Vuzov, Fizika (Zagreb) **1**, 111 (1983).
[5] S. A. Gredeskul, M. Zusman, Y. Avishai, and M. Ya. Azbel, Phys. Rep. **288**, 223 (1997).
[6] A. M. Kosevich, *The Theory of Crystal Lattice* [in Russian], Vishcha Shkola, Kharkov (1988).

[7] T. N. Theis, J. P. Kotthaus, and P. J. Stiles, Solid State Commun. **24**, 273 (1977).
[8] T. Ando, Solid State Commun. **27**, 895 (1978).
[9] A. I. Akhiezer, I. A. Akhiezer, R. V. Polovin *et al.*, *Electrodynamics of Plasma* [in Russian], Nauka, Moscow (1974).
[10] I. A. Akhiezer, Zh. Eksp. Teor. Fiz. **40**, 954 (1961) [Sov. Phys. JETP **13**, 667 (1961)].
[11] D. Pines, *Elementary Excitations in Solids*, New York (1963).
[12] D. Pines and Ph. Noziere, *The Theory of Quantum Liquids*, New York (1966).
[13] A. Bret and C. Deutsch, Phys. Rev. E **48**, 2994 (1993).
[14] A. M. Ermolaev and Babak Haghighi, Fiz. Nizk. Temp. **25**, 600 (1999) [Low Temp. Phys. **25**, 446 (1999)].
[15] T. Ando, A. Fowler, and F. Stern, *Electronic Properties of Two-dimensional Systems*, American Physical Society, New York (1982).

Translated by R. S. Wadhwa

LATTICE DYNAMICS

Peculiarities of low-frequency excitation spectrum of $CsDy_{1-x}Bi_x(MoO_4)_2$

V. I. Kut'ko, S. S. Gerashchenko, and N. Yu. Nedbailo

*B. Verkin Institute for Low Temperature Physics and Engineering, National Academy of Sciences of the Ukraine, 310164 Kharkov, Ukraine**

(Submitted December 29, 1998; revised May 26, 1999)
Fiz. Nizk. Temp. **25**, 1320–1324 (December 1999)

Low-frequency IR transmission spectra for a series of isostructural single crystals of $CsDy_{1-x}Bi_x(MoO_4)_2$ ($x=0, 0.05, 0.1, 0.2, 0.3, 0.5,$ and 0.7) are measured at low temperatures ($T \simeq 6$ K). It is found experimentally that absorption band broadening takes place in the Bi concentration range $0.2 \leqslant x \leqslant 0.6$. The mechanism which may result in absorption spectrum blurring are considered. © *1999 American Institute of Physics.* [S1063-777X(99)01112-3]

Double alkali-earth molybdates are compounds with a layered structure displaying structural phase transitions of the type of cooperative Jahn–Teller effect (CJTE) at low temperatures.[1,2]

Weak interaction between the layers in these compounds in the presence of Davydov splitting at acoustic vibrational branches leads to the formation of low-frequency optical phonon modes.[3] Several electron–phonon modes in these compounds are active in structural phase transitions of the CJTE type. For this reason, an analysis of the low-frequency spectrum is a complicated experimental problem. It is interesting to measure low-frequency spectra in systems of solid mixtures in which Jahn–Teller ions are replaced by their diamagnetic analog. According to modern theoretical concepts, a structural disorder of the type of Jahn–Teller glass can emerge in such systems.[4,5] Besides, both components of the $CsDy_{1-x}Bi_x(MoO_4)_2$ mixture undergo structural phase transformations of various origin, which may also lead to the formation of a structural disorder of the glass type in the intermediate concentration region.[6,7]

This research aims at an analysis of the behavior of the low-frequency spectrum of the compound $CsDy_{1-x}Bi_x(MoO_4)_2$ in which Jahn–Teller Dy^{3+} ions are replaced by their diamagnetic analog Bi^{3+}.

EXPERIMENTAL

Measurements were made by using a vacuum diffraction spectrometer with a cooled InSb photodetector in the spectral range of measurements extends from 15 to 40 cm^{-1} at a sample temperature ~ 6 K. Single crystals of the system of solid mixtures $CsDy_{1-x}Bi_x(MoO_4)_2$ were grown by spontaneous crystallization from solution in melt. The sample size was $10\times 10\times (0.2-1)$ mm. Single crystals of $CsBi(MoO_4)_2$ and $CsDy(MoO_4)_2$ belong to the rhombic system (the space group D_{2h}^3 with two structural units in a unit cell). The crystal lattice parameters are $a=9.45, b=8.21, c=5.14$ and $a=9.51, b=7.97, c=5.05$ respectively.[8] Since the crystal lattice parameters for both components of the solid mixture differ insignificantly, we assume that isotopic substitution of Bi^{3+} ions for Dy^{3+} ions takes place in the mixture. The ratio of the components was determined from their concentration in the initial charge.

Figure 1 shows the transmission spectra in the range 15–40 cm^{-1} at a temperature ~ 6 K for various concentration of the mixture components. It can be seen that the absorption band $\nu \simeq 27$ cm^{-1} (for $x=0$) is smoothly displaced along the frequency scale without a noticeable change in the half-width when Dy^{3+} ions are replaced by the diamagnetic impurity Bi^{3+} for low concentrations $x \leqslant 0.1$. For the Bi^{3+} concentration $x=0.05$, the spectrum acquires the absorption band $\nu \simeq 22$ cm^{-1}, whose intensity is slightly higher than the intensity of the band $\nu \simeq 27$ cm^{-1}. As the Bi^{3+} concentration increases, the band $\nu \simeq 22$ cm^{-1} remains practically unshifted on the frequency scale.

For higher concentrations of Bi^{3+} ($x \geqslant 0.15$), the absorption bands merge into one, and the resultant absorption band is broadened anomalously for a Bi^{3+} concentration $x \geqslant 0.2$. For $x=0.7$, the transmission spectrum also acquires an absorption band $\nu \simeq 33$ cm^{-1}.

We processed spectra and determined half-widths of absorption bands for various concentrations of the components. Figure 2 shows the values of absorption band half-widths for the system of solid mixtures $CsDy_{1-x}Bi_x(MoO_4)_2$ for various values of concentrations of the components. It can be seen that the half-widths of the bands $\nu \simeq 27$ and 22 cm^{-1} increase abnormally in the concentration range $0.2 \leqslant x \leqslant 0.6$.

DISCUSSION OF EXPERIMENTAL RESULTS

Earlier investigations of the low-frequency vibrational spectrum of $CsDy(MoO_4)_2$ have proved that the main mechanism of its formation is associated with vibrations of $[Dy(MoO_4)_2]_{\infty\infty}$ and $Cs_{\infty\infty}$ layers as well as $[Dy(MoO_4)_2]_{\infty\infty}$ and $[Dy(MoO_4)_2]_{\infty\infty}+2Cs_{\infty\infty}$ layers relative to each other along the relevant directions in the crystal. This vibrational spectrum is successfully described by the

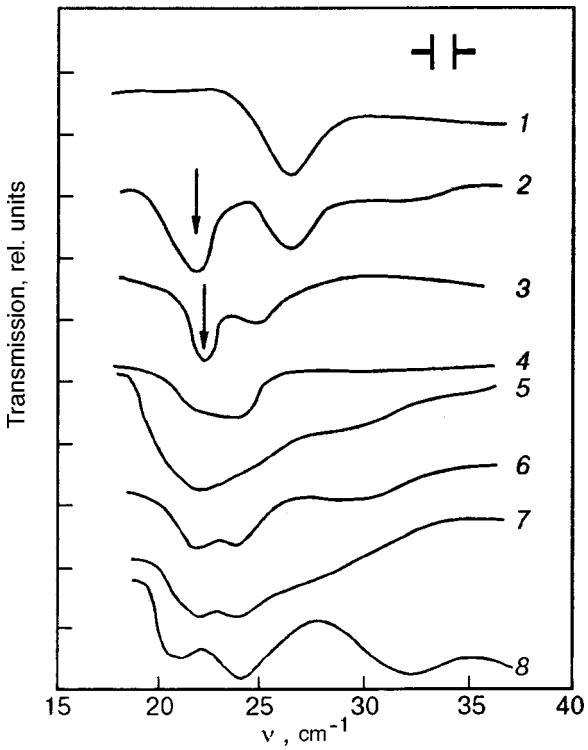

FIG. 1. Transmission spectrum of $CsDy_{1-x}Bi_x(MoO_4)_2$ single crystals at low temperature ($T \simeq 6$ K). Curves *1–8* correspond to $x = 0$, 0.05, 0.1, 0.15, 0.2, 0.3, 10.5, and 0.7, respectively. The arrow indicates the absorption band due to electron excitation of Dy^{3+} ions.

one-dimensional model.[9] The model used earlier for the vibrational spectrum of the $CsDy(MoO_4)_2$ crystal makes it possible to explain the behavior of the low-frequency vibrational spectrum of the compound $CsDy_{1-x}Bi_x(MoO_4)_2$ for various concentrations of its components. The vibrational spectrum of the mixture is formed by vibrations of $[Dy_{1-x}Bi_x(MoO_4)_2]_{\infty\infty}$ and $[Dy_{1-x}Bi_x(MoO_4)_2]_{\infty\infty} + 2Cs^+$ layers relative to each other. The corresponding frequencies vary with the reduced mass of the two layers: $[Dy_{1-x}Bi_x(MoO_4)_2]_{\infty\infty}$ and $[Dy_{1-x}Bi_x(MoO_4)_2]_{\infty\infty}$

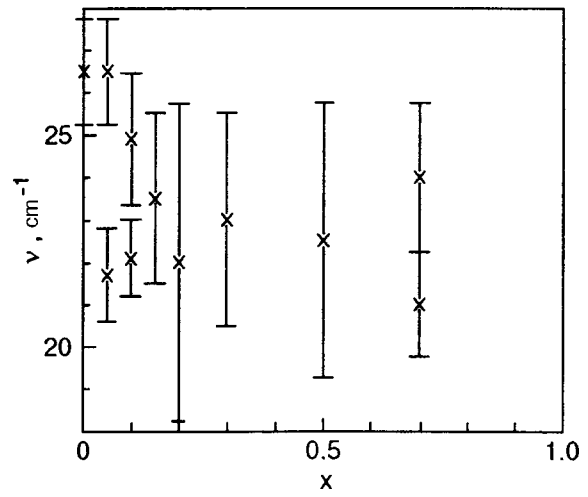

FIG. 2. Dependence of absorption band half-widths on the concentration of components of the $CsDy_{1-x}Bi_x(MoO_4)_2$ mixture.

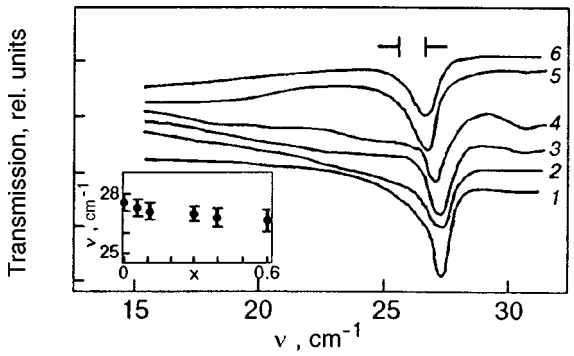

FIG. 3. Transmission spectrum of $KDy_{1-x}Y_x(MoO_4)_2$ single crystals at low temperature ($T \simeq 6$ K). Curves *1–6* correspond to $x = 0$, 0.05, 0.1, 0.3, 0.4, and 0.6, respectively. The inset shows the concentration dependence of half-width of the vibrational absorption band.

$+ 2Cs^+_{\infty\infty}$. The Bi^{3+} and Dy^{3+} ions have a uniform statistical distribution within a layer, and hence the reduced mass of the two layers is

$$\mu = \frac{\langle m_1 \times m_2 \rangle}{\langle m_1 \rangle + \langle m_2 \rangle},$$

were $\langle m_1 \rangle$ and $\langle m_2 \rangle$ are the masses of the layers statistically averaged over impurities. In view of the uniform distribution of the impurity over various layer packets, the reduced mass does not change upon a transition form layer to layer. For this reason, a $CsDy_{1-x}Bi_x(MoO_4)_2$ crystal is a packet of layers of the same mass with the corresponding weight components of Dy^{3+} and Bi^{3+} ions, which are proportional to the concentrations of the relevant ions. The masses of layer packets, and accordingly the reduced mass, vary smoothly with the concentrations of the mixture components.

According to our estimates, the change in the reduced mass upon a transition from $CsDy(MoO_4)_2$ to $CsBi(MoO_4)_2$ amounts to $\Delta\mu/\mu \simeq 0.07$. Provided that the force constant of interaction between $[Dy_{1-x}Bi_x(MoO_4)_2]_{\infty\infty}$ layer packets, which is associated with the interaction between Cs^+ and O^{2-} ions, does not change significantly, the isotopic shift of low-frequency optical modes must be $\Delta\nu/\nu \simeq 0.03$. For the vibrational mode $\nu \simeq 27\ \text{cm}^{-1}$ measured by us, this shift is $\Delta\nu \simeq 1\ \text{cm}^{-1}$. The isotopic shift is smaller than the dispersion of a branch in the Brillouin zone ($\Gamma \simeq 5\ \text{cm}^{-1}$), and hence the $\nu \simeq 27\ \text{cm}^{-1}$ band in the solid mixture $CsDy_{1-x}Bi_x(MoO_4)_2$ must display a one-mode behavior according to general considerations. Such a one-mode behavior was also observed by us for a system of solid mixtures $KDy_xY_{1-x}(MoO_4)_2$ and $KEr_{1-x}Y_x(MoO_4)_2$ with a similar crystalline structure.[10,11] Figure 3 shows absorption spectrum for various values of concentration x in a $KDy_{1-x}Y_x(MoO_4)_2$ crystal in the region of low-frequency vibrational mode ($\nu \simeq 28\ \text{cm}^{-1}$). It can be seen from the figure that the absorption band is shifted smoothly along the frequency scale upon a change in the reduced mass of two layers from one extreme position to the other without a noticeable change in the half-width. Such a behavior of vibrational modes was also observed in the spectrum of $KEr_{1-x}Y_x(MoO_4)_2$ and can be explained on the basis of general concepts concerning the formation of the spectrum in

these compounds. In the case under investigation, the low-frequency vibrational mode obviously also displays one-mode behavior, but in the intermediate concentration range we cannot unambiguously state this in view of superposition of spectra.

The absorption spectra of mixed $CsDy_{1-x}Bi_x(MoO_4)_2$ crystals with $x \sim 0$ display an absorption band $\nu \simeq 22\,\mathrm{cm}^{-1}$ (see Fig. 1). According to experimental data obtained earlier,[12] this band is associated with an electron transition to the first Stark energy level of the fundamental multiplet $^6H_{15/2}$ of the Dy^{3+} ion, split by the crystal field. Since this band must be observed in the spectrum of the high-temperature phase of $CsDy(MoO_4)_2$ ($T > T_c$),[12] while the vibrational mode $\nu \simeq 27\,\mathrm{cm}^{-1}$ must be manifested below the phase transition point ($T < T_c$),[9] we assume that phase separation takes place in mixed $CsDy_{1-x}Bi_x(MoO_4)_2$ crystals at low temperatures ($T \simeq 6\,\mathrm{K}$). This is also confirmed by experimental observations of phase separation in a pure $CsDy(MoO_4)_2$ crystal below the phase transition point ($T < T_c$) as a result of application of an external pressure along the normal to the layers.[13] According to the prevailing theoretical concepts, such a separation is possible in tricritical systems.[14,15] The intrusion of Bi^{3+} ions into $CsDy(MoO_4)_2$ is similar to the creation of a normal pressure since the crystal lattice parameter corresponding to the separation between layers in $CsBi(MoO_4)_2$ is smaller than in $CsDy(MoO_4)_2$. Thus, in the range of intermediate concentration, we observe an overlapped spectrum from two phases of the crystal: the absorption band corresponding to the vibrational mode of the low-temperature phase and the electron absorption band $\nu \simeq 22\,\mathrm{cm}^{-1}$ of the high-temperature phase.

We observe the threshold blurring of the spectrum upon a change in concentration upon a change in the concentration range $0.2 \leqslant x \leqslant 0.6$ (see Fig. 2). Such a behavior does not fit to the generally accepted mode of variation of the electron band half-width in the case of replacement of paramagnetic ions by diamagnetic impurities. In the systems of solid mixtures $KDy_{1-x}Y_x(MoO_4)_2$ and $KEr_{1-x}Y_x(MoO_4)_2$ investigated earlier and having a similar structure, the replacement of the paramagnetic Dy^{3+} and Er^{3+} ions by the diamagnetic impurity Y^{3+} caused a smooth decrease in half-widths as well as intensities of electron absorption bands corresponding to transitions to the lowermost electron state of paramagnetic ions upon an increase in the concentration of the diamagnetic impurity.[10,11] Hence we assume that interactions appearing in the strongly nonequilibrium high-temperature phase of the $CsDy_{1-x}Bi_x(MoO_4)_2$ system in the intermediate concentration range ($0.2 \leqslant x \leqslant 0.6$) lead to absorption spectrum blurring. We propose several mechanism that can lead to spectrum blurring.

First, an electron excitation can be regarded as an impurity-induced excitation in view of its insignificant delocalization in the crystal. Two cases can be realized here. In the first case, the impurity excitation interacts weakly with the crystal lattice and is of a quasi-local nature. In the second case, the excitation interacts with the vibrational spectrum and is responsible for its resonant excitation. This is manifested in a change in the density of states in the spectrum of a perfect crystal, viz., a change in its width and frequency for certain wave vectors, i.e., a spectrum rearrangement takes place. The rearrangement can be normal or abnormal by nature. Normal rearrangement leads to the splitting of the continuous spectrum into two branches by the electron mode and to the formation of a gap between them. However, the spectrum rearrangement can be abnormal when the impurity mode gets into the region of quasi-one-dimensional oscillations.[16,17]

In the case under investigation, the first electron excitation of Dy^{3+} ions ($\nu \simeq 22\,\mathrm{cm}^{-1}$) gets into the region of continuous spectrum of acoustic vibrational mode with the limiting frequency at the boundary of the Brillouin zone $\nu \simeq 27\,\mathrm{cm}^{-1}$. For a low concentration of Bi^{3+} ions, the electron mode intersects the acoustic mode within the Brillouin zone in which the density of states of the vibrational spectrum is relatively low. Consequently, we observe in the spectrum a narrow electron absorption band. As the Bi^{3+} concentration increases, the acoustic branch is shifted to the low-frequency region. The spectral position of the electron energy level in this case is displaced towards the Brillouin zone boundary. Since the specrta of layered crystals have a sharp peak in the low-frequency range due to a weak interaction between the layers, the maximum density of vibrational states corresponding to the zone boundary,[18] this may lead to an anomalous rearrangement of the crystal spectrum due to the interaction of the electron mode with the acoustic vibrational mode, leading to delocalization of the electron excitation, i.e., the broadening of the electron absorption band.

Second, the compound $CsDy(MoO_4)_2$ displays a first-order structural phase transition of the CJTE type ($T_c \simeq 40\,\mathrm{K}$), while $CsBi(MoO_4)_2$ displays a first-order structural phase transition associated with anharmonism at interlayer vibrations ($T_c \simeq 135\,\mathrm{K}$). Apparently, a competition of distortions emerging below phase transition points may take place in a solid mixture of these compounds. Since the phase transition in $CsDy(MoO_4)_2$ is accompanied by multiplication of the unit cell, while no multiplication takes place in $CsBi(MoO_4)_2$, such a competition observed at low temperatures in a strongly nonequilibrium state normally leads to a disordered crystal lattice of the spin glass type. In $CsDy_{1-x}Bi_x(MoO_4)_2$, the interlayer vibrational mode is active during the phase transition, and hence we can assume that disorder appears at interlayer links. In this case, the fluctuation of the distance Δa between layer packets is smaller than the distance in the initial phase ($a = a_0 + \Delta a$ and $\Delta a \ll a_0$, where a_0 is the separation between layer packets in the initial structure). Hence the structural disorder in our system in this model resembles one-dimensional glass or one-dimensional liquid rather than one-dimensional alloy.

In our analysis of the dynamics of crystal lattice of $CsDy_{1-x}Bi_x(MoO_4)_2$ in the intermediate concentration range, we assume that elastic constants of interlayer interaction vary with the distance between layer packets. The vibrational mode corresponding to these elastic constants must change frequency also, which must lead to blurring of the vibrational mode in the region of intermediate concentrations. The electron mode must display a similar behavior in view of its strong coupling with these phonon mode.

We believe that the contribution of the mechanism of dynamic interaction between the electron and phonon spectral branches to the absorption spectrum blurring is decisive in the intermediate concentration region, but the second mechanism can also make a contribution. It should be noted in conclusion that the sample with $x=0.7$ had a relatively poor quality, i.e., contained inclusions of the solvent, and hence we assume that the band $\nu \simeq 33\,\mathrm{cm}^{-1}$ can be due to the spectrum of the solvent.

The authors are grateful to A. B. Beznosov for fruitful discussions of the results of this research.

*E-mail: kutko@ilt.kharkov.ua

[1] A. I. Zvyagin, T. S. Stetsenko, V. G. Yurko, and P. A. Vaishnoras, Pis'ma Zh. Éksp. Teor. Fiz. **17**, 190 (1973) [JETP Lett. **17**, 135 (1973)].
[2] I. V. Skorobogatova and A. I. Zvyagin, Fiz. Nizk. Temp. **4**, 800 (1978) [Sov. J. Low Temp. Phys. **4**, 381 (1978)].
[3] M. S. Borodin and I. V. Blonskii, *Exciton Processes in Layered Crystals* [in Russian], Naukova Dumka, Kiev (1986).
[4] M. A. Ivanov, V. Ya. Mitrofanov, and A. Ya. Fishman, Fiz. Tverd. Tela (Leningrad) **20**, 3023 (1978) [Sov. Phys. Solid State **20**, 1744 (1978)].
[5] F. Mehran and K. W. H. Stevens, Phys. Rev. **B27**, 2899 (1983).
[6] Yu. A. Popkov, A. V. Van'kevich, L. A. Shuvalov, and R. M. Fedosyuk, Fiz. Nizk. Temp. **19**, 195 (1993) [Low Temp. Phys. **19**, 138 (1993)].
[7] E. Courtens, Ferroelectrics **72**, 229 (1987).
[8] P. V. Klevtsov and R. F. Klevtsova, Zh. Strukt. Khim. **18**, 419 (1977).
[9] V. I. Kut'ko, Fiz. Nizk. Temp. **24**, 383 (1998) [Low Temp. Phys. **24**, 291 (1998)].
[10] V. I. Kut'ko, I. V. Skorobogatova, V. A. Bagulya *et al.*, Fiz. Nizk. Temp. **17**, 1023 (1991) [Sov. J. Low Temp. Phys. **17**, 533 (1991)].
[11] V. I. Kut'ko, Yu. N. Kharchenko, N. M. Nesterenko, and A. A. Gurkas, Fiz. Nizk. Temp. **22**, 785 (1996) [Low Temp. Phys. **22**, 603 (1996)].
[12] E. N. Khats'ko and A. S. Chernyi, Fiz. Nizk. Temp. **7**, 1048 (1981) [Sov. J. Low Temp. Phys. **7**, 509 (1981)].
[13] I. V. Skorobogatova, E. M. Savchenko, and A. I. Zvyagin, Izv. Akad. Nauk SSSR, Ser. Fiz. **47**, 491 (1983).
[14] M. San Miguel and J. D. Gunton, Phys. Rev. **B23**, 2317 (1981).
[15] M. San Miguel, J. D. Gunton, G. Dee, and P. S. Sahni, Phys. Rev. **B23**, 2334 (1981).
[16] M. A. Ivanov, Yu. G. Pogorelov, and M. N. Borvinko, Zh. Éksp. Teor. Fiz. **70**, 610 (1976) [Sov. Phys. JETP **43**, 317 (1976)].
[17] M. A. Ivanov and Yu. V. Skrypnik, Fiz. Nizk. Temp. **16**, 1171 (1990) [Sov. J. Low Temp. Phys. **16**, 677 (1981)].
[18] E. S. Syrkin and S. B. Feodos'ev, Fiz. Nizk. Temp. **5**, 1076 (1979) [*sic*].

Translated by R. S. Wadhwa

BRIEF COMMUNICATIONS

On the theory of phase separation in systems metallized as a result of doping

M. A. Ivanov

*G. V. Kurdyumov Institute of Metal Physics, National Academy of Sciences of the Ukraine, 252152 Kiev, Ukraine**

V. M. Loktev

*N. N. Bogolyubov Institute of Theoretical Physics, National Academy of Sciences of the Ukraine, 252143 Kiev, Ukraine***

(Submitted April 13, 1999)
Fiz. Nizk. Temp. **25**, 1325–1328 (December 1999)

The mechanism of formation of an inhomogeneous ground state of weakly doped systems, consisting of the domains of metallic and insulating phases, is proposed. According to this mechanism, the formation of the charge-neutral metallic regions with the highest possible concentration of free charge carriers (and hence of the dopants generating them) is shown to be thermodynamically advantageous. © *1999 American Institute of Physics.* [S1063-777X(99)01212-8]

1. The ground state of the cuprate planes of weakly doped high-temperature superconductors (HTSC) has been the subject of lively discussion during recent years (see, for example, Ref. 1). As a matter of fact, the host oxides are known[2–4] to be AFM insulators whose conductivity results from heterovalent doping or is due to a change in their oxygen content. In either case, metallization is caused by a Mott transition which leads to the emergence of free carriers in the system and to the formation of a Fermi level.[5,6]

Nevertheless, the origin of dopant/ions (let alone the way in which they are introduced) affects their distribution in the obtained samples. For example, while Sr^{2+} ions remain practically immobile in $La_{2-x}Sr_xCuO_4$ even at rather high temperatures $T \lesssim 1400$ K, the subsystem of O^{2-} ions in $La_2CuO_{4+\delta}$ or $(YBa_2Cu_3O_{6+\delta})$ may diffuse quite easily over the lattice at temperatures right up to $T \approx 200$ K.[7] Consequently, the doped system tends towards equilibrium in the second version and becomes inhomogeneous and two-phased, the metallic phase consisting of oxygen-enriched regions (domains) and the insulating region deplete in oxygen. There is no long-range magnetic ordering in domains of the first type,[2,8] while all characteristic features of an AFM insulator are preserved in domains of the second type.

For example, neutron diffraction studies of the HTSC $La_2CuO_{4+\delta}$ show[7] that samples with excess oxygen in the range $0.01 \lesssim \delta \lesssim 0.055$ are separated into metallic (with $\delta \approx 0.055$, the superconducting transition temperature $T_c \approx 32$ K, and hence the Neel temperature $T_N = 0$ K) and insulating domains (with $\delta \lesssim 0.01$ and $T_N = 250$ K). The domains in both the phases, separated by domain walls, are quite large in size ($\sim 10^{-3}$ Å) in all directions.

Measurements in $La_{2-x}Sr_xCuO_4$[9] and manganites[10] show that in the case of a weak diffusion of dopants, the compounds also display a tendency towards the formation of domains, albeit of much smaller size, and the doping leading to such a state is called topological doping.[11] Among other things, the weakly doped $La_{2-x}Sr_xCuO_4$ system displays a striped structure of CuO_2 planes, consisting of extended metallic and insulating domains whose cross-sectional size does not exceed a few lattice constants. The description of the reasons and mechanisms of emergence of such self-organizing structures is one of the most important problems in the HTSC theory at present.

2. Several models have been proposed for explaining the emergence of such domains in cuprates. One such model (see Ref. 12), which owes its origin to Nagaoka[13] (see Ref. 14 also), attributes the origin of conducting domains to a considerable decrease in the kinetic energy of a carrier (hole in HTSC) moving in a paramagnetic (as well as ferromagnetic (FM)) medium as compared to an AFM medium in which each jump of the carrier from one ion to another is inevitably accompanied by a violation of the initial spin ordering. However, a free oxygen hole in an HTS is frustrated and is located in the zero exchange field of localized spin of ions Cu^{2+}, thus being free from the above-mentioned constraints.[2,15]

Another version of stratification, or the Emery–Kivelson[11,16] charge fluctuation model (see also Ref. 17), associates the formation of metallic strips with competition between long- and short-range interaction of dopants. The analysis is based on the model of effective spins close to the Ising model in which the role of the former is played by the AFM exchange between distant neighbors and of the latter by the FM exchange between long-range spins in a square lattice. Assuming that one component of the effective spin corresponds to the presence and the other to the absence of the dopant, we can choose the suitable parameters for defining a structure in which FM strips of width 3–5 lattice con-

stants alternate with similar strips with opposite spins, the structure being identical to the sequence of metallic and insulating domains in HTSC, although the correctness of the model in the latter case is not obvious. If, however, the dopants do not diffuse and constitute a uniform background (on the average), it is assumed that, being comparatively light, the carriers are expelled from the AFM domains and form striped AFM disordered metallic domains which are found to be charged. It was proved convincingly by Phillips (see Ref. 11) that such an ordering must be unfavorable from the energy point of view because of a large Coulomb interaction that is not compensated within domains. The neutralization of this interaction is not discussed under the Emery–Kivelson approach.[16]

3. However, we believe that splitting into domains is an inevitable property of doped metals. Indeed, the energy of the initial insulator assumed as the starting point changes upon the introduction of dopants following the creation of free carriers as well as slow-moving ions in the system. Let us calculate the binding energy ε per carrier. It is determined (see, for example, Ref. 18) by two main contributions coming from the Hartree-Fock energy $\varepsilon_{\rm free}$ of the free Fermi gas and the Coulomb interaction $\varepsilon_{\rm Coul}$ which in turn consists of two parts, viz., the energy $\varepsilon_{\rm Coul}^{hh}$ of repulsion between uniformly distributed carriers, and the energy $\varepsilon_{\rm Coul}^{hi}$ of attraction between the carriers and the negatively charged dopant ions.[1)]

The first contribution is positive and is determined by the average kinetic energy of carriers. Taking into consideration the two-dimensional nature of motion of holes in HTSC, we can present this contribution in the form

$$\varepsilon_{\rm free}=\frac{1}{2}\langle\varepsilon_F\rangle;\quad \varepsilon_F=\frac{\hbar^2\mathbf{k}_F^2}{2m_h}, \tag{1}$$

where ε_F and $\mathbf{k}_F$ are the Fermi energy and wave vector respectively, and m_h is the effective hole mass. Assuming that the number density of holes in a layer is n_h and that each hole occupies an area πr_h^2, i.e., $\pi r_h^2=n_h^{-1}$, we arrive at the relation $k_F=\sqrt{2}r_h^{-1}$, i.e., $\langle\varepsilon_F\rangle=(\hbar^2\pi/2m_h)n_h$.

Let us now estimate $\varepsilon_{\rm Coul}$. For this purpose, we break the crystal[18] into Wigner–Seitz cells and obtain in the first approximation the Coulomb energy of the $2D$ system within one such cell. As a result of simple computations, we get[2)]

$$\varepsilon_{\rm Coul}=\varepsilon_{\rm Coul}^{hh}+\varepsilon_{\rm Coul}^{hi}=-\frac{4}{3}\sqrt{\pi}e^2n_h^{1/2}, \tag{2}$$

where $\varepsilon_{\rm Coul}^{hh}=2e^2/3r_h$, and $\varepsilon_{\rm Coul}^{hi}=-2e^2/r_h$. It can be seen from Eq. (2) that this energy is negative. In other words, there exists a metallic bond in the system when the forces of Coulomb attraction dominate over repulsive forces. It can also be verified that if the cells are neutral as a whole, the interaction between them is much weaker than that defined by Eq. (2).

It was mentioned above that other contributions also exist for real systems, but they do not affect the estimates and qualitative conclusions. It follows from Eqs. (1) and (2) that the Coulomb term dominates for quite small n_h. The total energy minimum corresponds to the concentration $\tilde{n}_h=(16/9\pi)a_B^{-2}\approx10^{16}\,\mathrm{cm}^{-2}$ (a_B is the Bohr radius), which is much larger[3)] than real densities of free holes in CuO_2 layers ($\lesssim10^{14}\,\mathrm{cm}^{-2}$).

Thus, for a given concentration of dopants in the sample, their redistribution leading to the emergence of regions with maximum possible carrier concentration (though not exceeding $\tilde{n}_h$) and regions with zero (or few) carriers is more advantageous from the energy point of view. Each region having an area $\sim\pi r_h^2$ must remain electrically neutral since the energy gain is not realized otherwise.

Apparently, the entropy of mixing is a factor obstructing such a redistribution. However, it can be seen easily that even for large values of T, the contribution to the free energy per dopant is of the order of T, which is considerably smaller than (2).

4. Under real conditions, doping is carried out at high temperatures (heterovalent substitution) or under high pressures (addition of oxygen). In any case, the system must disintegrate due to energy considerations into two types of electrically neutral regions, viz., metallic regions with a high concentration of dopants (and carriers) and insulating regions. Although such a tendency does exist, it is realized under conditions of a finite (and generally weak) diffusion of dopants which thus controls the disintegration process. Hence the nature of the prevailing structural state in the investigated HTSC systems depends significantly on thermodynamics as well as kinetics of their preparation.

The highest possible concentration of fermions in metallic domains is defined as the limiting solubility of dopants in a given material. For example, the surplus oxygen in $La_2CuO_{4+\delta}$ is confined to $\delta_{\max}\approx0.1$.[7]

The established instability of the homogeneous state of a doped metal still does not reveal the form of the structure of its inhomogeneous state. It was mentioned above that this instability is the result of the kinetics of the heavy subsystem, and the domain size is determined by the rate of sample preparation: the higher the rate, the smaller the size of the structure formed. Such regularities are observed for HTSC[7] in which small as well as coarse domains can be formed depending on the conditions of growth and the type of dopant. As regards their shape, it is well known that decomposition processes occurring in alloys (see Ref. 19) often lead to stripe- or lamellar-type structures formed by alternating domains of different phases. The advantage of such structures can be ensured, for example, by the minimum value of ther total surface energy of domain walls. On the other hand, the type of domains can be ''dictated'' by ordering dopants also. For example, it is advantageous from the symmetry and energy points of view that their structure in cuprate layers of HTSC be of a transverse-homogeneous chain type.[20] In our opinion, it cannot be ruled out that the latter circumstance is an additional factor in the formation of the stripe (i.e., transverse-inhomogeneous) ordering of dopants interacting with free charge carriers.

5. Thus, we propose that the domain (including stripe) structure of samples in the metal state observed for HTSC is due (to a considerable extent) to decomposition processes occurring during sample preparation, in which each domain

remains charge-compensated. In the proposed model of domain formation, the antiferromagnetism of initial compounds as well as the mobility of holes as a lighter subsystem do not play a signifiant role, and long-range AFM correlations are suppressed even at the insulating stage due to exchange and elastic perturbations.[8] However, a theoretical description of the formed $3D$ structure involves the introduction of additional concepts concerning the kinetics of dopants at a given T, taking into account the fact that small domains are disadvantageous due to the developed interface, and the growth of large-scale structure is limited by the ionic mobility of thermal activation origin and also depends on the elastic properties of the medium. Hence it should be quite interesting to carry out experimental studies of the variation in shape and size of domains depending on the conditions (e.g., cooling rate) of HTSC sample preparations with various doping impurities.

*E-mail: ivanov@imp.kiev.ua
**E-mail: vloktev@bitp.kiev.ua

[1)]For the sake of simplicity, we neglect the terms associated with correlation and free energies.

[2)]We omit static permittivity ($\sim 30-50$) for HTSC) which can be taken into account in a trivial manner.

[3)]It should be noted that such concentrations, which are unattainable even in ordinary metals, in HTSC are also due to impossibility of dilution of such an amount of dopants (~ 1 per unit cell) in these materials.

[1] A. A. Zakharov, Perspekt. Tekhn. **6**, 2 (1999).
[2] V. M. Loktev, Fiz. Nizk. Temp. **22**, 3 (1996) [Low Temp. Phys. **22**, 1 (1996)].
[3] N. M. Plakida, *High-Temperature Superconductivity* [in Russian], Intern. Edu. Program, Moscow (1996).
[4] Yu. A. Izyumov, Phys. Usp. **169**, 225 (1999) [*sic*].
[5] M. A. Ivanov, V. M. Loktev, Yu. G. Pogorelov, and Yu. V. Skripnik, Fiz. Nizk. Temp. **17**, 716 (1991) [Sov. J. Low Temp. Phys. **17**, 377 (1991)].
[6] M. A. Ivanov, V. M. Loktev, and Yu. V. Skripnik, Fiz. Nizk. Temp. **22**, 1186 (1996) [Low Temp. Phys. **22**, 907 (1996)].
[7] B. O. Wells, Y. S. Lee, M. A. Kastner *et al.*, Science **277**, 1067 (1997).
[8] M. A. Ivanov, V. M. Loktev, and Yu. G. Pogorelov, Zh. Eksp. Teor. Fiz. **101**, 596 (1992) [Sov. Phys. JETP **74**, 317 (1992)].
[9] J. M. Tranquada, B. J. Sternlieb, J. Axe *et al.*, Nature (London) **375**, 561 (1995).
[10] S. Mori, C.-H. Chen, and S. W. Cheong, Nature (London) **392**, 473 (1998).
[11] V. J. Emery and S. A. Kivelson, Preprint Cond. Mat./9902179 (1999).
[12] E. L. Nagaev, Usp. Fiz. Nauk **168**, 833 (1996) [*sic*].
[13] Y. Nagaoka, Phys. Rev. **147**, 392 (1966).
[14] E. V. Kuz'min, G. A. Petrakovskii, and E. A. Zavadskii, *Physics of Magnetically Ordered Materials* [in Russian], Nauka, Novosibirsk (1976).
[15] V. M. Loktev, Fiz. Nizk. Temp. **19**, 375 (1993) [Low Temp. Phys. **19**, 263 (1993)].
[16] U. Low, V. J. Emery, K. Fabricius, and S. K. Kivelson, Phys. Rev. Lett. **72**, 1918 (1994).
[17] T. Muton and H. Kontani, Preprint cond-mat/9904440 (1999).
[18] C. Kittel, *Quantum Theory of Solids*, J. Wiley and Sons, New York (1963).
[19] J. W. Christian, *The Theory of Transformations in Metals and Alloys*, Vol. 1, Pergamon Press, New York (1975).
[20] V. M. Loktev and H. M. Tatarenko, Phys. Status Solidi B **166**, 191 (1991).

Translated by R. S. Wadhwa

Sound attenuation in the superconducting amorphous alloy ZrTiCuNiBe

E. V. Bezuglyĭ, A. L. Gaiduk, and V. D. Fil

*B. Verkin Institute for Low Temperature Physics and Engineering, National Academy of Sciences of the Ukraine, 310164 Kharkov, Ukraine**

W. L. Johnson

California Institute of Technology, Pasadena, CA 91125, USA

G. Bruls, B. Lüthi, B. Wolf, and S. V. Zherlitsyn

Physikalisches Institut, Universitat Frankfurt, 60054 Frankfurt, Germany
(Submitted May 25, 1999)
Fiz. Nizk. Temp. **25**, 1329–1333 (December 1999)

The superconducting energy gap and the parameter η determining the intensity of electron scattering at two-level systems in amorphous ZrTiCuNiBe are determined from the results of measurements of sound attenuation. The mechanism of adiabatic renormalization of the amplitude of coherent tunneling is used for a quantitative description of the peculiarities of sound absorption in the vicinity of T_c. © *1999 American Institute of Physics.*
[S1063-777X(99)01312-2]

Preliminary measurements of the velocity v and absorption Γ of sound in the amorphous alloy $Zr_{1.2}Ti_{13.8}Cu_{12.5}Ni_{10}Be_{22.5}$ have revealed[1] an interesting peculiarity in its behavior in the vicinity of the superconducting transition temperature T_c. It was found that the value of $T_{cm} \approx 0.9\,\mathrm{K}$ determined from magnetic measurements exceeds the transition temperature $T_c \approx 0.83\,\mathrm{K}$ at which a nonzero difference is observed in the velocities of sound in superconducting (s) and normal (n) phases. It was proposed that such a behavior may be due to magnetic depairing leading to the gapless s-phase in the temperature interval $T_{cm}-T_c$. Since our earlier measurements[1] were made in a temperature interval limited from below ($T \gtrsim 0.4\,\mathrm{K}$), it should be interesting to study the behavior of Γ at lower temperatures. In view of a close analogy in the behavior of electron acoustic absorption coefficient in superconductors and the relaxation absorption of sound in two-level systems (TLS) in the s-phase, one could expect a nonexponential drop in $\Gamma_s(T)$ in the low-temperature ''tail,'' or an exponential decrease but with a much smaller gap if the magnetic depairing effects are significant. It is shown in the present work that the $\Gamma_s(T)$ dependence at low temperatures can be described quite correctly by the tunnel model (TM)[2] in the framework of the standard BCS approximation, which rules out the gapless phase hypothesis. The refined value of the transition temperature for the bulk of the sample was found to be close to T_c, while the value of T_{cm} determined from magnetic measurements is apparently associated with the surface phase. However, the behavior of Γ in the vicinity of T_c does not conform to the standard TM: the drop in $\Gamma_s(T)$ below T_c begins much later than what is predicted by TM. Besides, in a certain temperature interval below T_c, the absorption is slightly higher than $\Gamma_n(T)$. Such effects were observed earlier in the amorphous alloy $Pd_{30}Zr_{70}$ and were explained qualitatively by the electron renormalization of the parameter of TLS interaction with an elastic wave.[3] However, possible mechanisms of such a renormalization were not discussed and quantitative estimates of its magnitude were not obtained in Ref. 3. We shall use the mechanism of adiabatic renormalization of the amplitude of coherent tunneling[4] to explain the peculiarities of sound absorption in the vicinity of T_c. This approach gives an acceptable quantitative description of the dependence $\Gamma_s(T)$.

The basic postulate of TM, which was confirmed irrefutably in experiments (see the review by Hunklinger and Raychaudhuri[2]), is the assumption that glasses have double-well potentials with a tunneling link between the wells whose density of states $\overline{p}$ is constant in the space of the parameters ξ and $\ln \Delta_0$ (ξ is the asymmetry of a double-well potential and Δ_0 the amplitude of coherent tunneling). The response of the TLS system to an external perturbation is determined by the average over the TLS ensemble. For the sake of convenience, averaging is usually carried out by using new variables $E=\sqrt{\xi^2+\Delta_0^2}$ and $u=\Delta_0/E$ in which the density of states of TLS is independent of E:

$$g(E,U)=\frac{\overline{p}}{u\sqrt{1-u^2}} \equiv g(u). \tag{1}$$

Under the conditions of the experiment ($\omega \ll T$, ω being the frequency of acoustic vibrations), the attenuation of sound associated with the TLS is determined by the relaxation mechanism and is described by the following standard expression:[2]

$$\left(\frac{\Gamma v}{\omega}\right)_{\mathrm{rel}} = \int_0^{E_g/T} \frac{d\varepsilon}{\cosh^2(\varepsilon/2)} \int_0^1 C_g(u)(1-u^2)\frac{\omega\nu}{\omega^2+\nu^2}\,du. \tag{2}$$

Here $\varepsilon = E/T$, $E_g \gg T$ is the limiting energy, and ν the relaxation frequency. In Eq. (2) and below, we have used the

system of energy units ($\hbar = k = 1$). The order of magnitude of the TLS contribution to the velocity and attenuation of sound is determined by the parameter C. In the standard TM,[2] this quantity is a constant: $C = C_0 = \overline{p\gamma^2}/(\rho v^2)$ ($\gamma = 1/2(\partial\xi/\partial e)$ is the deformation potential, e the deformation, and ρ the density), although a number of experimental facts can be explained only by assuming that C depends on E, u or T.

The TLS relaxation is due to their interaction with electrons as well as phonons, although the contribution of the latter can be disregarded for $T \lesssim 1$ K. The intensity of interaction of TLS with electrons is determined by the dimensionless parameter $\eta = 2n_0(V^2_{kk'})^{1/2}$, where n_0 is the density of electron states at the Fermi level and $\overline{V^2_{kk'}}$ is the square of the matrix element of electron scattering at TLS from the state $\mathbf{k}$ to the state $\mathbf{k}'$, averaged over the Fermi surface.

In the standard TM, the interaction of TLS with electrons is considered in the framework of the perturbation theory in parameter η^2, which does not change the system of energy levels.[5] The entire distinction between a metallic glass and an amorphous insulator is reflected just in the emergence of a new relaxation channel with a characteristic rate

$$\nu = \frac{\pi\eta^2}{2} T u^2 J(\varepsilon). \tag{3}$$

In the n-phase, $J(\varepsilon) = J_n(\varepsilon) = (\varepsilon/2)\coth(\varepsilon/2)$ and $\nu \approx \eta^2 T u^2$. As long as $\omega \ll T$, there always exist TLS with $\nu_{\text{opt}} \sim \omega$, and the absorption (2) is practically independent of temperature (''plateau'' region).

In the s-state, we must use instead of $J_n(\varepsilon)$ the function $J_s(\varepsilon,\Delta)$($\Delta = \Delta_s/T, \Delta_s$) is the superconducting energy gap:[6]

$$J_s(\varepsilon,\Delta) = \frac{1}{2}\int_\Delta^\infty d\varepsilon' \frac{f(-\varepsilon')}{\sqrt{\varepsilon'^2-\Delta^2}} \left\{ \frac{\varepsilon'(\varepsilon'-\varepsilon)-\Delta^2}{\sqrt{(\varepsilon'-\varepsilon)^2-\Delta^2}} \times \frac{f(\varepsilon'-\varepsilon)}{f(-\varepsilon)} \Theta[(\varepsilon'-\varepsilon)^2-\Delta^2]\,\mathrm{sgn}(\varepsilon'-\varepsilon) + (\varepsilon \to -\varepsilon) \right\}, \tag{4}$$

where $f(x)$ is the Fermi function and $\Theta(x)$ is the step Θ-function. The function $J_s(\varepsilon,\Delta)$ is frequently encountered in the theory of kinetic properties of superconductors. It has a discontinuity at $\varepsilon = 2\Delta$, while $aJ_s(\varepsilon,\Delta) \to 2f(\Delta)$ for $\varepsilon \ll 2\Delta$. As a result of a rapid drop in the value of J_s below T_c, the maximum relaxation rate ($u = 1$) becomes less than ω starting from a certain temperature while $\Gamma_s(T)$ ''freezes.''

A nonperturbative analysis[4,7] revealed a more complicated pattern. Even at $T = 0$, the initial coherent tunneling amplitude Δ_0 in the n-phase is renormalized as the adiabatic part of the interaction of TLS with electrons is taken into consideration:

$$\Delta_0^* \approx \Delta_0 \left(\frac{\Delta_0}{\omega_0}\right)^{\eta^2/4-\eta^2}, \tag{5}$$

where ω_0 is the energy of the order of Debye energy.

For $T \neq 0$, the TLS ensemble can be divided arbitrarily into three intervals according their position on the E-scale in the n-state.

(1) The coherent tunneling region $E^* \sqrt{\xi^2 + \Delta_0^{*2}} > T$

(2) The region $E^* < T < 4\tilde{E}/(\pi\eta^2)$ of coherent tunneling with an amplitude $\tilde{\Delta} = \Delta_0 \times (2\pi T/\omega_0)^{\eta^2/4}$ and the energy splitting $\tilde{E} = \sqrt{\xi^2 + \tilde{\Delta}^2}$. Going over to renormalized variables E^* and $\tilde{E}$ as well as to u^* and $\tilde{u}$ during averaging in each of the regions 1 and 2, relations (2) and (3) remain valid.

(3) The low-energy TLS $T > 4\tilde{E}/(\pi\eta^2)$. In this region also, the tunneling is incoherent and has an amplitude $\tilde{\Delta}$. However, the vanishing of the factor $(1-\tilde{u}^2)$ from Eq. (2) is a reflection of the fact that the incoherent transitions between broadened levels occur with a variation of energy even in the symmetric case. The relaxation frequency

$$\nu_3 \approx \frac{2}{\pi\eta^2} T \tilde{u}^2 \tilde{\varepsilon}^2 \frac{1}{j(\tilde{\varepsilon})} \tag{6}$$

also changes in region 3.

It would appear that as a result of a decrease in ν_3 for small $\tilde{\varepsilon}$ [Eq. (6)], the contribution to Γ from the part of TLS with $\tilde{E} < \sqrt{\omega T}$ must decrease. However, this decrease is compensated by an increase in the contribution from symmetric TLS, and the partial contribution from region 3 to Γ remains practically the same as that calculated in the standard TM. The contribution from region 2 also remains unchanged. Only the contribution from coherently tunneling TLS (region 1) undergoes significant variation. Upon a transition to the variables E^* and u^*, the density of states $g(u^*)$ (1) is renormalized as a result of a nonlinear relation (5) between Δ_0^* and Δ_0, and acquires an additional factor $(1-\eta^2/4)$. The parameter C is also renormalized accordingly. If the boundary between regions 1 and 2 is located at $E^* \sim T$, the resulting value of Γ in the n-phase decreases in spite of the fact that the denominator in (2) decreases the contribution from the high-energy TLS. Below T_c, the nonlinear relation (5) is rapidly transformed into a linear relation:[4] $\Delta_0^* \approx \Delta_0(\Delta_s/\omega_0)^{\eta^2/4}$, renormalization of C vanishes, and $\Gamma_s(T)$ below T_c may increase before ''freezing out.''

Let us now discuss the experimental results. Figure 1 shows the dependence $\Gamma_s(T)/\Gamma_n(T_c)$ for transverse sound. The normalization factor $\Gamma_n(T_c)^{-1}$ used for presenting the results can be easily determined from the variation of the amplitude of the acoustic signal between T_c and the deep superconducting state.

In the region of the low-temperature ''tail,'' the renormalization $g(u)$ can be disregarded. The following estimate is obtained from (1), (2) and (4):

$$\frac{\Gamma_s(T)}{\Gamma_n(T_c)} = \frac{2\pi\eta^2}{3\omega} T e^{-\Delta_s/T}, \quad (T/T_c < 0.3). \tag{7}$$

According to this equation, the low-temperature region $\Gamma_s(T)$ must become linear in coordinates $\ln(\Gamma_s(T)T^{-1}), T^{-1}$.

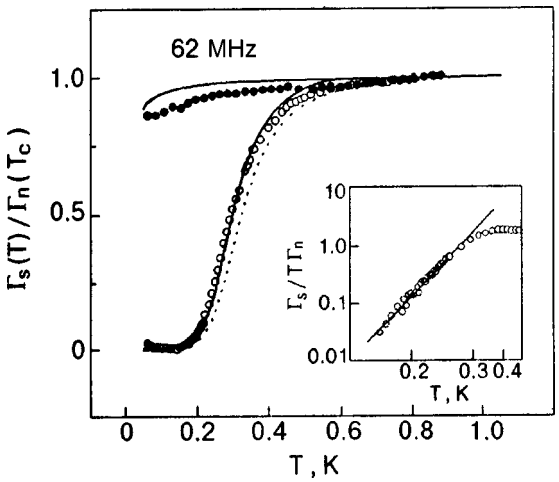

FIG. 1. Temperature dependence of attenuation in n (●) and s (○) states. The solid curves correspond to calculations for $\eta=0.65$ and $T_c=0.83$ K and the dotted ones to $T_c=0.9$ K. The inset illustrates the evaluation of $\Delta_s(0)$ and η. The solid line corresponds to the linear approximation.

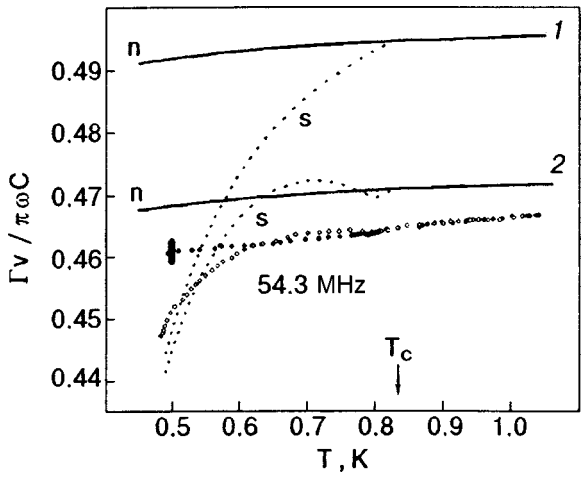

FIG. 2. Behavior of attenuation in the vicinity of T_c in n (●) and s (○) states. The experimental recordings are averaged, and the noise level is indicated by the bold vertical line. Curves *1* and *2* are obtained without and with renormalization respectively; $\eta=0.65$, $d=1.2$.

as can be seen from the inset to Fig. 1. The slope of the approximating straight line is determined by the superconducting energy gap which is in good accord with the BCS value: $\Delta_s(0)/T_c=1.7\pm0.1(T_c=0.9\,\mathrm{K})$ or $\Delta_s(0)T_c=1.8\pm0.1(T_c=0.83\,\mathrm{K})$. Intersection of the approximating straight line with the ordinate axis leads to the estimate $\eta=0.65\pm0.05$. These data can also be used to refine the value of T_c for the bulk of the sample. The slope of the approximating straight line and its interaction with the ordinate axis (see inset to Fig. 1) are by no means connected with the choice of T_c. For a complete evaluation of $\Gamma_s(T)$, we must use the specific value of T_c. It can be seen from Fig. 1 that the theoretical curve for $T_c=0.83$ K is in much better accord with the experimental data.

The closeness of $\Delta_s(0)/T_c$ to the BCS value indicates that peculiarities in the behavior of $\Gamma(T)$ in the vicinity of T_c are not connected with the magnetic depairing effects. Let us now discuss the applicability of the hypothesis of the electron renormalization of C to the description of the behavior of $\Gamma_s(T)$.

Figure 2 shows the data on variation of $\Gamma_s(T)$ and $\Gamma_n(T)$ in the vicinity of T_c, measured with a higher resolution than in Fig. 1. The results are normalized to the value $C_0=2.85\cdot10^{-5}$ obtained from the slope of $\nu_s(\ln T)$ in the deep superconducting state ($T\lesssim0.3$ K).[1)] The normalized value of $\Gamma(T_c)$ in the standard TM must be close to 0.5 for $\omega\ll T$. Renormalization (decrease) of C naturally shifts Γ towards lower values. However, it has not been possible to measure the value of attenuation with an accuracy better than 1%, which would allow an analysis of the shift of the experimental dependence relative to the theoretical one. Hence we consider only relative position of the lines $\Gamma_s(T)$ and $\Gamma_n(T)$ (the latter value is obtained in a magnetic field $H\approx2$T) which could be measured with a much higher degree of accuracy (Fig. 2).

The meaning of the ''anomaly'' in Γ discussed above can be seen clearly from a comparison of the experimental dependences with the theoretical ones obtained in the standard TM (curve *1* in Fig. 2). According to calculations, a decrease in absorption begins at T_c and continues as the steepness increases upon a decrease in temperature. The experimental dependence clearly displays a different behavior: $\Gamma_s(T)$ does not display any variation at T_c within the limits of resolution, and a tendency towards an increase in $\Gamma_s(T)$ over $\Gamma_n(T)$ is observed at lower temperatures. In any case, $\Gamma_s(T)$ remains practically unchanged over a wide temperature range $T<T_c$. More clearly manifested effects of this kind were detected earlier in the alloy $Pd_{30}Zr_{70}$.[3] It was also suggested in Ref. 3 that these anomalies can be associated with the electron renormalization of the parameter C.

The renormalization of C indeed takes place in the alloy investigated by us. An irrefutable proof of this is the intersection the dependences $\nu_s(T)$ and $\nu_n(T)$ at a quite low temperature T_{cr} (its value for 62 MHz is $T_{cr}=0.055$ K). The scale of renormalization is quite significant ($\delta C/C_0\sim0.25$) and is about double the quantity $\eta^2/4\sim0.09-0.12$, which allows us to assume the existence of several mechanisms of renormalization.[2)] Moreover, incompatibility of the scale of $\delta C/C_0$ with the anomalies in $\Gamma_s(T)$ indicates that these mechanisms affect only insignificantly the TLS forming the relaxation attenuation for $T\sim T_c$. It should be recalled that the main contribution to $\Gamma(T)$ comes from asymmetric TLS with $u_{opt}\sim\sqrt{\omega/T}\ll1$. One possible mechanism of renormalization, which takes into account the fluctuational rearrangement of the barrier in a double-well potential, is associated only with the symmetric TLS[8] and apparently makes no contribution to $\Gamma(T)$.

The adiabatic renormalization does not impose any constraints on the possible values of u.[7] In spite of the fact that the condition $\varepsilon>1$ moves the coherently tunneling TLS to the region of action of the truncating factor in (2), their partial contribution to $\Gamma(T)$ may be quite significant on the scale of Fig. 2.

For the purpose of numerical computations, we used the model energy dependence of the renormalization parameter

$$\frac{C}{C_0}=1-\Theta(\varepsilon-d)[1+(2f(\Delta)-1)\Theta(2\Delta-\varepsilon)]\frac{\eta^2}{4}, \quad (8)$$

where d is a free fitting parameter. The first cofactor in the term describing renormalization in Eq. (8) defines the boundary between the regions 1 and 2. Since the coherent amplitude Δ_0^* decreases exponentially for $\varepsilon<1$,[4] such an approximation seems to be quite reasonable. The second cofactor in (8) takes into account the fact that only normal excitations can contribute to renormalization for $\varepsilon<2\Delta$.

The results of calculations are also presented in Fig. 2 (curves *2*). The interval of approximate ''independence'' of $\Gamma_s(T)$ can be matched with that observed for a given value $\eta=0.65$ for a quite reasonable value of $d=1.2\pm0.1$. It can be seen that the calculated dependence $\Gamma_s(T)$ varies initially below T_c in the same manner as in the standard TM. Subsequently, $\Gamma_s(T)$ displays a kink with a reversal of the sign of $d\Gamma/dT$ at $T=2\Delta_s/d$. The emergence of the kink is a consequence of the use of a step approximation in (8). As long as $2\Delta_s$ does not exceed the value of $E=Td$, superconductivity does not have any effect on renormalization. Apparently, the restriction on the renormalization of C imposed from below by a smooth function of energy decreases the variation of $\Gamma_s(T)$ in the vicinity of T_c and eliminates the kink. The same result is also arrived at by the broadening of the superconducting transition which is quite natural for an amorphous sample. Hence it can be really expected that $\Gamma_s(T)$ will not change at T_c, as is indeed observed in the experiments.

Thus, the evolution of $\Gamma_s(T)$ near T_c is determined by two factors, viz., a drop in $\Gamma_s(T)$ due to a decrease in the relaxation rate ν, and an increase in $\Gamma_s(T)$ as a result of ''freezing out'' of the renormalization of C. In contrast to the latter factor, the former is frequency-dependent, and hence the resulting variation of Γ_s will also depend on frequency. Upon a decrease in ω, the temperature interval in which $\Gamma_s(T)>\Gamma_n(T)$ must expand, and vice versa. In particular, calculations show that an increase in frequency by an order of magnitude (measurements were made just at these frequencies by Esquinazi *et al.*[3]) completely masks the effect of the second factor for the same values of η, T_c, and d. However, Esquinazi *et al.*[3] carried out measurements on glass with $T_c\simeq2.5$ K. In this region, ν is determined mainly by phonons and depends weakly on the state of the electron subsystem. Under these conditions, the ''freezing out'' of renormalization must give an even more pronounced effect than in our experiments, as was apparently observed by Esquinazi *et al.*[3]

In conclusion, let us formulate the main results. The experimental dependence of the absorption of sound in the amorphous superconducting alloy $Zr_{41.2}Ti_{13.8}Cu_{12.5}Ni_{10}Be_{22.5}$ was used to determine the superconducting energy gap (which is found to be practically identical to the gap obtained in the BCS theory) and the parameter η characterizing the intensity of interaction of TLS with electrons. The departures from the predictions of the standard tunneling model observed in the vicinity of T_c can be explained qualitatively and quantitatively by the adiabatic renormalization of the coherent tunneling amplitude.

The authors are obliged to Prof. G. Weiss for drawing their attention to the publications by Kagan and Prokof'ev[4] and Stockburger *et al.*[7]

This research was partially supported by the State Foundation on Fundamental Research in Ukraine (grant No. 2.4/153) and by Deutsche Forschungsgemeinschaft via SFB 252. One of the authors (W. L. J.) wishes to thank the US Energy Department for grant (No. DE-FG03-86ER45242), while S. V. Zh. is grateful to the von Humboldt Foundation for financial support.

*E-mail: fil@ilt.kharkov.ua

[1)]This value of C_0 is double the analogous value presented in Ref. 1. The departure is due to the fact that the value of C_0 was estimated in Ref. 1 by using the linear dependence $\nu_n(\ln T)$ whose slope depends significantly on the renormalization of C. The latter was not taken into consideration in Ref. 1. The value of η presented in Ref. 1 is also found to be exaggerated for the same reason.

[2)]The effect of renormalization of C on the velocity of sound will be considered in a separate publication.

[1] A. L. Gaiduk, E. V. Bezuglyi, V. D. Fil, and W. L. Johnson, Fiz. Nizk. Temp. **23**, 1139 (1997) [Low Temp. Phys. **23**, 857 (1997)].
[2] S. Hunklinger and A. K. Raychaudhuri, in *Prog. in Low Temp. Phys.* (Ed. by D. F. Brewer), Vol. 9, North-Holland, Amsterdam (1986).
[3] P. Esquinazi, H.-M. Ritter, H. Neckel *et al.*, Z. Phys. B: Condens. Matter **64**, 81 (1986).
[4] Yu. Kagan and N. V. Prokof'ev, Zh. Éksp. Teor. Fiz. **97**, 1698 (1990) [Sov. Phys. JETP **70**, 957 (1990)].
[5] J. L. Black, B. L. Gyorffy, and J. Jäckle, Philos. Mag. B **40**, 331 (1979).
[6] J. L. Black and P. Fulde, Phys. Rev. Lett. **43**, 453 (1979).
[7] J. Stockburger, U. Weiss, and R. Görlich, Z. Phys. B: Condens. Matter **84**, 457 (1991).
[8] K. Vladar and A. Zawadowski, Phys. Rev. B **28**, 1564, 1582, 1696 (1983).

Translated by R. S. Wadhwa